N 62 65787

CASE FILE
COPY

NATIONAL ADVISORY COMMITTEE FOR AERONAUTICS

WARTIME REPORT

ORIGINALLY ISSUED
August 1944 as
Memorandum Report

WIND—TUNNEL TESTS OF THE $\frac{1}{8}$-SCALE POWERED
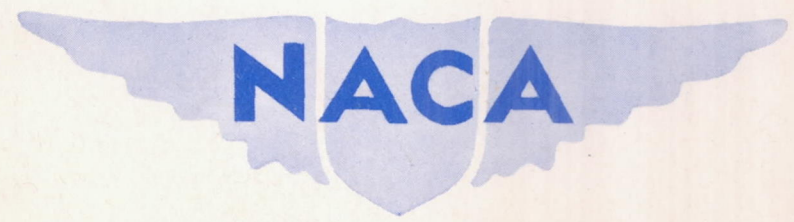
MODEL OF THE CURTISS XBTC—2 AIRPLANE

II — PRELIMINARY INVESTIGATION OF

LATERAL STABILITY AND CONTROL

By Arthur R. Wallace

Langley Memorial Aeronautical Laboratory
Langley Field, Va.

NACA

WASHINGTON

NATIONAL ADVISORY COMMITTEE FOR AERONAUTICS

<u>MEMORANDUM REPORT</u>

for the

Bureau of Aeronautics, Navy Department

WIND-TUNNEL TESTS OF THE $\frac{1}{8}$-SCALE POWERED

MODEL OF THE CURTISS XBTC-2 AIRPLANE

II - PRELIMINARY INVESTIGATION OF

LATERAL STABILITY AND CONTROL

By Arthur R. Wallace

INTRODUCTION

At the request of the Bureau of Aeronautics, tests
were made of the $\frac{1}{8}$-scale model of the Curtiss XBTC-2
airplane in the LMAL 7- by 10-foot tunnel. The results
of a preliminary investigation of longitudinal stability
and control are given in part I (reference 1).

When lateral-stability tests of the original model
were made, it was found: First, that a rudder-force
reversal was evident; and, second, that a large reduc-
tion in effective dihedral was shown when flaps were
lowered and take-off power applied. In an attempt to
remove the rudder-force reversal, various dorsal fins
and a modified vertical tail were tested. In an attempt
to reduce the change in effective dihedral with flap
deflection and power, the following modifications were
tested: the outboard flaps skewed from their original
position (effectively swept back), wing tips which could
be made to turn up when the flaps were lowered, and three
modifications to the wing plan form.

The present report also includes some estimates of
flying qualities which were computed from the data herein.

A new model is to be built and tested which will
incorporate modifications as judged best from the present
tests.

MODEL

The original model was supplied by the Columbus
division of the Curtiss-Wright Corporation. It was
equipped with a six-blade, dual-rotating propeller which
was not to scale, its diameter being 1.813 feet as com-
pared to the scale value of 1.771 feet. The model was
not checked for accuracy but was found to be faired and
finished in a satisfactory manner. The original model is
shown in figure 1. Cowl flaps were made at LMAL as shown
on figure 2. Some details of the aileron are shown in
figure 3. The various modifications were constructed by
the Navy, the Curtiss-Wright Corporation, or the LMAL.
They are as follows:

Modifications	Figure No.
Swept-back outer wing panel	4
Rectangular outer wing panel	5
Rectangular wing	6
Upturned wing tips	7
Skewed flap positions	8
Canopy opening	9
Dorsal fins	10
Revised vertical tail	11

For all wings tested, the dihedral of the center
panel was 0° and of the outer panel 10°, measured at
the leading edge of the chord line.

The swept-back outer wing panel was formed by
pivoting the original outer wing panel about a line so
that the total wing area and incidence remained about
constant. The wing sections of the outer panels were
thus at an angle to the air stream for this condition.

The rectangular outboard wing panel is rectangular
from the break outward giving a larger total area. The
rectangular wing was formed by the rectangular outer

panel of figure 5 and a rectangular center section (figure 6). The rectangular wing has approximately the same area as the original wing.

The upturned wing tips replaced the original wing tips. The wing area and aspect ratio were increased; the modification was made in this manner to avoid cutting the aileron.

The sweep or skew of the outboard flap was changed by pivoting about the outboard fitting (fig. 8). Since the original flap fittings were used, the gap between the flap and the wing and the flap angles changed when the flap was skewed. The gaps obtained with the original fittings were quite large for the skewed positions, and it was felt that the lift would be reduced. Consequently, the gap was made smaller and most of the tests were run with the small gap.

The canopy opening, although not quite like that of the airplane, is believed to simulate the airplane aerodynamically.

The revised vertical tail had the same plan form and section as the original vertical tail. The rudder hinge line was moved back 0.86 inch on the model and the overhanging balance reduced to a minimum.

The power plant consisted of an induction motor, a dual-rotation gearbox, and the dual-rotating propeller.

TEST AND RESULTS

Test conditions.- The tests were made in the LMAL 7- by 10-foot tunnel at dynamic pressures of 9.21 pounds per square foot for power-on tests in the landing configuration and 16.37 pounds per square foot for all other tests, corresponding to airspeeds of about 60 and 80 miles per hour. The test Reynolds numbers were about 560,000 and 746,000 based on the wing mean aerodynamic chord of 12.26 inches. Because of the turbulence factor of 1.6 for the tunnel, effective Reynolds numbers were about 896,000 and 1,192,000.

Coefficients and symbols.- The results of the tests are presented in standard NACA coefficients of forces and moments. Rolling-, yawing-, and pitching-moment coefficients are given about the center-of-gravity location shown in figure 1 (22 percent of the mean aerodynamic chord of the original wing). The data are referred to a system of axes in which the Z axis is in the plane of symmetry and perpendicular to the relative wing; the X axis is in the plane of symmetry and perpendicular to the Z axis, and the Y axis is perpendicular to the plane of symmetry (fig. 12).

The coefficients and symbols are defined as follows:

C_L lift coefficient (Z/qS)

C_{D_R} resultant-drag coefficient (X/qS)

C_Y lateral-force coefficient (Y/qS)

C_l rolling-moment coefficient (L/qSb)

C_{l_p} damping in roll $\dfrac{\partial C_l}{\partial (pb/2V)}$

C_m pitching-moment coefficient (M/qSc)

C_n yawing-moment coefficient (N/qSb)

C_h hinge-moment coefficient $\left(H/qb\bar{c}^2\right)$

$T_c{}'$ effective thrust coefficient (T/qS)

V/nD propeller advance-diameter ratio

where the quantities are defined below and in figure 12

$\left.\begin{array}{l} X \\ Y \\ Z \end{array}\right\}$ forces along axes

$\left.\begin{array}{l} L \\ M \\ N \end{array}\right\}$ moments about axes

H hinge moment of a control surface

T   effective thrust

q   dynamic pressure $\left(\frac{1}{2}\rho V^2\right)$

S   wing area (6.34 square feet on model except for original center panel with rectangular outer panels which is 7.26 square feet and for the original wing with upturned wing tip which is 6.46 square feet. The coefficients for the up-turned wing-tip modification, however, are based on 6.34 square feet.)

c   wing mean aerodynamic chord (12.26 inches on model. This value of c is used as a basis for C_m for all wings even though original center panel with rectangular outer panel has larger actual mean aerodynamic chord.)

$\bar{c}$ root mean square chord of a control surface back of hinge line

b   wing span (6.25 feet on model. This value of b is used as a basis for C_n and C_l for all wings even though original wing with upturned wing tips has a span of 6.5 feet.)

b   with subscripts, span of control surface

V   air velocity

D   propeller diameter (1.813 feet on model)

n   revolutions per second

and

t   time, seconds

ρ mass density of air

α angle of attack of thrust line, degrees

ψ angle of yaw, degrees

β angle of sideslip, degrees; $\beta = -\psi$ in this report

ϕ angle of roll, degrees, measured from horizontal; positive when right wing is low

r   yawing velocity, degrees per second; positive when
          the nose is moving to the right

p   rolling velocity $\partial\phi/\partial t$, radians per second (except
          as noted); positive when the airplane is rotating
          clockwise when viewed from the rear

i_w angle of wing incidence with respect to thrust line,
          degrees; positive when the trailing edge is down

i_t angle of stabilizer with respect to thrust line,
          degrees; positive when trailing edge is down

δ control-surface deflection, degrees

β_F front-propeller-blade angle at 0.75 radius

β_R rear-propeller-blade angle at 0.75 radius

Γ_e effective dihedral angle, degrees $\left(C_{l_\psi}\right.$ divided
          by 0.0002, a good approximation but not strictly
          accurate for all plan forms$\big)$

Subscripts:

a   aileron (a_r, a_l right and left aileron)

e   elevator

r   rudder

f   flap

ψ denotes partial derivatives of a coefficient with
          respect to angle of yaw $\left(\text{example:}\ C_{l_\psi} = \dfrac{\partial C_l}{\partial\psi}\right)$

i   inboard

o   outboard

    Corrections.- All data have been corrected for tares
caused by the model support strut. Jet-boundary correc-
tions have been applied to the angles of attack, the drag
coefficients, and the tail-on pitching-moment coeffi-
cients. The corrections were computed as follows:

$$\Delta \alpha = 57.3 \delta_w \frac{S}{C} C_L \quad (\text{degrees})$$

$$\Delta C_D = \delta_w \frac{S}{C} C_L{}^2$$

$$\Delta C_m = -57.3 \left(\frac{\delta_T}{\sqrt{q_t/q}} - \delta_w \right) \frac{S}{C} \frac{\partial C_m}{\partial i_t} C_L$$

where

δ_w jet-boundary correction factor at the wing

δ_T total jet-boundary correction at the tail

S model wing area (6.34 sq ft)

C tunnel cross-sectional area (69.59 sq ft)

$\frac{\partial C_m}{\partial i_t}$ change in pitching-moment coefficient per degree change in stabilizer setting as determined in tests

q_t/q ratio of effective dynamic pressure over the horizontal tail to free-stream dynamic pressure

All jet-boundary corrections were added to the test data.

Test procedure.- Propeller calibrations were made by measuring the resultant drag of the clean model at 0° angle of attack for a series of propeller speeds. Thrust coefficients were determined from the relation

$$T_c{}' = C_D - C_{D_R}$$

where C_D is the drag coefficient of the model with propeller removed, and C_{D_R} is the resultant drag coefficient with propeller operating. The results of the calibration are presented in figure 13.

The thrust coefficient available at any lift coefficient is given on figure 14. These data were supplied by the Curtiss-Wright Corporation. Since constant power is

simulated, only one point on the curve will be for level flight for a given model configuration. Lower values of T_c' will be for the airplane descending and higher values will be for the airplane climbing. With the original center section and rectangular outer panels, the wing area was increased and the coefficients were based on the actual wing area. Since the relation between T_c' and C_L depends on the wing area and wing loading, certain assumptions about airplane weight had to be made. One possibility is to assume that the wing loading remained constant with the corresponding increase in airplane gross weight. Another possibility is that the airplane weight would remain constant with the corresponding reduction in wing loading. The case of constant airplane weight is called "power A" while the case of constant airplane wing loading is called "power B." The engine power is identical for the two cases.

Most of the results of this report are presented in two types of plots: first, the aerodynamic coefficients are plotted against yaw, and second, the lateral-stability derivatives are plotted against lift coefficient. Power-on yaw tests were made at a constant angle of attack and propeller speed. Since lift coefficient varies with yaw, the variation of T_c' versus C_L given on figure 14 is strictly followed only at zero yaw. Lateral-stability derivatives were obtained from pitch tests at -5° and 5° yaw by assuming a straight-line variation between those points. Propeller speed for these tests was varied to follow T_c' versus C_L given on figure 14 in the same manner as for the pitch tests at zero yaw given in reference 1. The large-symbol points on the plots of lateral-stability derivatives were obtained by measuring slopes from the yaw tests. The large-symbol points are considered more accurate than the small-symbol points at the specific lift coefficient.

In the text and on the figures, the model configuration is given as "cruising" or "landing." These conditions except as noted are described as follows:

(a) Cruising configuration:

All flaps retracted
Landing gear retracted
Cowl flaps closed
Slats retracted

(a) Cruising configuration (continued):

Propeller blade angles $\beta_F = 30\frac{1}{2}^{\circ}$, $\beta_R = 29\frac{1}{2}^{\circ}$,

for the original wing, and $\beta_F = 23\frac{1}{2}^{\circ}$,

$\beta_R = 22\frac{1}{2}^{\circ}$ for all other wing plan forms.
(This change in blade angle was found to have a negligible effect, reference 1.)

(b) Landing configuration:

Inboard flaps, $\delta_{f_i} = 50^{\circ}$

Outboard flaps, $\delta_{f_o} = 50^{\circ}$

Landing gear extended
Cowl flaps, 25°
Outboard slat extended (the 13-inch portion shown on fig. 1)
Propeller blade angles $\beta_F = 23\frac{1}{2}^{\circ}$, $\beta_R = 22\frac{1}{2}^{\circ}$

When not stated, the wing used will be the original wing. Since the original and revised vertical tail have identical plan forms and sections, the vertical tail is not always stated. When not given, the original dorsal fin was used. Stabilizer settings are given in the following table:

Wing	Cruising configuration (deg)	Landing configuration (deg)
Original	1.0	1.0
Swept-back	-2.9	-2.0
Rectangular outer panels	-1.2	-1.7
Rectangular	-3.2	-2.3

No attempt was made to have the same stabilizer setting because stabilizer settings were set for the longitudinal-stability tests. The differences in stabilizer setting is not believed to affect the lateral-stability characteristics, because of the system of axes used in presenting the data.

Computation of aileron and rudder control forces.-
Aileron control forces were computed from the following
formula:

$$F_a = \frac{142.4\left(C_{h_{a_l}} - C_{h_{a_r}}\right)}{C_L}$$

which is based on the following information supplied by
the Curtiss-Wright Corporation:

    Wing loading, W/S = 39.4 pounds per square foot
    Total aileron movement, 30^0
    Total stick movement, 41.7^0
    Stick length, 29 inches to center of hand grip

The wing-tip helix angle was computed as follows:

$$\frac{pb}{2V} = 0.8 \frac{C_l}{C_{l_p}}$$

where p is the rolling velocity in radians per second;
C_{l_p} is the damping in roll (0.408) obtained from refer-
ence 2. The factor of 0.8 is an arbitrary value which
approximates the reduction in rolling velocity due pri-
marily to adverse yaw at low speeds and wing twist at
high speeds determined from a number of flight tests of
conventional airplanes. For the tests a wire 0.007 inch
in diameter was fixed at 10 percent of the wing chord
on the upper surface in an attempt to simulate full-scale
transition conditions more closely.

    Rudder-pedal forces were computed from the following
formula:

$$F_r = K \frac{C_{h_r}}{C_L}$$

where K = 2324 for the original tail and K = 1193
for the revised tail which is based on the following
information supplied by the Curtiss-Wright Corporation:

    Wing loading, W/S = 39.4 pounds per square foot
    Total rudder movement, 60^0
    Total pedal movement, 30.64^0
    Radius of pedal about center of rotation,
        12 inches

A refinement was made in the calculations for the revised vertical tail by including a correction for strain-gage deflection. Calibration of this deflection gave a value of $\frac{\Delta\delta_r}{C_{h_r}} = -7.32$ for the windmilling condition (q = 16.37) and a $\frac{\Delta\delta_r}{C_{h_r}} = -4.12$ for the take-off power condition (q = 9.21). The result was subtracted from the nominal rudder angle to get the corrected rudder angle. The maximum correction was about 3°. This correction has been made to plots of δ_r against ψ or C_n but not to the data giving C_n against ψ because the correction would vary with ψ for the latter case. The strain gage for the aileron and original tail was much more rigid so that deflection was negligible.

DISCUSSION

Effect of wing plan form and power. (a) Small angles of yaw.- Figure 15 compares C_{Y_ψ}, C_{n_ψ}, and C_{l_ψ} of various wing plan forms for the range of power and flap conditions. The variation of C_{n_ψ} and C_{Y_ψ} is much greater with flight conditions than with wing plan form. C_{n_ψ} varies from a maximum of about -0.0040 for the landing configuration with take-off power to a minimum of -0.0005 for the cruising configuration with propeller windmilling. C_{Y_ψ} varies from about 0.040 for the landing configuration with take-off power to about 0.008 for the cruising configuration with propeller windmilling. C_{l_ψ} varies considerably with both plan form and power. The variation is illustrated in table I. Effective dihedral is $8\frac{1}{2}^\circ$ to $11\frac{1}{2}^\circ$ $\left(C_{l_\psi} = 0.0002 \text{ is }\right.$ equivalent to 1° effective dihedral$\left.\right)$ in the cruising or dive condition. These values may be too large for desirable flying qualities. The original wing loses effective dihedral with increase in lift coefficient and flap deflection whereas the other wing plan forms gain in effective dihedral. All the wings lose effective

dihedral when power is applied. Since the effective
dihedral in any given flight condition may be changed by
changing the geometric dihedral, the relative merit of
the various plan forms can probably best be judged by
the bottom line of the table. This line gives the change
in effective dihedral from the dive or cruising condi-
tion to the most adverse condition, landing configuration
with a take-off power at a high C_L. A small or zero
change in effective dihedral is desirable. The least
change occurs with the rectangular wing, $-6\frac{1}{2}^{\circ}$, and the
greatest change occurs with the original wing, $-21\frac{1}{2}^{\circ}$,
with the swept-back and rectangular outer panels lying
in between $-9\frac{1}{2}^{\circ}$, -10°. The effective dihedral of the
model with the swept-back outer panels decreases sharply
near maximum lift (fig. 15(a)). This fact indicates
that the leading wing tip is probably stalling first.
There is a large variation in stalling characteristics
of the different wing plan forms, but this subject has
been discussed in reference 1.

The increment in the lateral-stability derivatives
caused by power have been isolated on figure 16 by sub-
tracting the windmilling values of figures 15(a) and
15(c) from the power-on values of figures 15(b) and 15(d).
The subtraction for figure 16(a) was performed with
values taken at the same angle of attack while the sub-
traction for figure 16(b) was performed with values taken
at the same lift coefficient. Since the results on
figure 16 represent fairly small differences of large
values, most of the scatter between various wing plan
forms may be considered to be experimental error.

The increase in C_{Y_ψ} with power can be primarily
explained as follows: A yawed propeller produces a con-
siderable side force. The magnitude of this side force
increases markedly with T_c', and hence with C_L for
the power-on condition. The lateral force produced by
the vertical tail increases with T_c' because of the
greater dynamic pressure ratio in the slipstream as T_c'
is increased. The lateral force of the fuselage probably
also increases with T_c' as a result of being in the
slipstream. Opposed to the increase in C_{Y_ψ} with T_c'

is the fact that sidewash resulting from propeller operation decreases the angle of attack of the vertical tail and fuselage.

Directional stability also increases with C_L when power is on. This fact indicates that the increased vertical-tail load due to the slipstream times its moment arm about the center of gravity produces the largest yawing moments. The increase of the propeller side force times its moment arm and the change in fuselage moment are the lesser effects.

The variation in C_{l_ψ} with plan form and flap deflection is illustrated in reference 3. The reason for the loss in effective dihedral with increase in T_c' can be primarily explained as follows: When an airplane is yawed, the slipstream tends to follow the relative wind lying somewhere between the longitudinal axis and the wind axis. The trailing side of the wing receives more slipstream than the leading side, thus causing a greater increase in lift on the trailing side than on the leading side. This effect is destabilizing since it is opposite to the rolling moment produced by positive dihedral.

The increase in C_L due to the propeller force and the slipstream over the wing is shown in figure 16(a). The value of ΔC_{l_ψ} on figure 16 varies considerably with change of wing. Since the rectangular wing has the least area in the slipstream, reduction in effective dihedral due to power may be expected to be smallest for this case which is borne out to a large extent by the results. As all the other wings had the same center section, the difference shown between them is largely unexplained. Some of the difference may be attributed to the difference in span-load distribution across the center section with the various outboard panels.

(b) Large angles of yaw.- In addition to giving slopes shown by the large symbols in previous figures, figures 17 and 18 show the effect of large angles of yaw on the aerodynamic characteristics. Characteristics of the model in yaw with tail off are shown in figure 19 and 20. Where the power effect is small (the windmilling condition and the low lift-coefficient condition with take-off power) C_{Y_ψ} and C_{n_ψ} with tail on continue

to large angles of yaw with little change. C_{l_ψ} reduces
markedly at large angles of yaw. Since C_l never reverses
sign at large angles of yaw, the change in slope is
believed to be of little importance. Displacement of
the C_m curves, one from another, is caused chiefly
by the different stabilizer settings and wing mean aero-
dynamic chord positions. C_{D_R} decreases with angle of
yaw as a result of the system of axis used. While C_{D_R}
along the axis used reduces with yaw, C_{D_R} along the
wind axis actually increases with yaw as would be expected.
C_L does not change much with yaw. When the power effect
is large (take-off power at a high C_L), the same trends
are shown except as follows: With tail on C_{n_ψ} decreases
considerably with yaw in the cruising configuration
(fig. 17(d)) and changes sharply for the landing configu-
ration, becoming quite highly positive beyond -20° of
yaw (fig. 18(b)). This sharp change in C_{n_ψ} probably
occurs when the tail leaves the slipstream. With tail
off and power on, C_{n_ψ} is highly positive (fig. 20(b))
but becomes highly negative at small yaw angles when the
tail is added (fig. 18(b)) indicating a large effect of
the tail when in the slipstream. When the tail leaves
the slipstream, its effectiveness decreases considerably
so that the high positive C_{n_ψ} of the tail-off curve
predominates.

(Although believed to have only a small effect on
the results, the following information is given for com-
pleteness. On figures 17 and 18 the original dorsal fin
was used with the original wing and dorsal D_I was used
for all other plan forms. On figures 17, 18, 19, and 20
the leading-edge slot was open to the fold line for the
original wing, but only the outboard portion (13 inches
on model) was open for the other plan forms.)

Effect of upturned wing tips.- The variation of the
lateral-stability derivatives with C_L is shown on fig-
ure 21. The dates (7-30-43 and 9-27-43) are the dates
of testing. There are only slight changes in C_{Y_ψ} and
C_{n_ψ} with take-off power due to the upturned wing tips;
however, the upturned wing tips cause a considerably
less stable C_{n_ψ} with windmilling power. Although there

is poor agreement between C_{l_ψ} obtained from pitch tests made at $\pm 5^\circ$ yaw and yaw tests (indicated by the large symbols), the increment in effective dihedral caused by the upturned wing tips for propeller windmilling is about 2.6° effective dihedral. For take-off power, however, even the increment is in poor agreement. The curves compared on figure 21 were obtained from data taken about 2 months apart with several model changes being made in the meantime; therefore, the data indicated by the large diamond and square of the same date are considered much more accurate. These points were obtained from figure 22 and indicate an increase of about $3\frac{1}{2}^\circ$ in effective dihedral due to upturned wing tips with take-off power. It may be concluded that, for the landing configuration, the upturned wing tips may be expected to increase the effective dihedral about $2\frac{1}{2}^\circ$ for the windmilling condition $(C_L \approx 1.6)$ and about $3\frac{1}{2}^\circ$ to 5° for the take-off power condition $(C_L \approx 2.7)$.

Effect of outboard flap modification.- The effect of skewing the outboard flap and removing the outboard flap is shown in figures 23, 24, and 25. As a convenience in testing, some of the tests were made with the tail and some without.

Table II has been prepared to correlate and summarize the effective dihedral results. The values of Γ_e are obtained from slopes measured from figures 23 and 24. The values of Γ_e with the asterisk (*) were obtained by adding or subtracting the contribution of the tail which was found by comparing figures 18 and 20 to be about 1° of Γ_e for the windmilling condition and 4° of Γ_e for the take-off power conditions at the angles of attack corresponding to the yaw tests. Skewing the flap from the original position of -14.5° to 0.7° gives a considerable improvement in effective dihedral while further skew to 11.3° gave no further improvement. Removing the flap entirely gave the most improvement; however, these modifications reduce $C_{L_{max}}$ as reported in reference 1. Figure 25 shows that skewing the outboard flap reduces the variation of effective dihedral with C_L similar to effect of sweeping the outboard wing panel back as previously discussed. Adding the tail to the case of $\Lambda_{f_o} = 0.7$ with take-off power would raise the

curve about 4° effective dihedral at the higher lift coefficients. Figure 23 shows that there is no measurable effect of changing the flap gap. Opening the slats increased the effective dihedral about 3.4° (fig. 24 and table II).

Effect of canopy opening.- Opening the canopy is shown to have no measurable effect on the variation of C_n with ψ between $\pm 10^\circ$ ψ (fig. 26). The difference in C_n at $\pm 15^\circ$ is not believed to indicate any dangerous tendency.

Aileron control.- The results of the tests of the left aileron are shown in figure 27. A transition wire 0.007 inch in diameter was placed on the upper surface of the wing at the 10-percent-chord station in an attempt to duplicate full-scale transition conditions more closely. The variation of wing-tip helix angle $pb/2V$ with stick force was computed for figure 28(a) for both ailerons. The results are reduced by multiplying by 0.8 to approximate the reduction in $pb/2V$ due primarily to adverse yaw and wing twist as previously mentioned. To check the validity of the 0.8 factor at a low speed with flaps down where adverse yaw is greatest, a theoretical time history of the motion following an abrupt full aileron deflection ($\pm 15^\circ$) was computed using a refinement of the step-by-step computation given in reference 4. The refinement was to use the slopes at the angle of sideslip under consideration instead of a single value of slope measured at zero sideslip. The results of the computation are given in figure 28(b). The model with the swept-back outer wing panels was chosen for the computation, because of the closer simulation of the airplane. The speed chosen was 94.4 miles per hour which is 120 percent of the minimum speed. The maximum $pb/2V$ at about 1 second is 0.082. To obtain 0.082, C_l/C_{l_p} would have to be multiplied by

0.86 instead of the usual factor of 0.8. The average $pb/2V$ for a 90° bank, where sideslip reaches a maximum, is only 0.067. To obtain 0.067, C_l/C_{l_p} would have to be multiplied by 0.70 instead of 0.8. As the speed increases this factor for a 90° bank would increase until at high speed the factor would be reduced by wing twist.

The Navy requirement F-8 and F-9 of reference 5 states in brief that a $pb/2V$ of 0.08 is required at

any speed between 140 percent of stalling speed and
80 percent of maximum speed with a control force not
exceeding 30 pounds. As shown, the average effective-
ness is too low at 140 percent of minimum speed, although
the maximum rate of roll meets the requirement (fig. 28(b)),
in the landing configuration and the control force is too
high at 80 percent of maximum speed. The ailerons meet
the requirement at the cruising speed of 220 miles per
hour.

Rudder-free characteristics.- Preliminary tests
showed that a reversal of yawing moment would occur, and
hence a reversal of rudder force, for the cruising con-
figuration with take-off power at a high α (fig. 29(a))
and for the landing configuration with windmilling or
take-off power (figs. 29(b) and 29(c)). While the reversal
occurs earlier for the windmilling condition, it was more
severe for the take-off power condition. Most of the
dorsal fins were therefore tested in the landing configu-
ration with take-off power. The addition of the dorsal
fins delays the reversal of yawing moments about as fol-
lows: original dorsal, 3°; dorsal D_1, 9°; dorsal D_2, $14\frac{1}{2}^\circ$.
These values can be obtained from figure 29(c) by the
proper addition and subtraction.

It was thought that a revised vertical tail of the
same plan form and area having a smaller chord rudder
might prove better because when the tail stalls a smaller
portion of the area would be deflected so that a greater
restoring moment in yaw would result. Because of the
dual-rotating propeller, the directional control supplied
by a smaller chord rudder should be sufficient. For the
windmilling condition, the revised vertical tail alone
eliminated the reversal of yawing moments (fig. 29(b)).
For the landing configuration with take-off power, the
revised vertical tail delays the reversal of yawing
moments about $5\frac{1}{2}^\circ$ ψ beyond that for the original tail
when results with the same dorsal fin are compared
(fig. 29(c)).

Rudder tests.- The test data of the original tail
are shown in figure 30 and the revised tail in figures 31,
32, and 33. Certain flying qualities computed from these
figures are presented on figures 34, 35, 36, and 37. The
rudder-free figure (fig. 29(b)) was also used to help
determine where rudder-force reversal occurred on the
original tail for figure 35.

The take-off power rudder calculations were made for a $C_L = 1.74$, although the take-off power rudder test data were taken at a $C_L = 2.77$ (fig. 33). T_c' was therefore higher for the test than it would be for the flight conditions computed. The calculations were made in this manner so that a better comparison could be made with the windmilling condition at 1.2 times the power-off minimum speed. For the take-off power results on figures 35 and 37, an interpolation was made between the windmilling condition (fig. 32) and the take-off power condition given on figure 33 for the T_c' difference.

In the cruising configuration, the revised tail could hold $11\frac{1}{2}°$ of sideslip; however, at high speed this value of sideslip would be reduced considerably because of high pedal forces (fig. 34). In the landing configuration, the revised tail can hold $10°$ of sideslip for windmilling power and $12°$ for take-off power at 94.4 miles per hour, which is about 1.2 times the minimum speed. For a maximum pedal force of 180 pounds as specified in reference 5, only $8\frac{1}{2}°$ of sideslip could be held with take-off power. The original tail holds $24°$ of sideslip or 2.4 times the value for the revised tail; however, a rudder-force reversal occurs at $16°$ sideslip which violates requirement E-3 of reference 5. The revised tail could be improved by increasing the overhanging balance. The original tail could be improved by increasing the dorsal-fin size and possibly reducing the deflection range.

Since there are no asymmetric yawing moments to trim with the dual-rotating propeller, the most severe requirement for the rudder is probably for neutralizing the adverse yaw of the ailerons. Rudder control for spin recovery may be the most severe rudder requirement. Spin-recovery tests are to be made in the NACA spin tunnel. The maximum adverse yaw of the ailerons was determined by adding the test C_n for the ailerons as given on figure 27 to the C_n due to rolling computed from the method given in reference 6. These estimates were placed on figures 36 and 37. Either vertical tail can easily neutralize the aileron adverse yawing moment.

CONCLUSIONS

The following conclusions may be drawn as to the lateral stability and control of the XBTC-2 airplane.

1. Wing plan form had a pronounced effect on the variation of effective dihedral with lift coefficient and flap deflection. Wing plan form had little effect on directional stability or lateral force.

2. The application of power, particularly at high lift coefficients, decreased the effective dihedral but increased the directional stability and lateral force.

3. With the upturned wing tips for the windmilling condition ($C_L \approx 1.6$), the effective dihedral was increased about $2\frac{1}{2}^\circ$, and with take-off power ($C_L \approx 2.7$), about $3\frac{1}{2}^\circ$ to 5°.

4. For the landing configuration, giving sweepback to the outboard flap or removing the outboard flap reduced the change in effective dihedral with lift coefficient but reduced the maximum lift coefficient obtainable.

5. Aileron effectiveness was marginal for the landing configuration and aileron control force was too high at high speed.

6. The rudder-force reversal was improved considerably by increasing the dorsal-fin size and also by reducing the rudder chord while maintaining the same vertical-tail area.

7. Aileron yawing moments, the only asymmetric yawing moments occurring in normal flight with a dual-rotating propeller, were easily neutralized by the rudder.

8. Rudder control for spin recovery may be the most severe rudder requirement. It is recommended that the narrow-chord rudder be checked for spin recovery as well as the larger rudder.

REFERENCES

1. Weil, Joseph, and Wells, Evalyn G.: Wind-Tunnel Tests of the 1/8-Scale Powered Model of the Curtiss XBTC-2 Airplane. I - Preliminary Investigation of Longitudinal Stability. NACA MR, June 1, 1944.

2. Swanson, Robert S., and Toll, Thomas A.: Estimation of Stick Forces from Wind-Tunnel Aileron Data. NACA ARR No. 3J29, 1943.

3. Betz, A.: Applied Airfoil Theory. Unsymmetrical and Non-Steady Types of Motion. Vol. IV of Aerodynamic Theory, div. J, ch. IV, sec. 4, W. F. Durand, ed., Julius Springer (Berlin), 1935, pp. 102-107.

4. Weick, Fred E., and Jones, Robert T.: The Effect of Lateral Controls in Producing Motion of an Airplane as Computed from Wind-Tunnel Data. NACA Rep. No. 570, 1936.

5. Anon.: Specification for Stability and Control Characteristics of Airplanes. SR-119, Bur. Aero., Oct. 1, 1942.

6. Pearson, Henry A., and Jones, Robert T.: Theoretical Stability and Control Characteristics of Wings with Various Amounts of Taper and Twist. NACA Rep. No. 635, 1938.

TABLE I.- EFFECT OF WING PLAN FORM ON EFFECTIVE DIHEDRAL

	Flight condition	Original (deg)	Swept back (deg)	Rectangular outer panels (deg)	Rectangular (deg)
1	Cruising configuration windmilling or power on, low C_L	$8\frac{1}{2}$	$9\frac{1}{2}$	10	$11\frac{1}{2}$
2	Landing configuration windmilling, high C_L	4	12	$14\frac{1}{2}$	17
3	Landing configuration take-off power, high C_L	-13	0	0	5
4	3 - 1	$-21\frac{1}{2}$	$-9\frac{1}{2}$	-10	$-6\frac{1}{2}$

NOTE: Table made from large symbols on figure 15.

NATIONAL ADVISORY
COMMITTEE FOR AERONAUTICS

TABLE II.- EFFECT OF OUTBOARD FLAP MODIFICATION

ON EFFECTIVE DIHEDRAL

[Original plan form, landing configuration]

Outboard flap condition	Power	C_L	α (deg)	Γ_e tail on (deg)	Γ_e tail off (deg)
$\Lambda_{f_o} = -14.5^o$ (original)	Windmilling	1.67	9.2	4	3[a]
$\Lambda_{f_o} = 0.7^o$ (both gaps)	----do-----	1.53	9.2	8.3[a]	7.3
$\Lambda_{f_o} = 11.3^o$	----do-----	1.41	9.1	8.3[a]	7.3
Flap up	----do-----	1.26	8.9	11.5[a]	10.5
$\Lambda_{f_o} = -14.5^o$ (original)	Take-off	2.85	10.6	-13	-17[a]
$\Lambda_{f_o} = 0.7^o$ (small gaps)	----do-----	2.57	10.4	-6[a]	-10
Flap up	----do-----	2.20	10.5	-4.6	-8.6[a]
Flap up (L.E. slot closed)	----do-----	2.22	10.5	-8.0	-12.0[a]

[a]Estimated from average effects of tail on Γ_e.

NOTE: For the cruising configuration with tail on at a
       low C_L, $\Gamma_e = 8.5^o$, power on or windmilling.

NATIONAL ADVISORY
COMMITTEE FOR AERONAUTICS

OUTLINE OF FIGURES ON $\frac{1}{8}$-SCALE MODEL OF XBTC-2 AIRPLANE

OUTLINE OF FIGURES - Continued

ROOT SECTION NACA 23014.7 (Approx) $i_w = 1.5°$
BREAK SECTION NACA 23016 $i_w - 1.5°$
THEO. TIP SECTION NACA 23008 $i_w = -0.8°$
WING AREA 6.34 SQ.FT, MAC 12.26 IN.
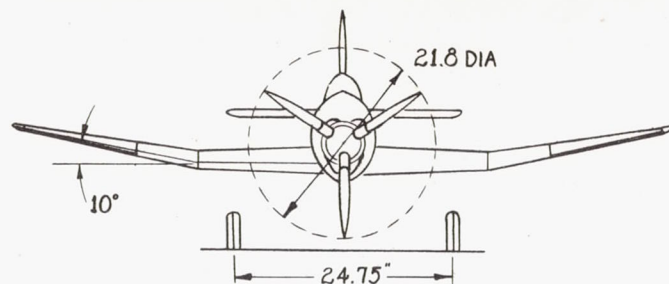
NATIONAL ADVISORY
COMMITTEE FOR AERONAUTICS
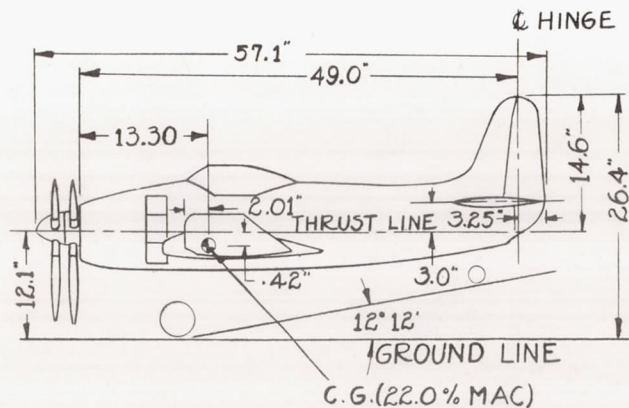
FIGURE /(a).-THREE-VIEW DRAWING OF ⅛-SCALE MODEL OF THE CURTISS XBTC-2 AIRPLANE.
(ORIGINAL MODEL)
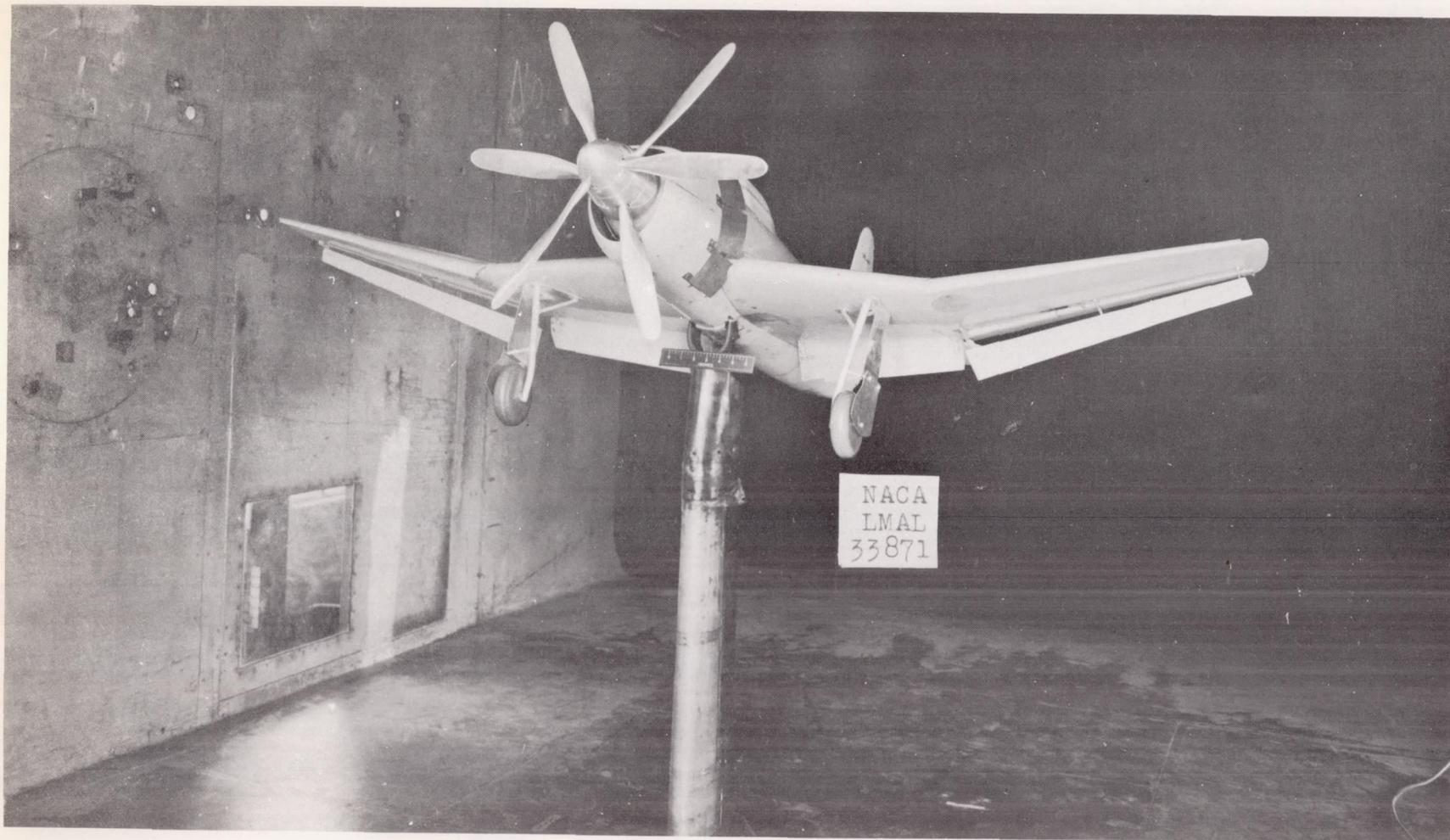
Figure 1(b).- The $\frac{1}{8}$-scale model of the XBTC-2 airplane in the LMAL 7- by 10-foot tunnel.
Landing configuration.
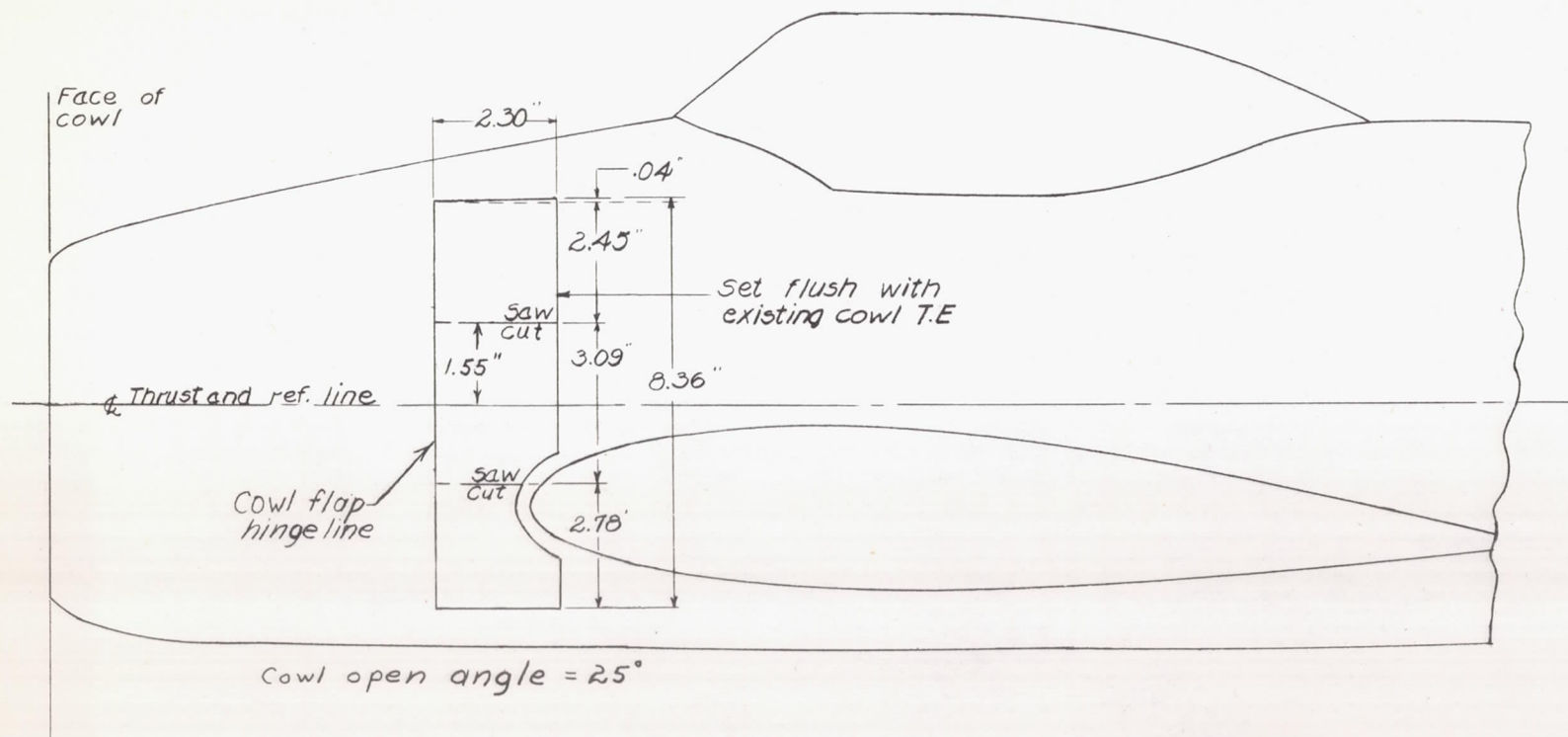
Figure 2 .- Side view of 1/8-scale model of XBTC-2 airplane showing cowl flap details.

16.44"   37.56"

3.22

¢ Airplane

5.93"

12.24"

20.31"

¢ AILERON BALANCE
¢ AILERON HINGE
20.20"

$$C_{h_a} = \frac{H_a}{q\, b_a\, \overline{c_a}^{\,2}}$$

$b_a = 20.2$ in on model
$\overline{c}_a = 1.425$ in on model

.54c_a
.40c_a
$c_a = .15c$

SEAL ¢

50°

INBOARD SECTION

.54c_a
.22c_a
$c_a = .15c$

SEAL ¢

50°

OUTBOARD SECTION
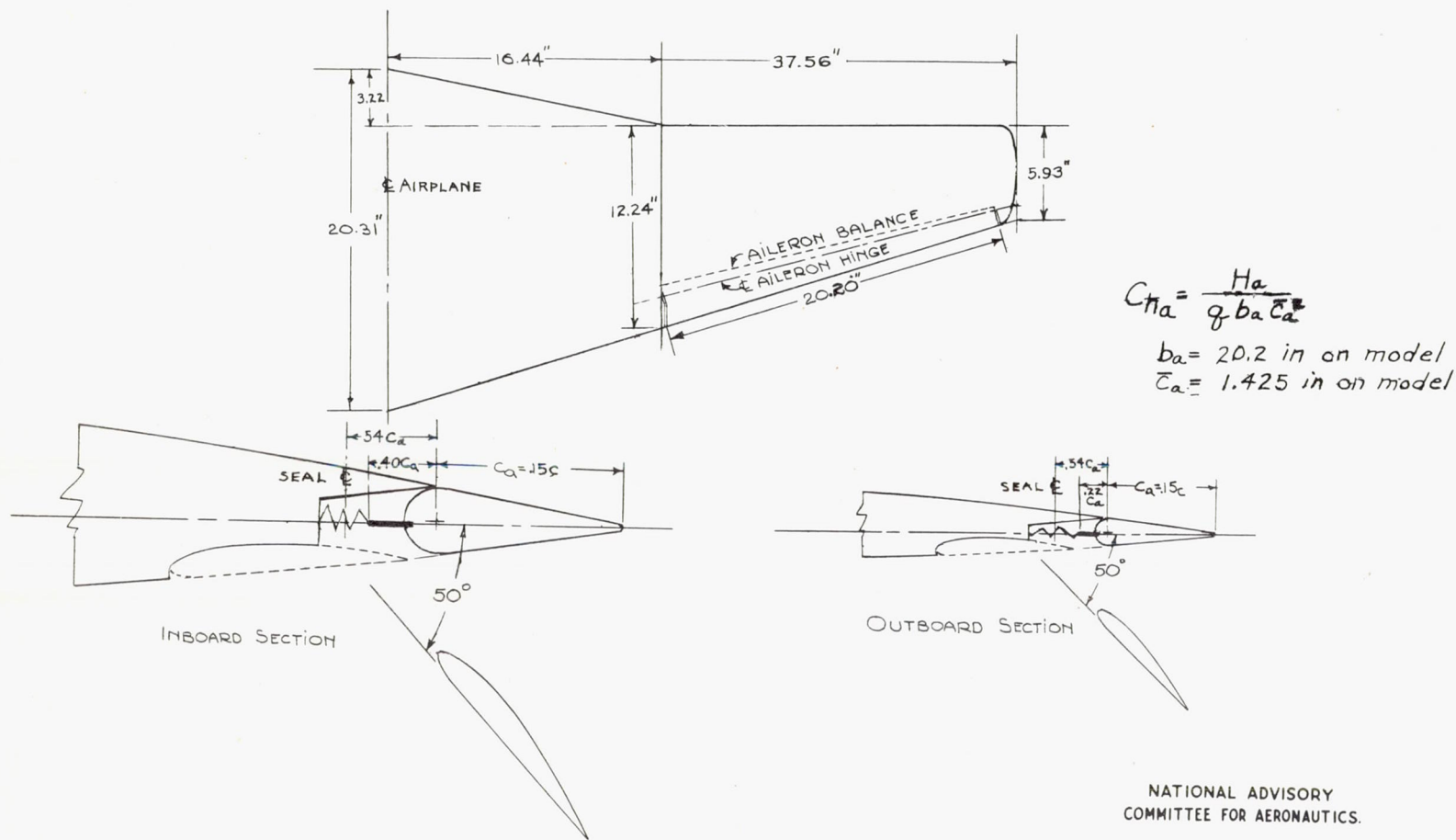
Figure 3.—Diagram showing aileron of XBTC-2 model tested with flaps neutral and flaps extended.
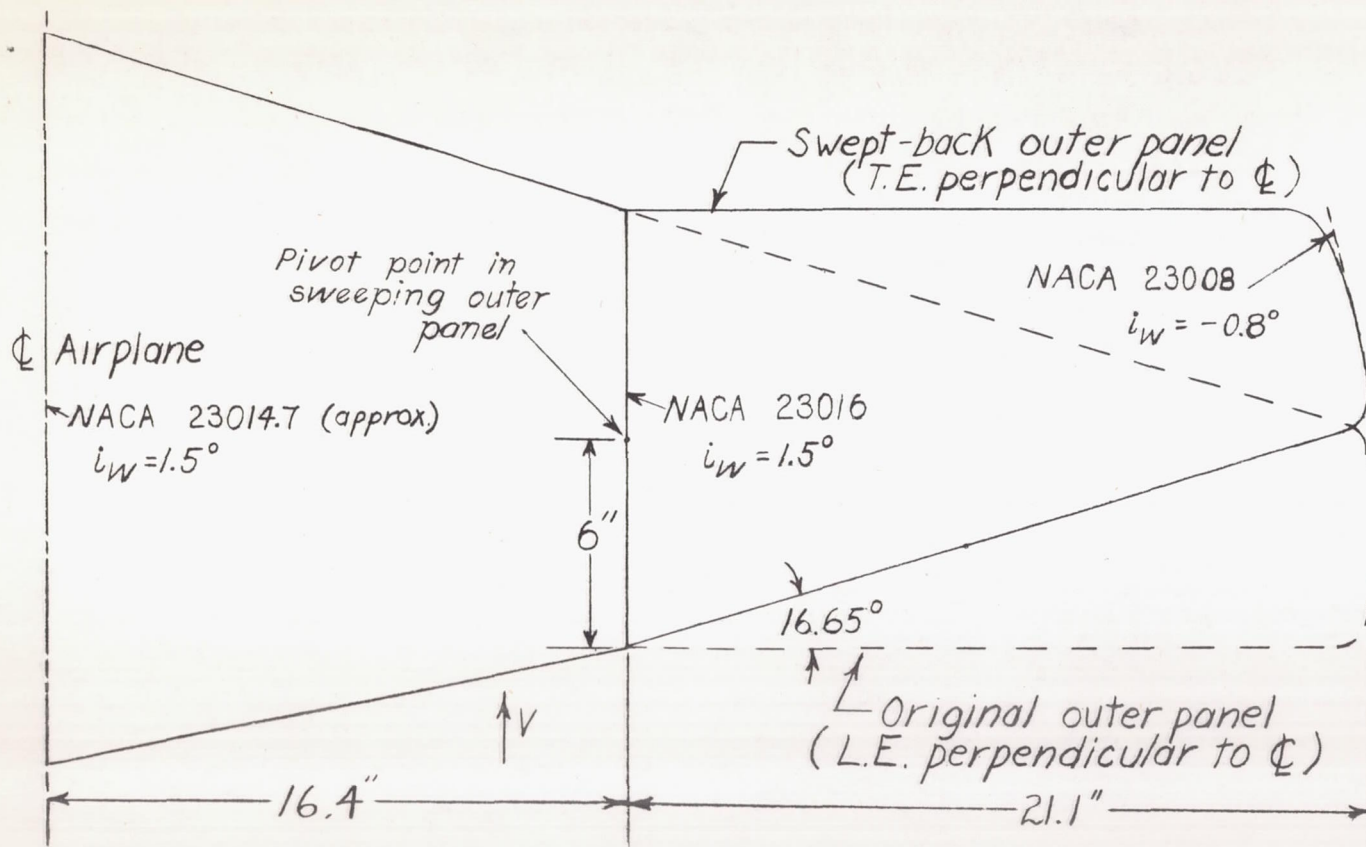
Figure 4.-Left wing panel of 1/8-scale model of XBTC-2 airplane showing swept-back outer panel modification.

Rectangular outer panel

Original outer panel

¢ Airplane

NACA 23014.7 (approx)
$i_w = 1.5°$

NACA 23016
$i_w = 1.5°$

NACA 23009
$i_w = -0.4°$

↑V

16.4"

21.1"
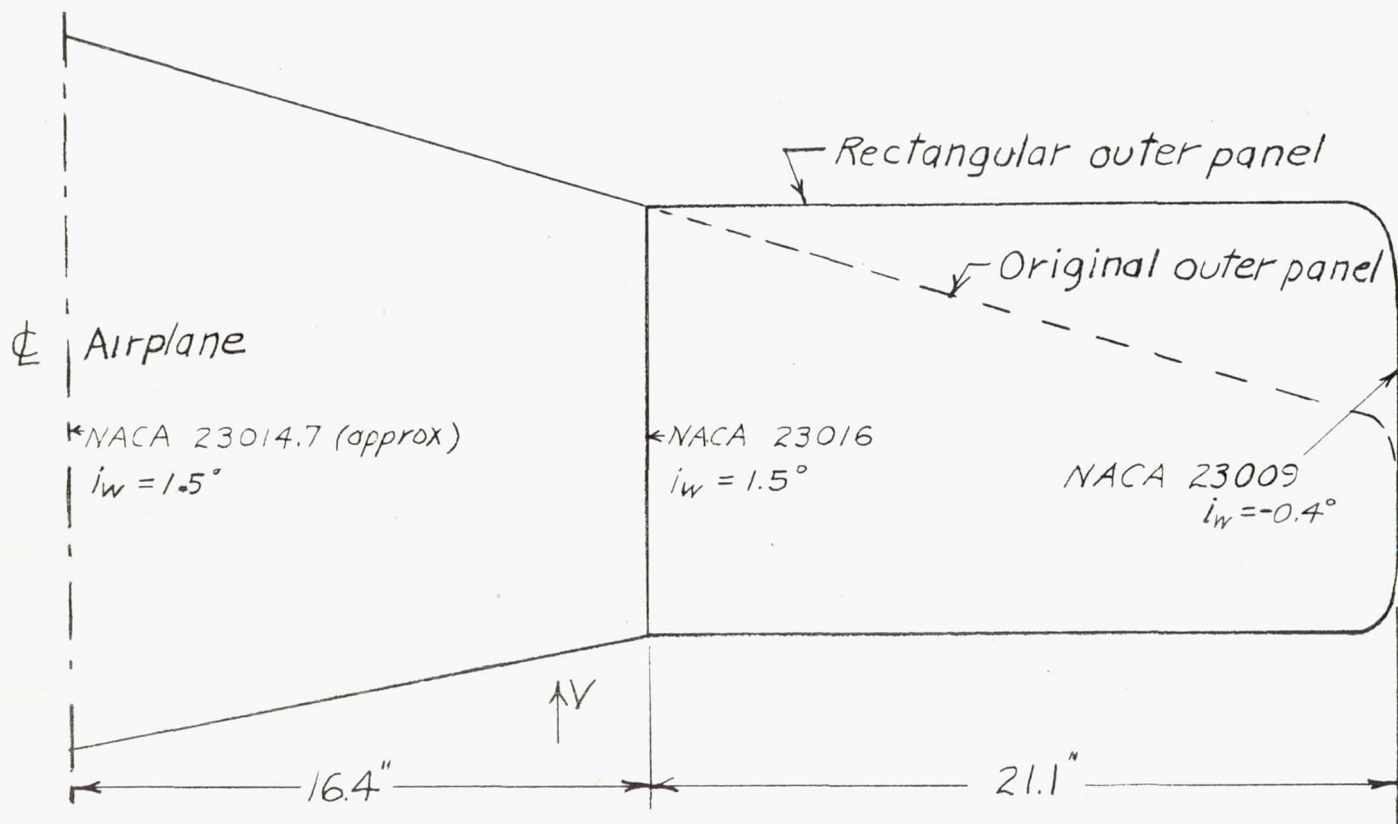
Total original wing area   6.34 sq ft
Total wing area (Rect. outer panels)   7.26 sq ft

NATIONAL ADVISORY
COMMITTEE FOR AERONAUTICS

Figure 5(a).Left wing panel of 1/8-scale model of XBTC-2 airplane showing rectangular outer panel modification.
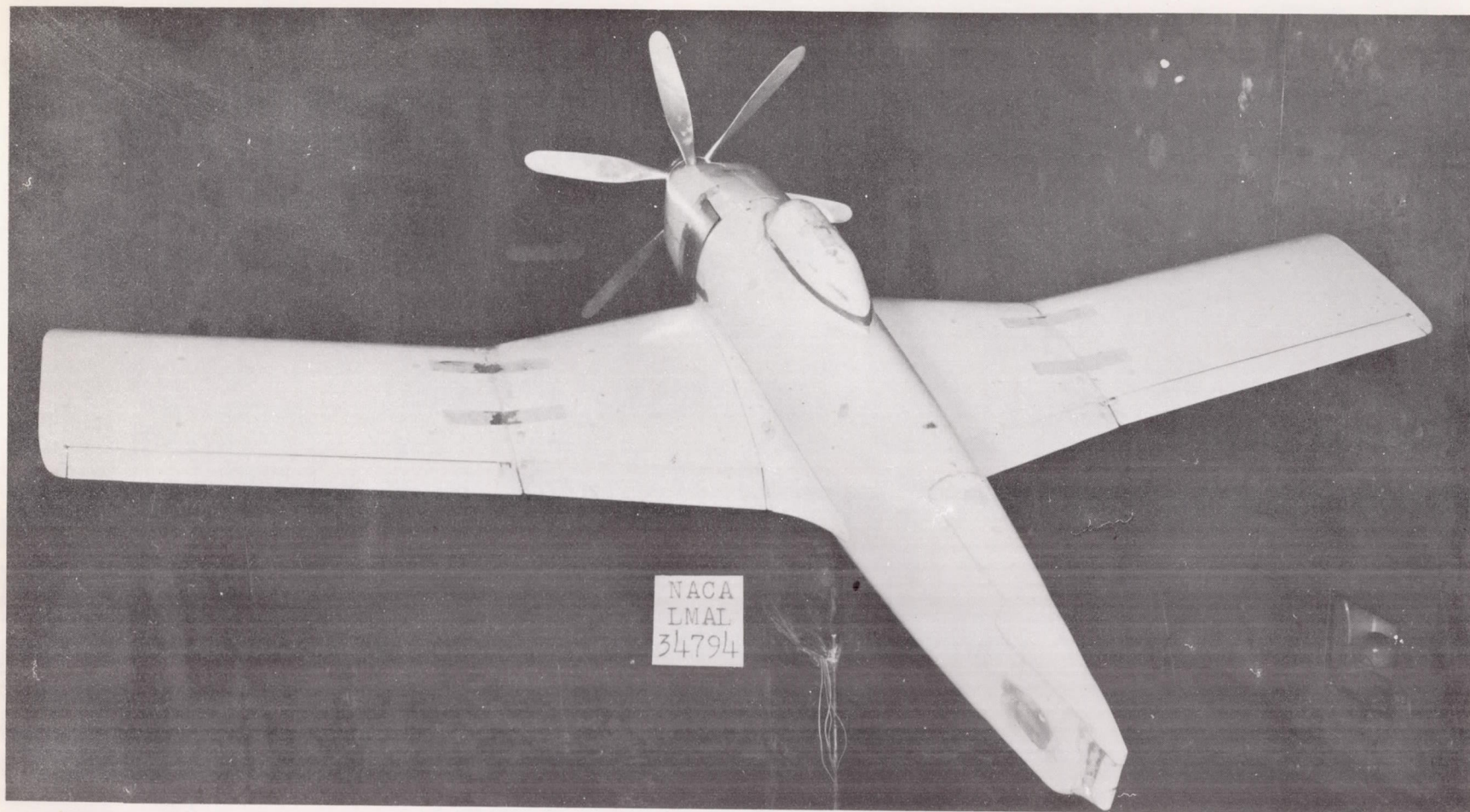
Figure 5(b).- The $\frac{1}{8}$-scale model of the XBTC-2 airplane with rectangular outer wing panels. Cruising configuration. Tail off.
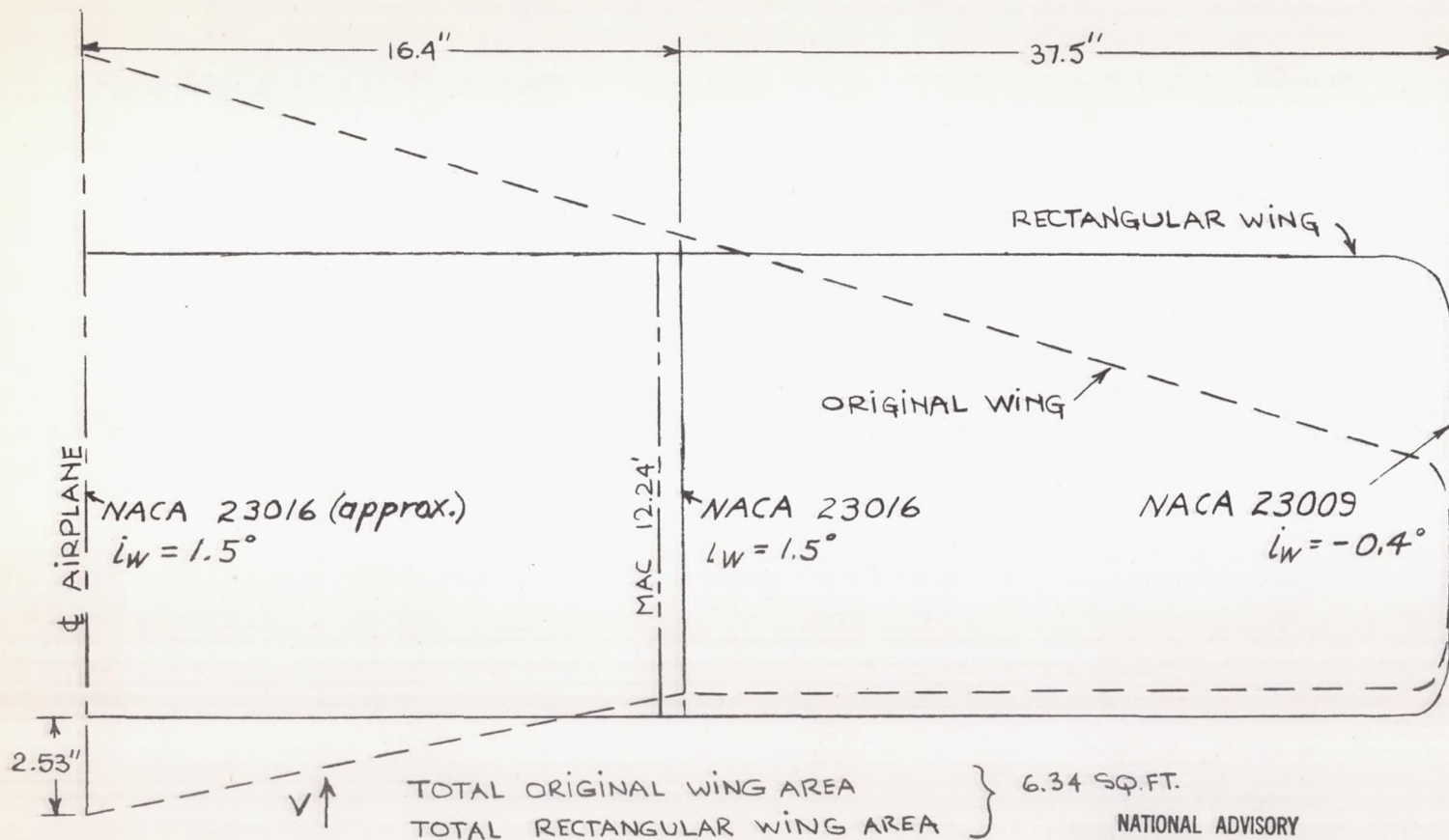
Figure 6.— Left wing panel of ⅛-scale model of
XBTC-2 airplane with rectangular planform.
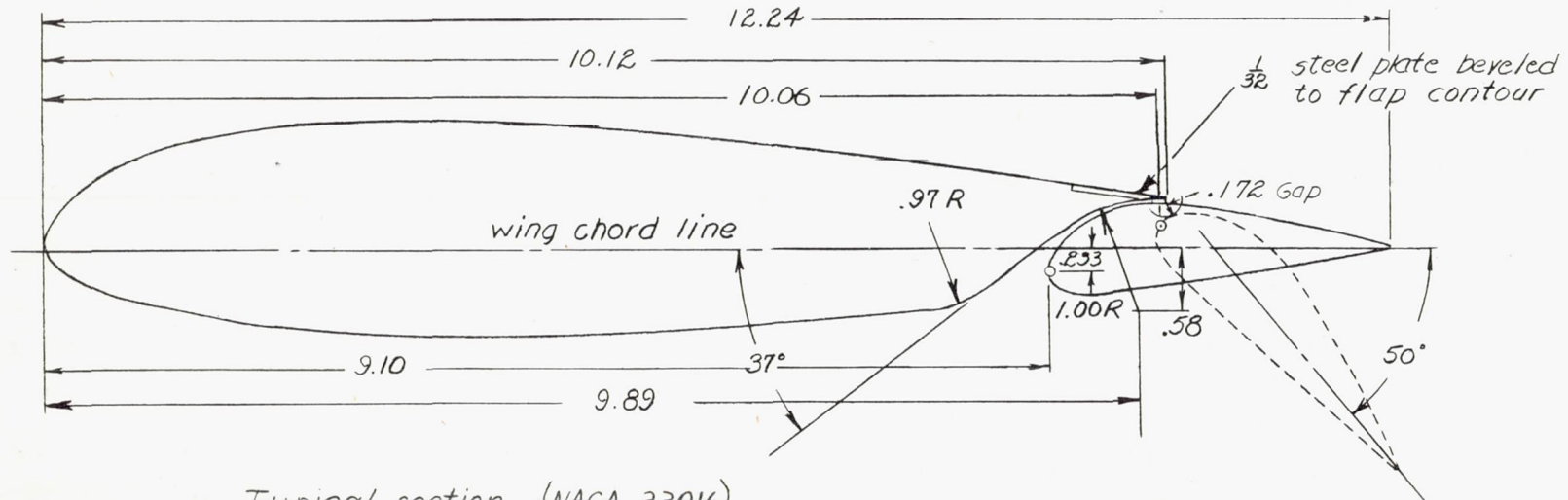
Typical section : (NACA 23016)

wing chord line

12.24
10.12
10.06
9.10
9.89

.97 R
37°
.233
1.00R
.58
.172 Gap
50°
1/32 steel plate beveled to flap contour

Flap nose section

x .233" .177R y_u wing chord y_L

All dimensions in inches
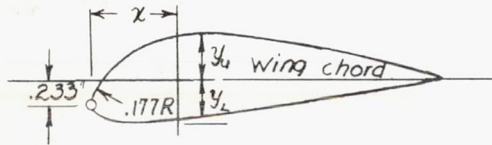
x	.049	.094	.167	.244	.323	.480	.636	.693	.793	.949	1.105	1.261
y_u	-.073	-.014	.081	.154	.212	.300	.359	—	.401	.417	.409	.388
y_L	.360	.387	.409	.421	.421	—	—	.376	—	—	—	—

Figure 6(b)- Details of slotted flap for 1/8-scale model of the XBTC-2 airplane. Rectangular wing.
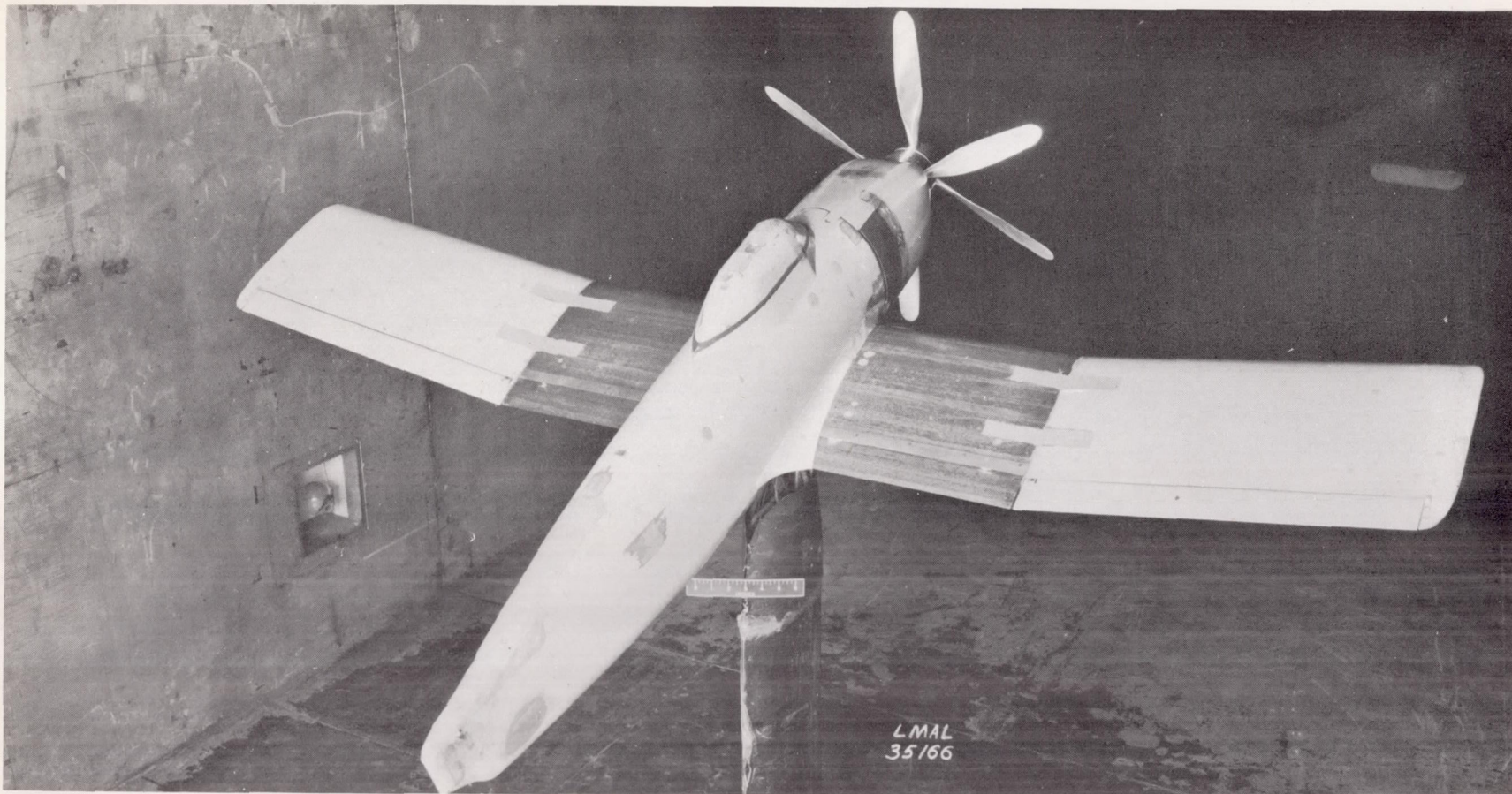
Figure 6(c).- The $\frac{1}{8}$-scale model of the XBTC-2 airplane with rectangular wing.   Cruising configuration.   Take-off.

Ȼ airplane

Upturned tip
faired like
original

Original
Tip

Leading Edge

$\frac{3}{4}$" $1\frac{1}{2}$"

L.E.

$37\frac{1}{2}$"

L.E

35°

L.E.

10°

Total wing area 6.46 ft²
(Coefficients based on original
area of 6.34 ft² and original
span of 6.25 ft.)
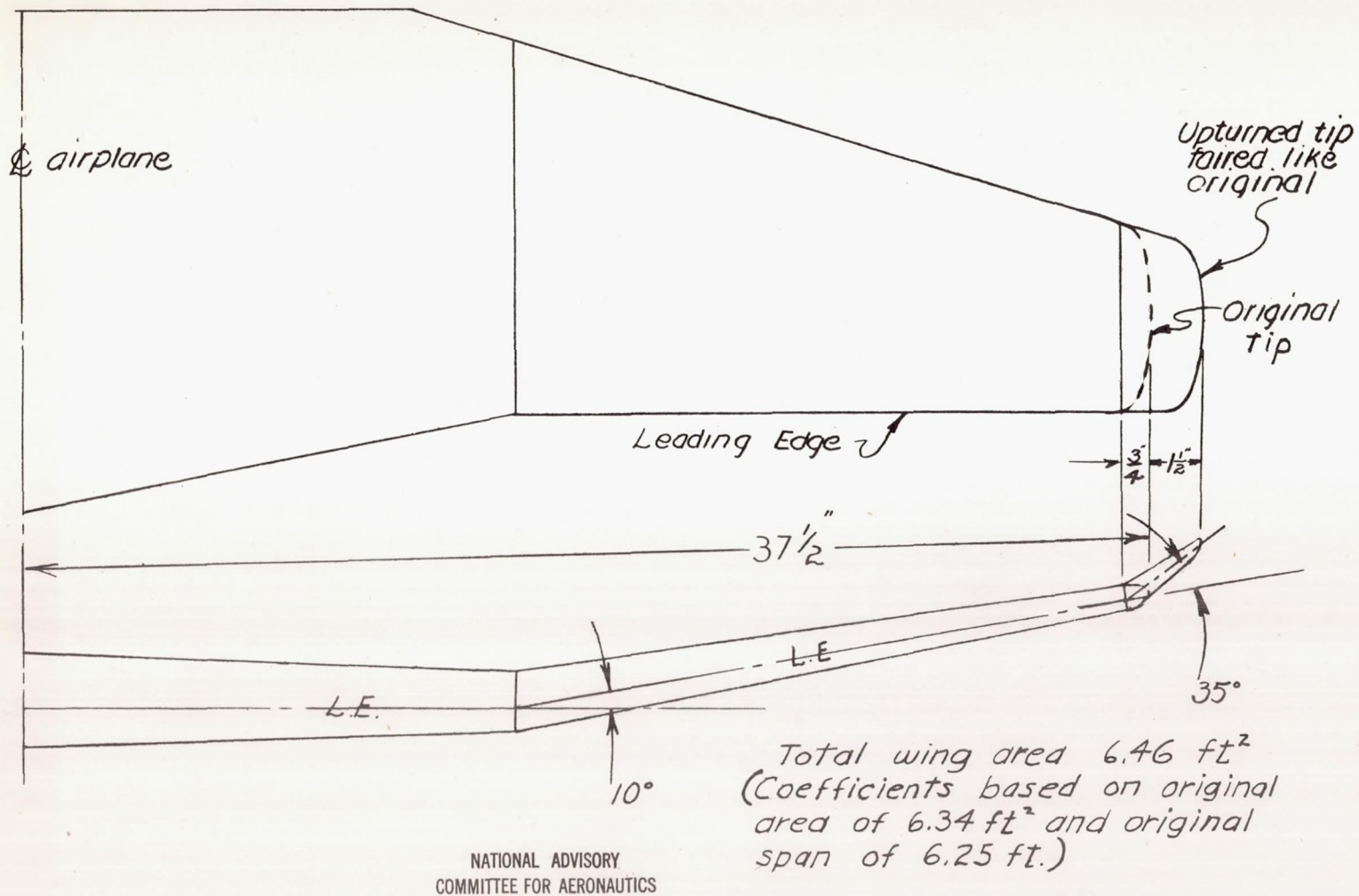
Figure 7(a)- Left wing panel of ⅛-scale model of XBTC-2 airplane showing
upturned wing tip.
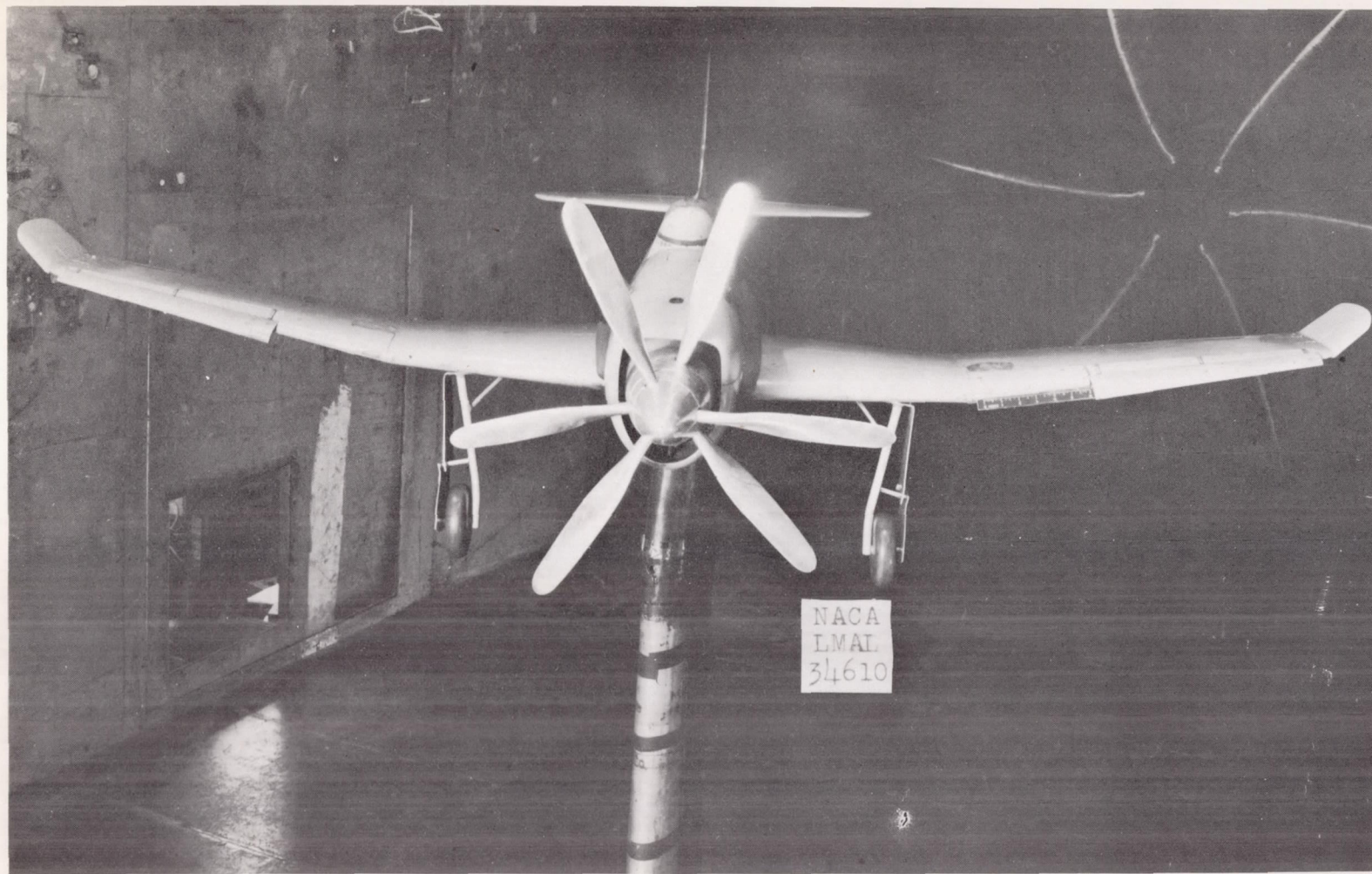
Figure 7(b).- The $\frac{1}{8}$-scale model of the XBTC-2 airplane with upturned wing tips. Landing configuration.

Section **A-A**

Section **B-B**

Small gap	Left	Right
Small gap	.89″	.76″
Large gap	1.15″	1.15″

Λ_{f_o}	g		c	
	Left	Right	Left	Right
-14.5° original	.37″	.33″	5.35″	5.35″
0.7° small gap	.36″	.41″	5.45″	5.45″
0.7° large gap	.56″	.59″	5.43″	5.45″
11.3°	.38″	.45″	5.49″	5.45″
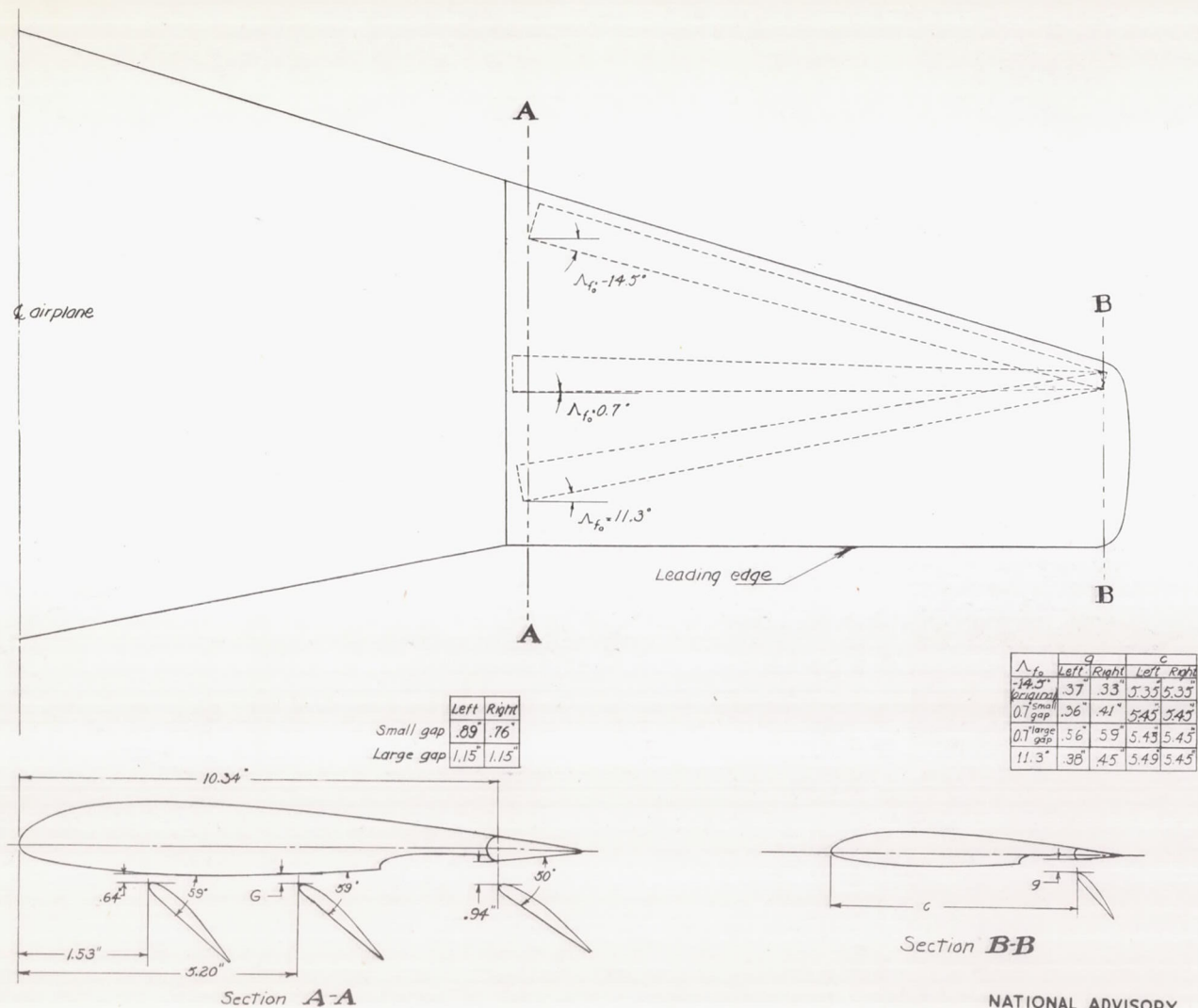
NATIONAL ADVISORY
COMMITTEE FOR AERONAUTICS.

Figure 8.- Left wing panel of ⅙ scale model of XBTC-2 airplane showing outboard flap positions tested.
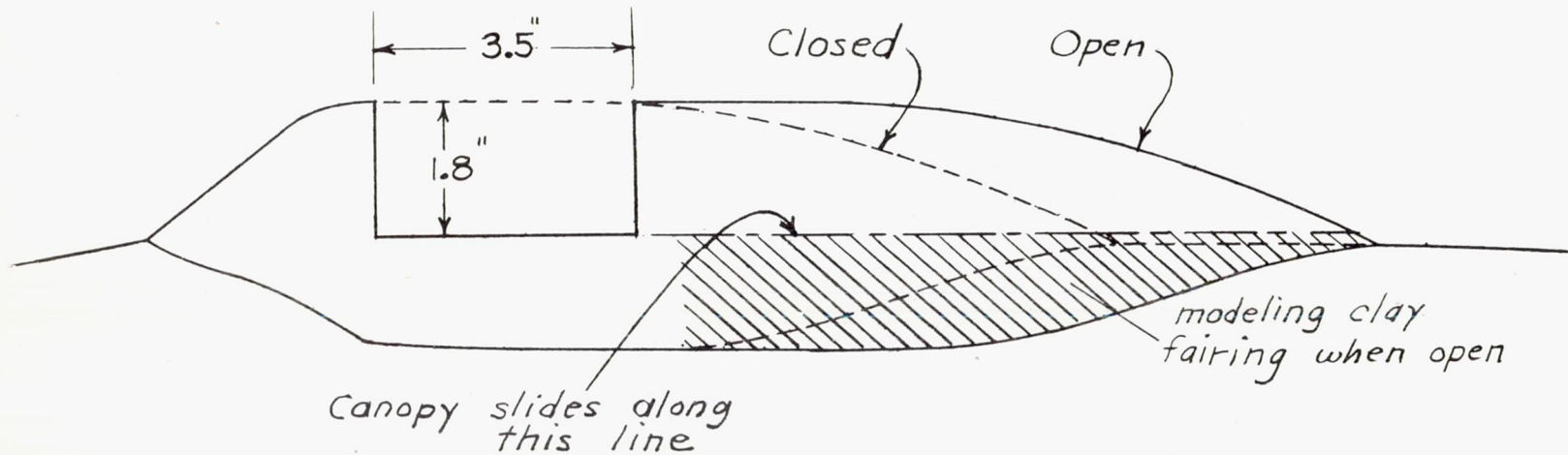
Figure 9. - Drawing showing canopy opening on
1/8-scale model of XBTC-2 airplane.

6.50 R.

12.48

D_2 D_1 Original   Approx 1" $\frac{1}{16}$

1"

9.75

FUSELAGE
CONTOUR

Thrust line

13.76

2.22

11.53

Figure 10- Dorsal fins tested on the ⅛-scale model
XBTC-2 airplane.

.022" .040" 12° av. Original 14° av. Revised

Section AA   Radius

	Original Tail	Revised Tail
Total area	.606 ft.²	.606 ft.²
Aspect ratio	2.45	2.45
Rudder area	.269 ft.²	.182 ft²
Balance area	.071 ft.²	Minimum
RMS chord	.221 ft.	.160 ft.
Rudder span	1.208 ft.	1.192 ft.

Both Airfoil Sections
NACA 0009-64 modified
aft of rudder beam.

$$C_{h_r} = \frac{H_r}{q\, b_r\, \overline{c}_r^{\,2}}$$

b_r, rudder span
$\overline{c}_r$, rudder RMS chord

5.02"
3.48"
.86"
.20"
1.69"
.54"   R   A

14.50"

℄ Original Rudder Hinge
℄ Revised Rudder Hinge

9.45"
1.53"
2.75"
2.75"
3.67"
3.25" R
3.0"
.41"
1.6"
Fuselage Hor. Ref. Line
.48"
1/8"
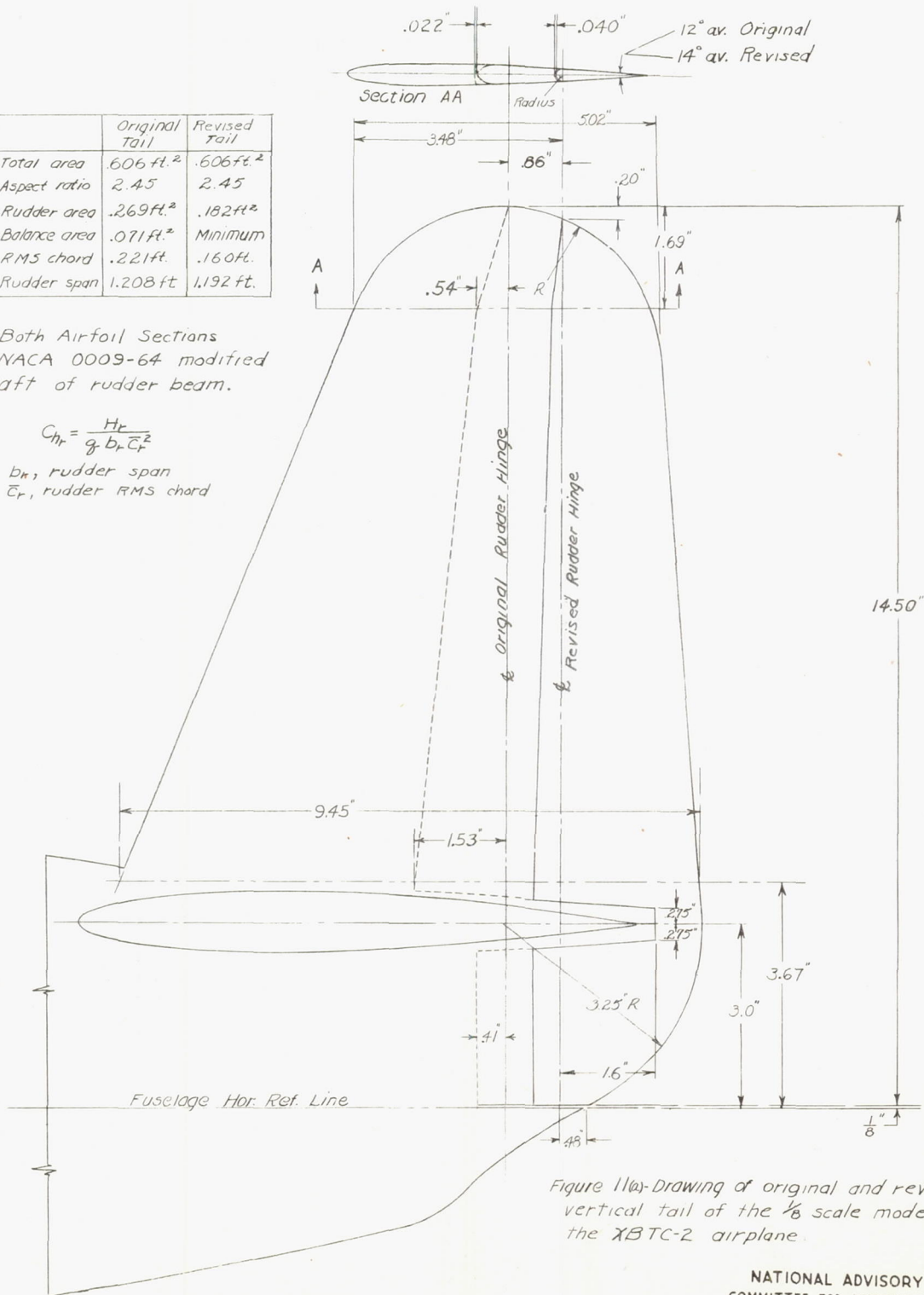
Figure 11(a)- Drawing of original and revised
vertical tail of the 1/8 scale model of
the XBTC-2 airplane.

NATIONAL ADVISORY
COMMITTEE FOR AERONAUTICS.

L-787
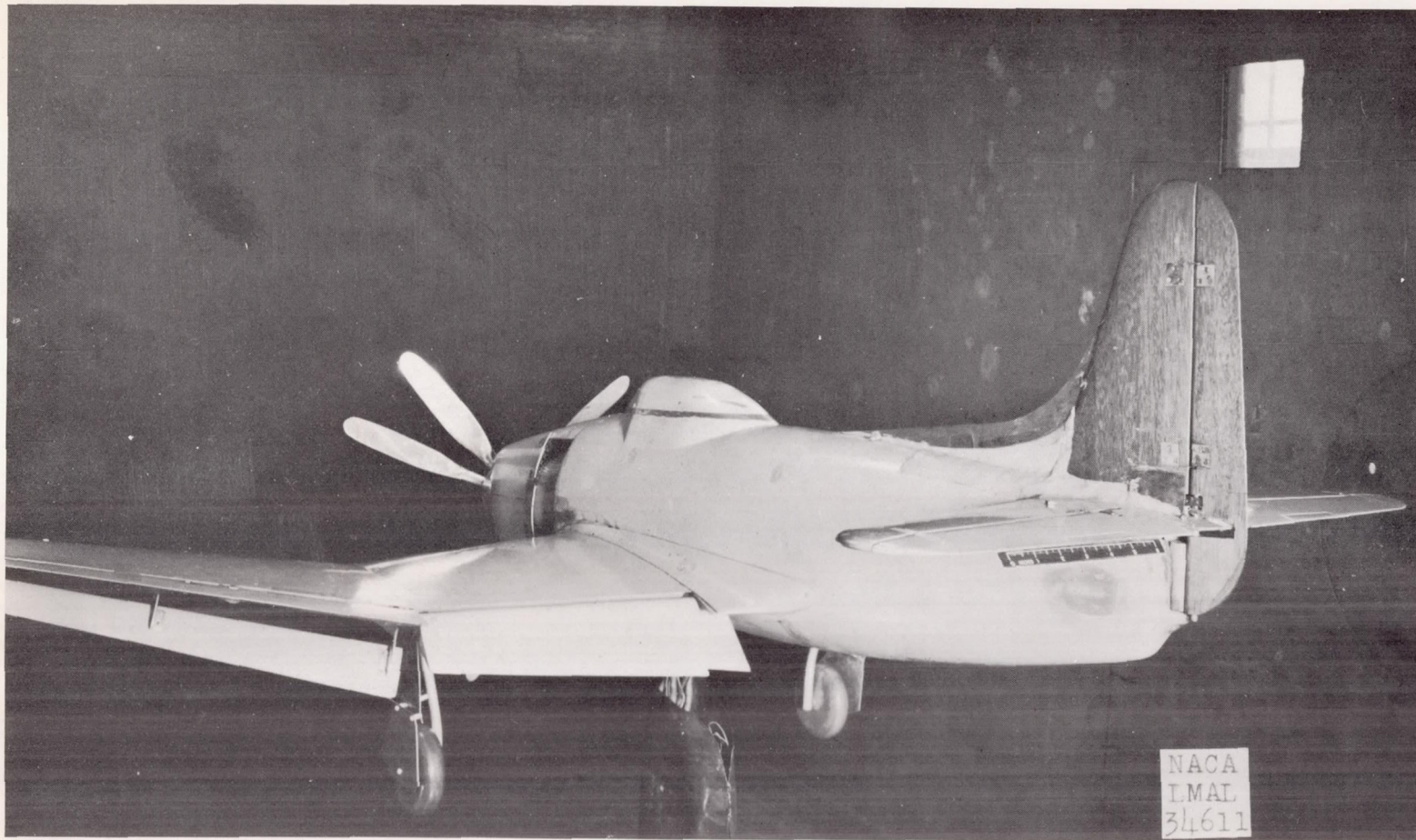
Figure 11(b).- The $\frac{1}{8}$-scale model of the XBTC-2 airplane with the revised vertical tail and dorsal fin, D_1. Landing configuration.
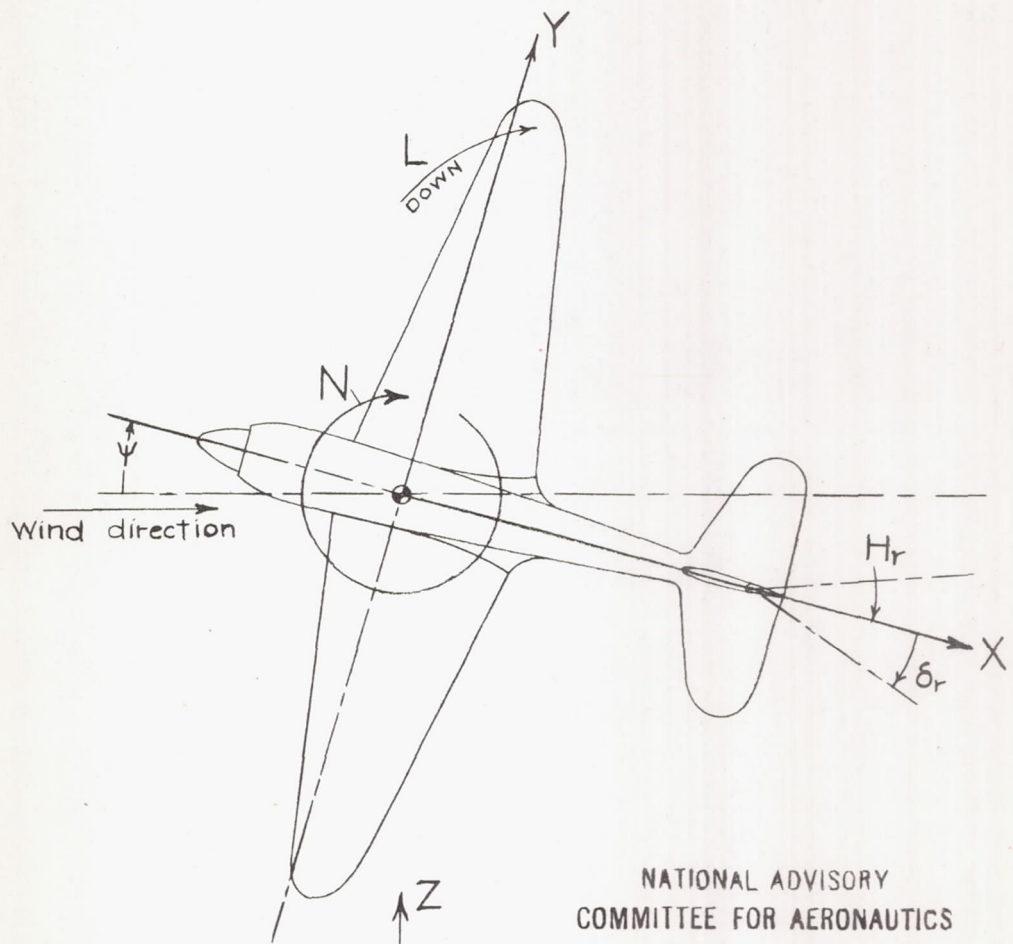
NATIONAL ADVISORY
COMMITTEE FOR AERONAUTICS
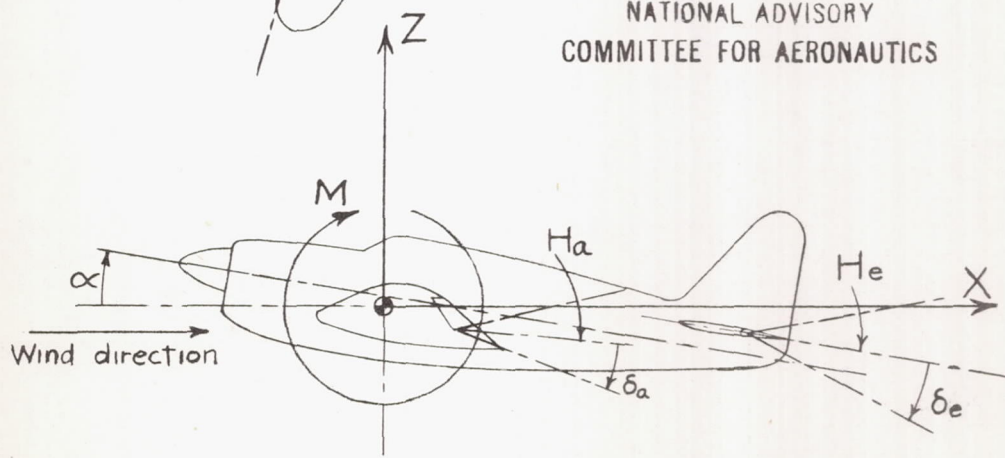
Figure 12.-Notation of the system of axes
and the control-surface hinge moments and
deflections. (Arrows indicate positive values.)
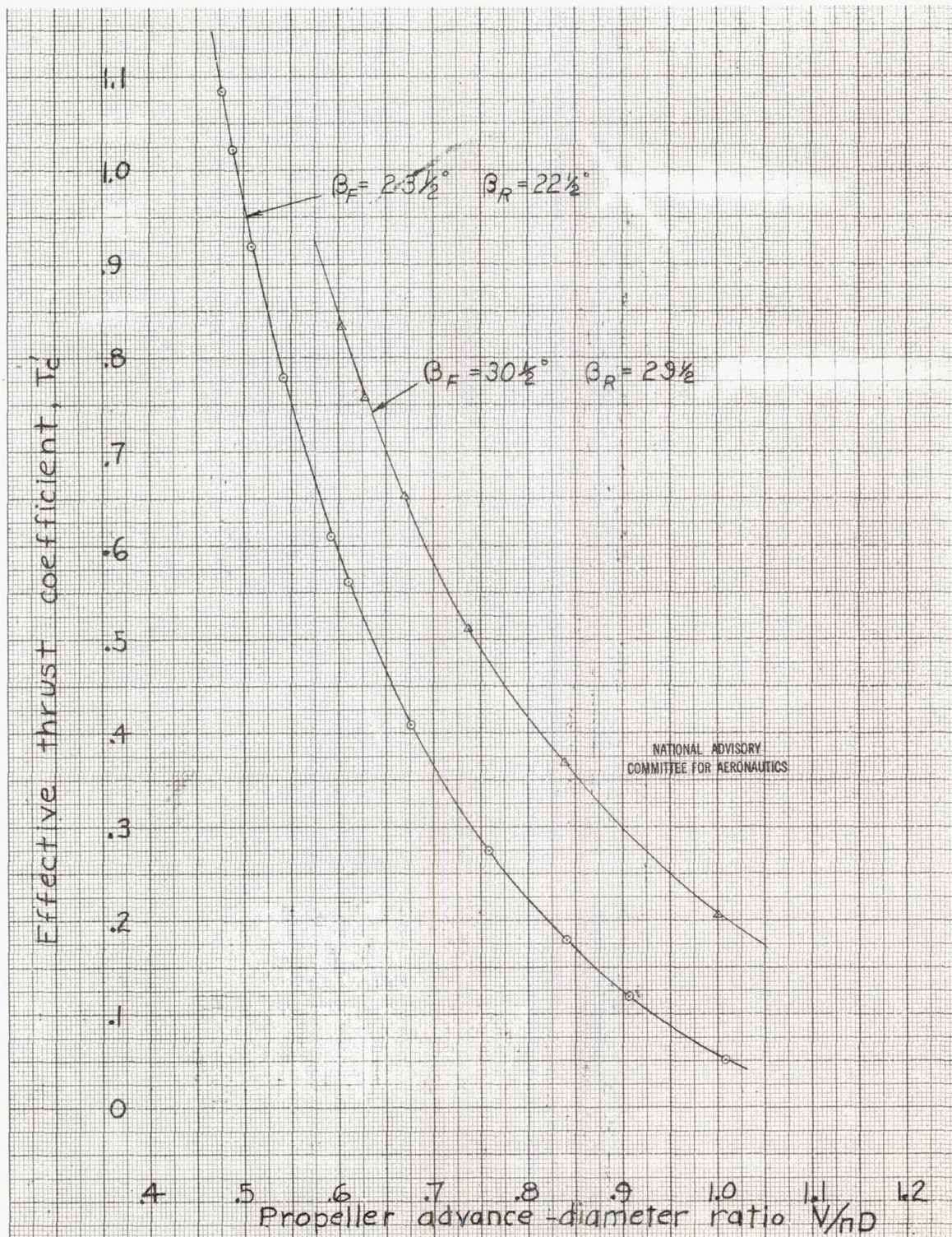
Figure 13.- Propeller calibration of the $\frac{1}{8}$-scale model of the XBTC-2 airplane. Cruising configuration, $\alpha = 0°$.

1.2

1.1

1.0

.9

.8

.7

.6

.5

.4

.3

.2

.1

0

Effective thrust coefficient, T_c'

Original wing
Rectangular wing
Wing with
swept-back outer
panels, W/s=39.4 lbs/ft²
also power A for
rectangular outer
wing panels W/s=34.4
lbs/ft²

Power B for
rectangular outer
wing panels
W/s = 39.4 lbs/ft²

Note: T_c' and C_L are based
on the following wing areas

Wing	Total area
Original	406 ft²
Swept-back	406 ft²
Rect out panel	465 ft²
Rectangular	406 ft²
Upturned tips	406 ft²

0   .4   .8   1.2   1.6   2.0   2.4   2.8

Lift coefficient, C_L

Figure 14.- Variation of effective thrust coefficient
with lift coefficient for the XBTC-2 airplane
with constant power and a constant speed
propeller. Take-off power, 3000 h.p. at 2700 rpm
at sea level. Gear ratio 0.39.

NATIONAL ADVISORY
COMMITTEE FOR AERONAUTICS
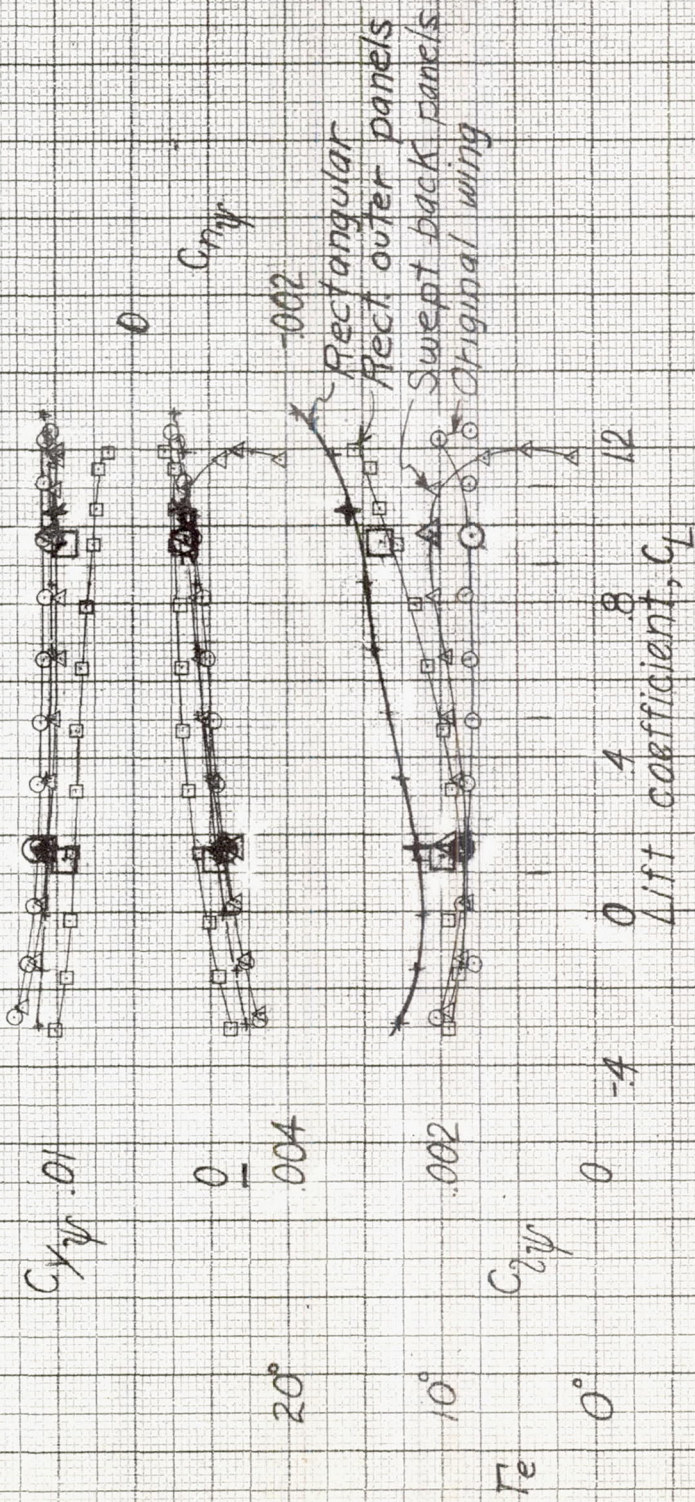
(a) Cruising configuration. Propeller windmilling.

Figure 15.- Effect of wing plan form on the variation of $C_{n\psi}$ and $C_{Y\psi}$ with C_L of the 1/8-scale model of the XBTC-2 airplane.
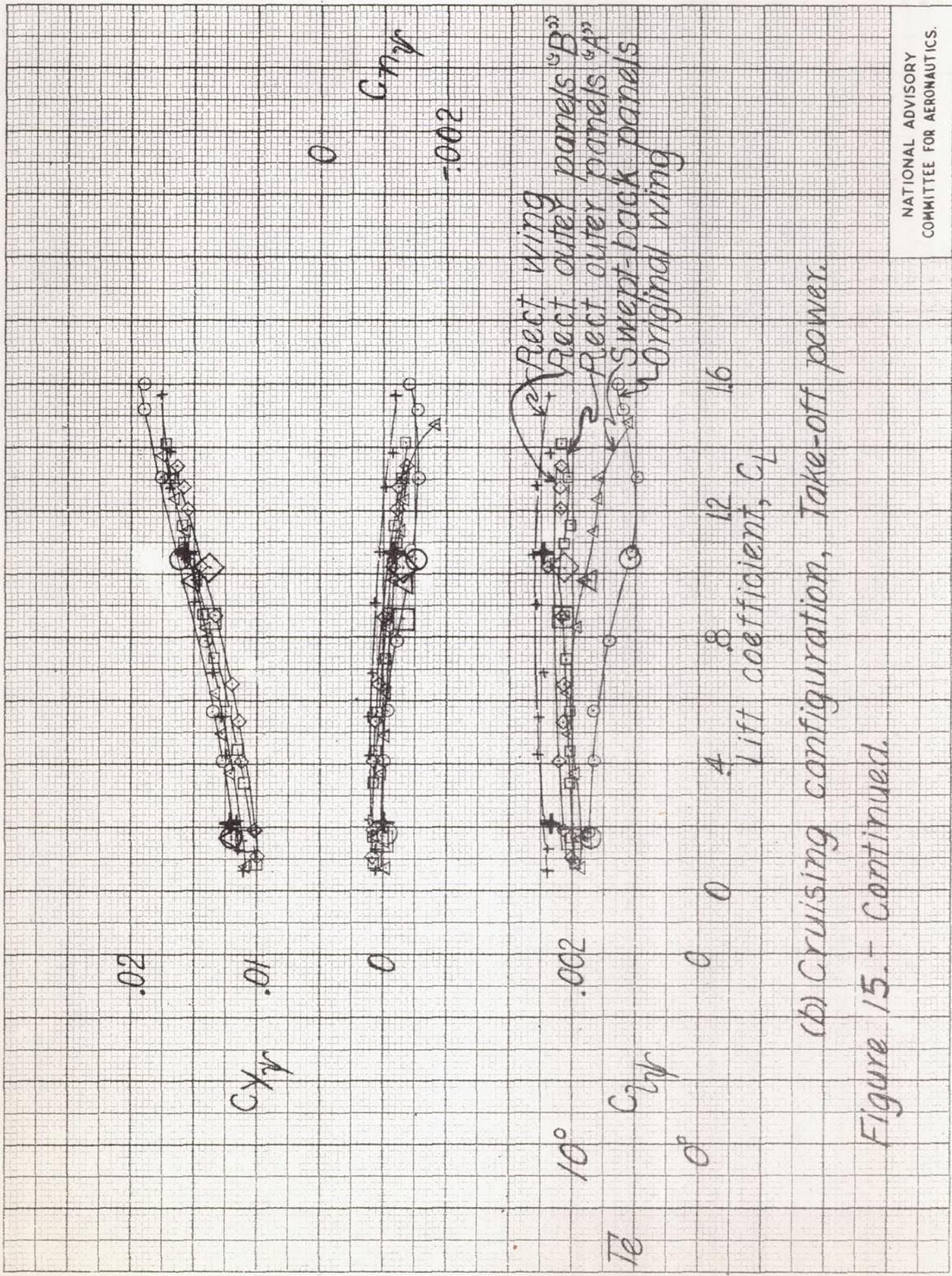
Rectangular
Rect. outer panels
Swept back panels
Original wing

Lift coefficient, C_L

$C_{Y\psi}$

$C_{n\psi}$

$C_{n\psi}$

$C_{l\psi}$

Γ_e

C_{n_r}

.002

0

-.002

C_{Y_r}

.02

.01

0

Rect wing
Rect outer panels "B"
Swept-back panels "A"
Rect outer panels "B"
Original wing

16

12

8

4

0

Lift coefficient, C_L

C_{h_g}

.002

0

Θ°

0

0

0

θr

(b) Cruising configuration, Take-off power.

Figure 15.- Continued.

NATIONAL ADVISORY
COMMITTEE FOR AERONAUTICS
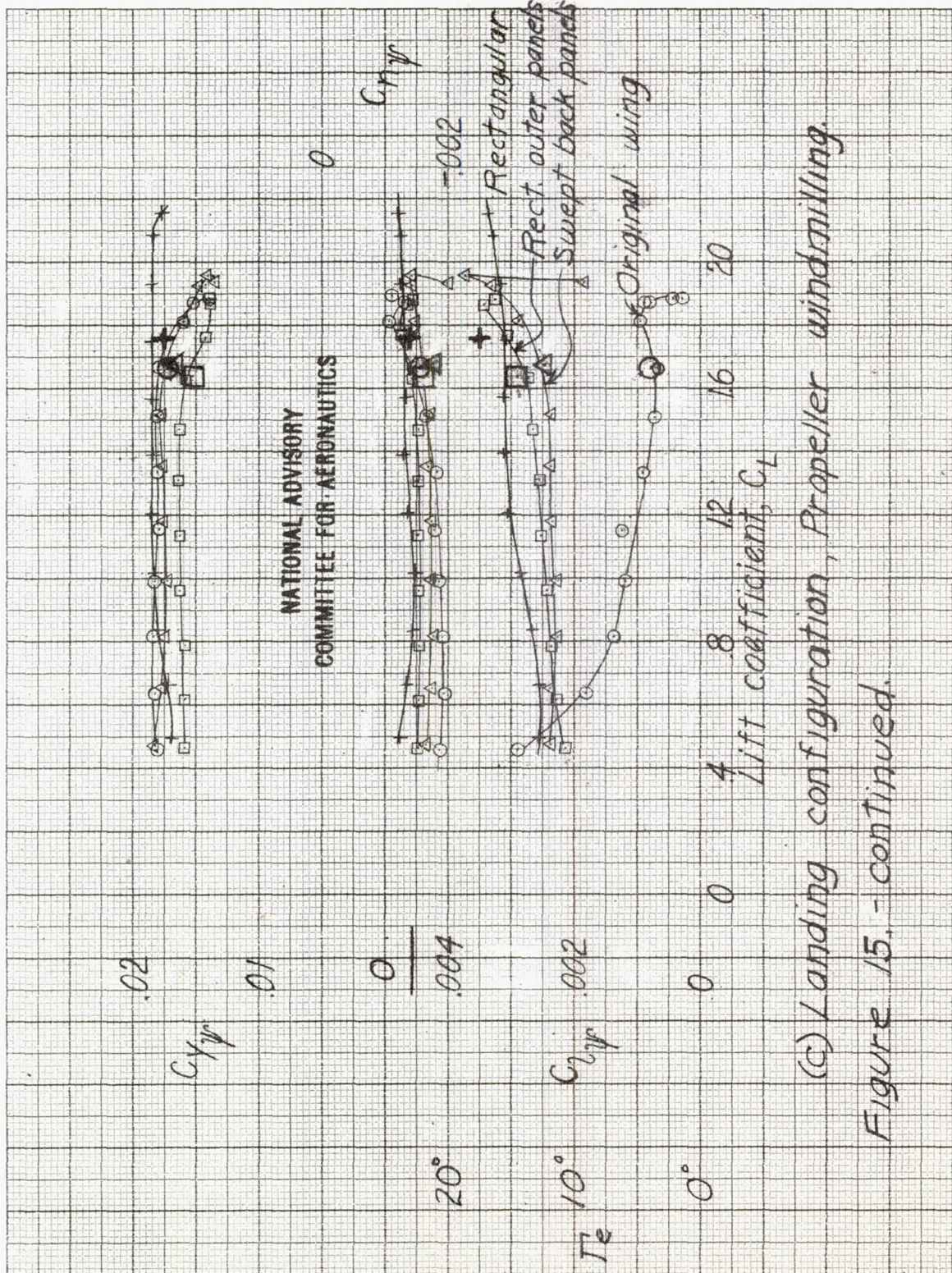
(c) Landing configuration, Propeller windmilling.

Figure 15.–continued.

NATIONAL ADVISORY
COMMITTEE FOR AERONAUTICS

(d) Landing configuration, Take-off power.

Figure 15.- concluded.
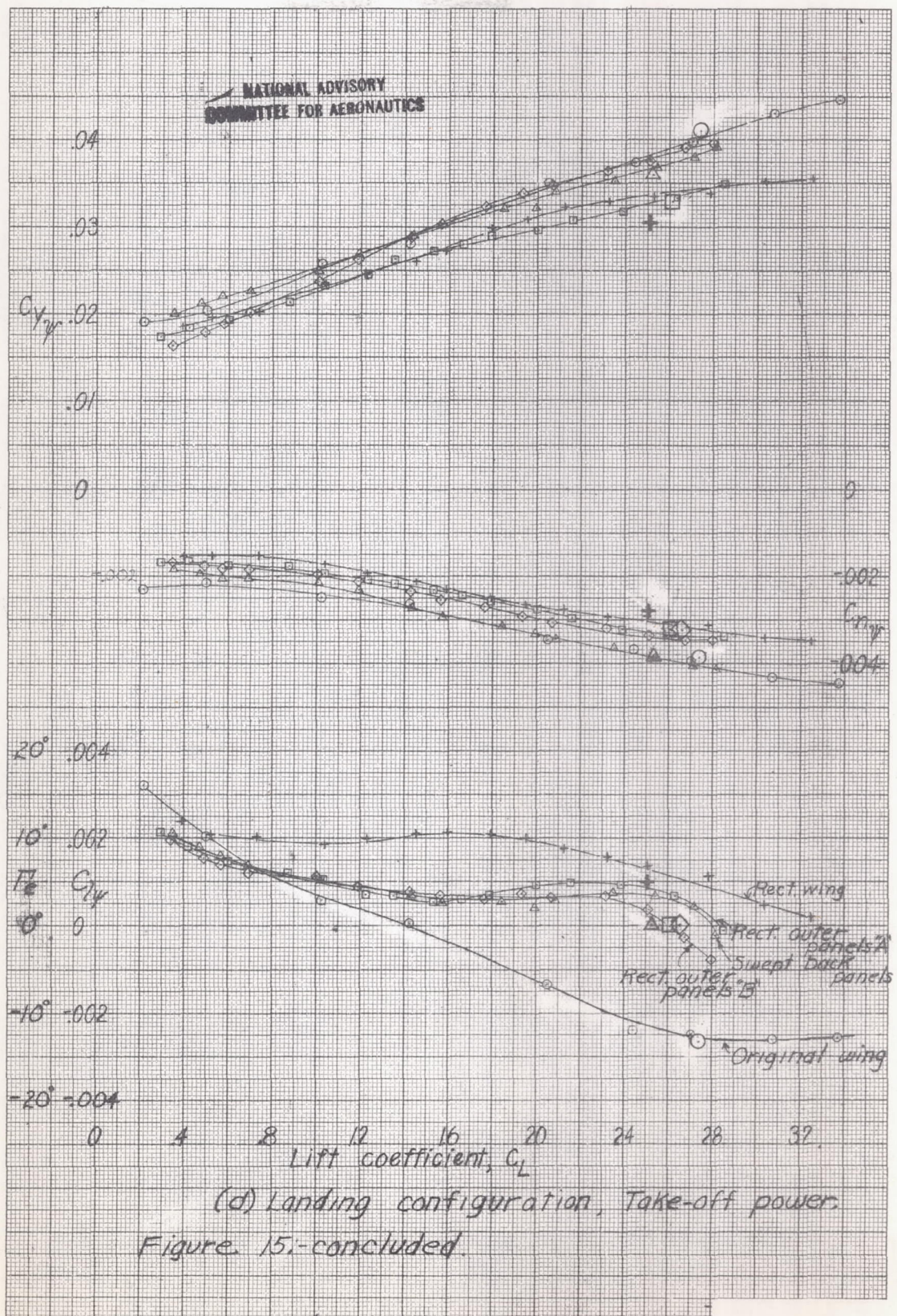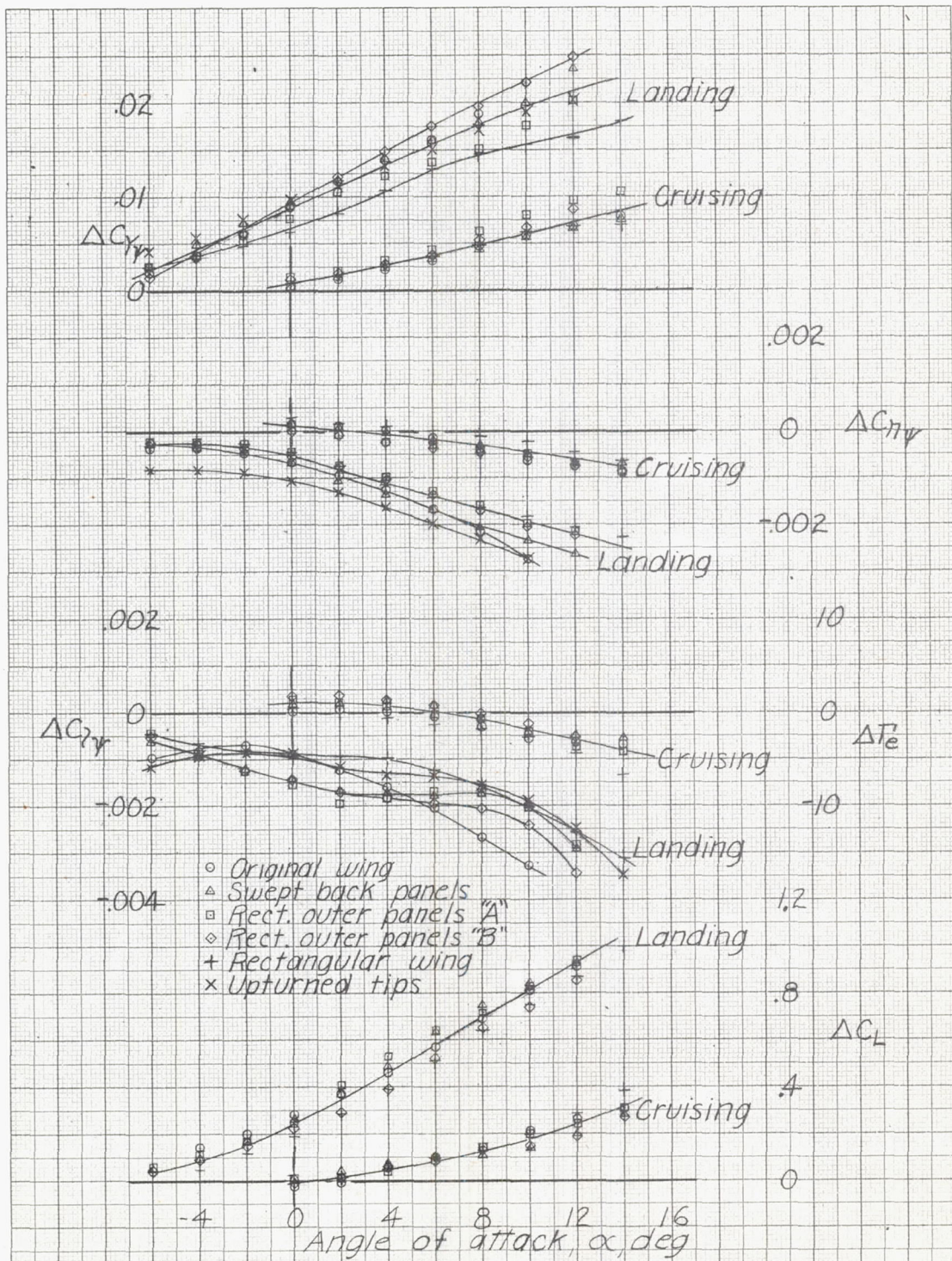
(a) Increments for same α.

Figure 16.- Increments of C_{Y_ψ}, C_{n_ψ}, C_{l_ψ}, and C_l due to take-off power for the $\frac{1}{8}$-scale model of the XBTC-2 airplane.

Cruise, Land
ⓓ   Original wing
△   Swept-back panels
□   Rect. outer panels "A"
◇   Rect. outer panels "B"
+   Rectangular wing
×   Upturned tips
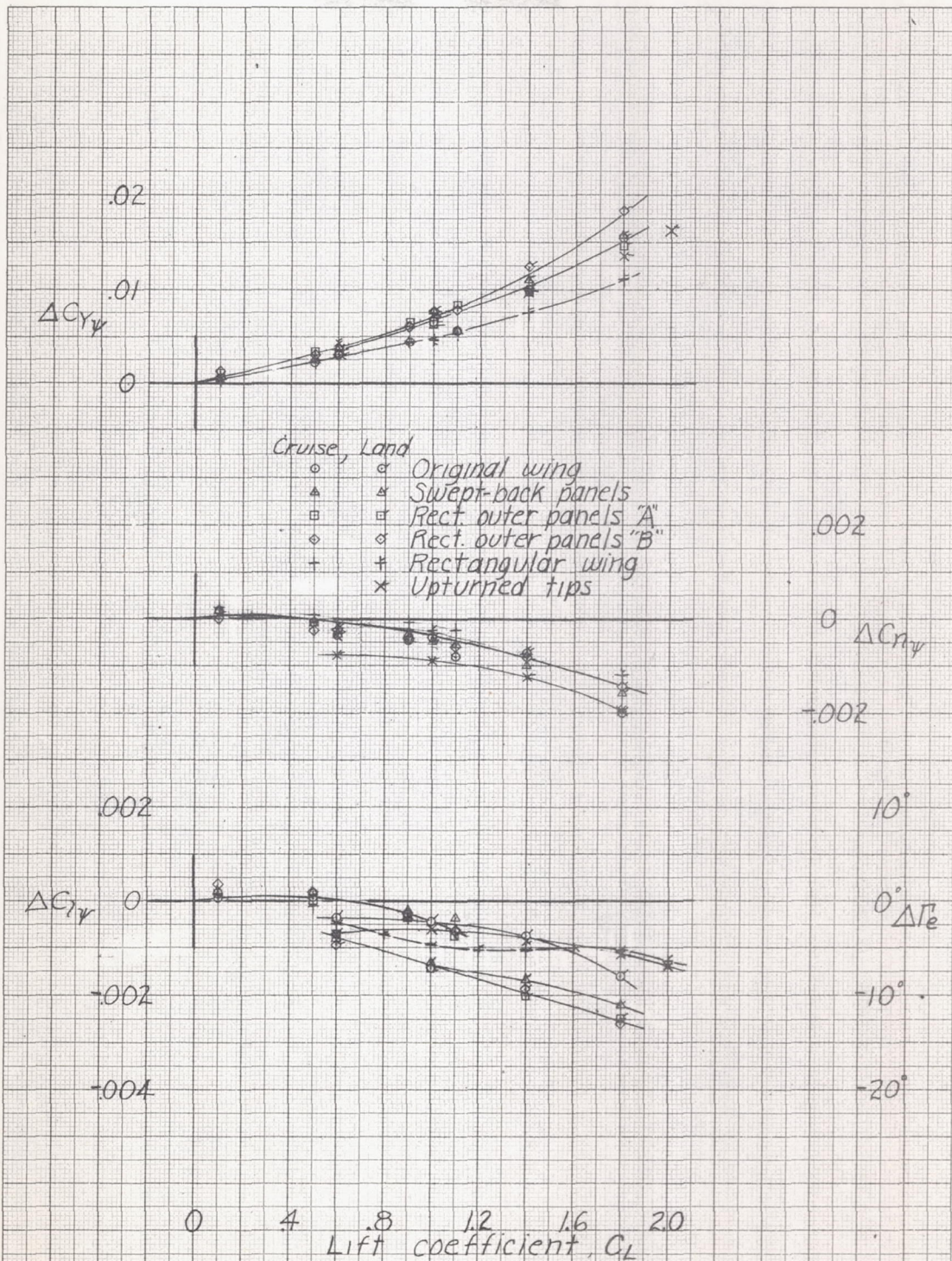
(b) Increments for same C_L.

Figure 16.- Concluded.
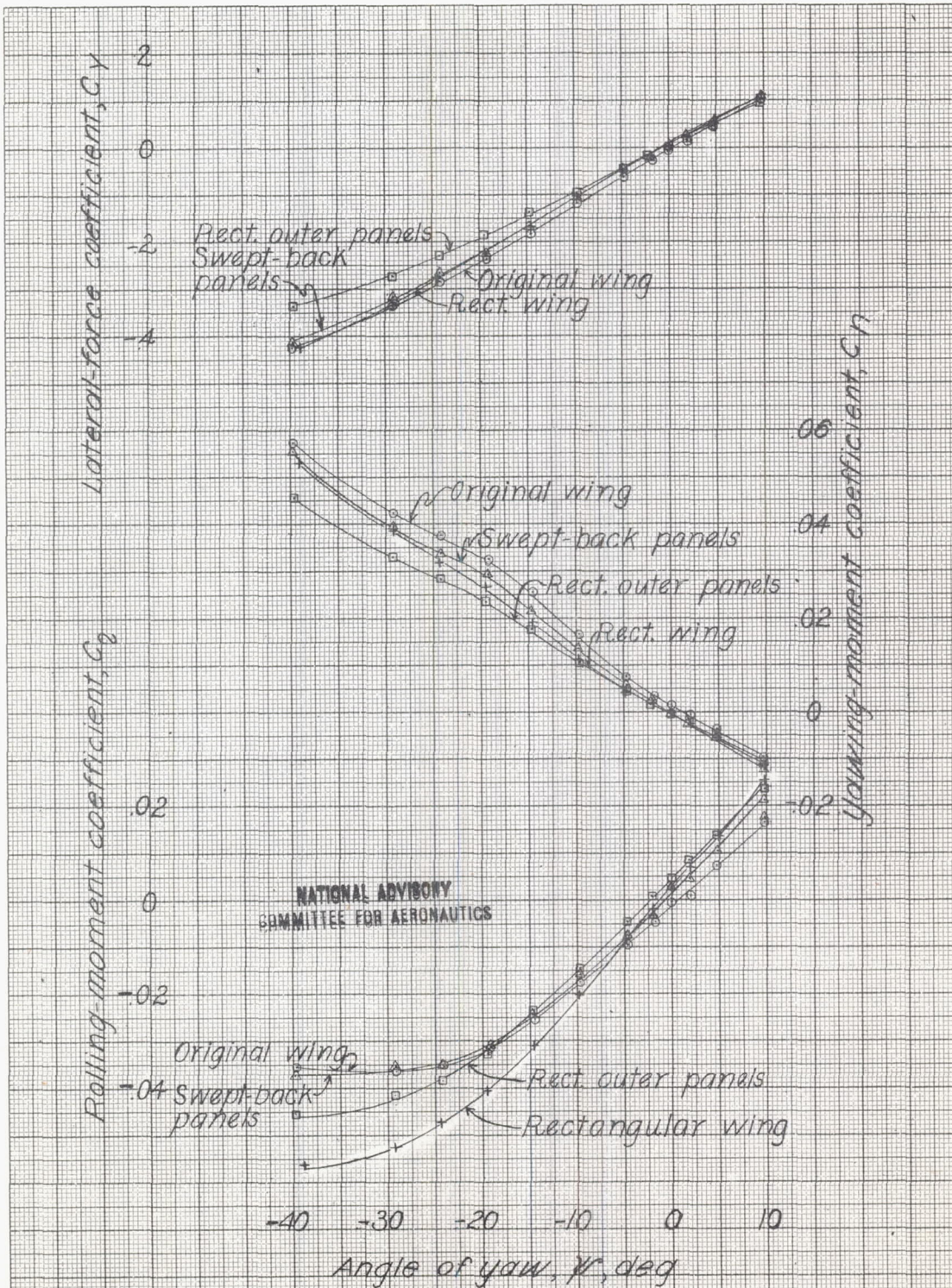
(a) Propeller windmilling, $\alpha \approx 0.2°$.

Figure 17.- Effect of wing plan form on the aerodynamic characteristics in yaw of the ⅛-scale model of the XBTC-2 airplane. Cruising configuration.

(a) concluded.

Figure 17.- continued.

(b) Take-off power, $\alpha \approx 0.1°$.

Figure 17.-continued.

Pitching-moment coefficient, C_m

.1

0

-1

Resultant-drag coefficient, C_{DR}

○ Original wing
△ Swept-back panels
□ Rect. outer panels
+ Rect. wing

0

-1

Lift coefficient, C_L

.4

0

-40   -30   -20   -10   0   10

Angle of yaw, ψ, deg

(b) concluded.

Figure 17.- continued.

Lateral-force coefficient, C_Y

Rolling-moment coefficient, C_l

Yawing-moment coefficient, C_n

Rect. outer panels

Rect. wing

Swept-back panels

Original wing

Swept-back panels

Original wing

Rect. wing

Rect. outer panels

NATIONAL ADVISORY
COMMITTEE FOR AERONAUTICS

Original wing

Swept-back panels

Rect. outer panels

Rectangular wing

Angle of yaw, ψ, deg
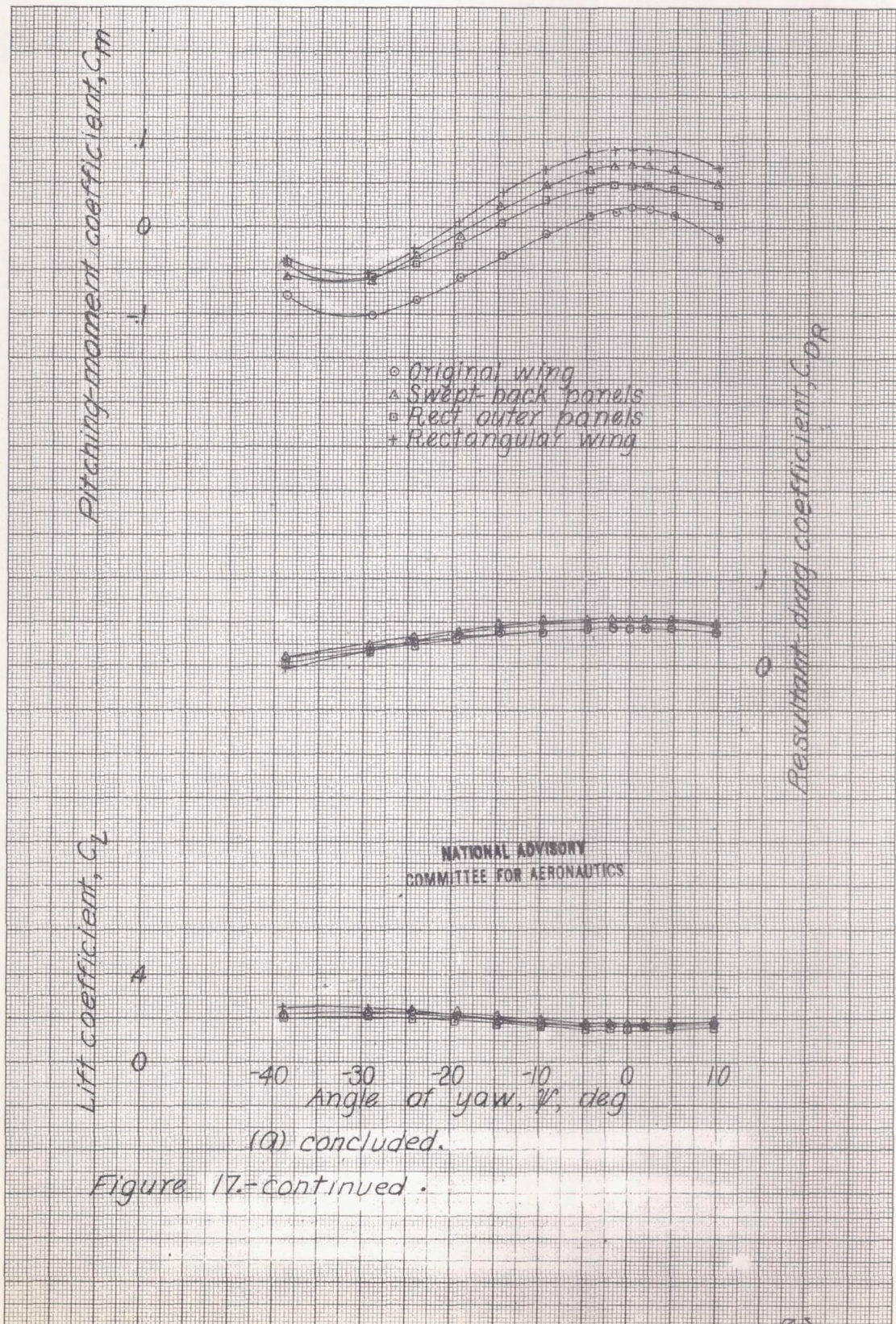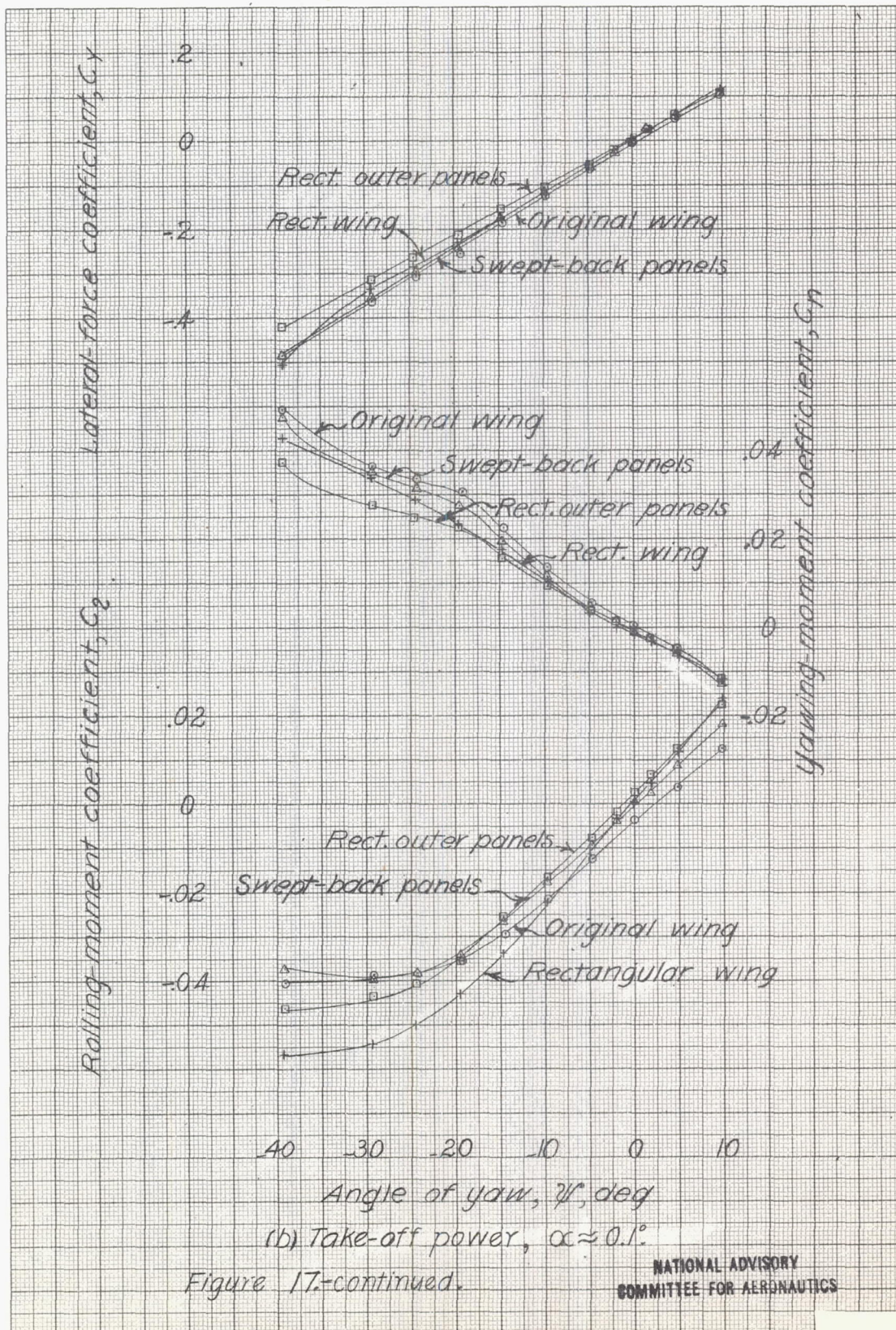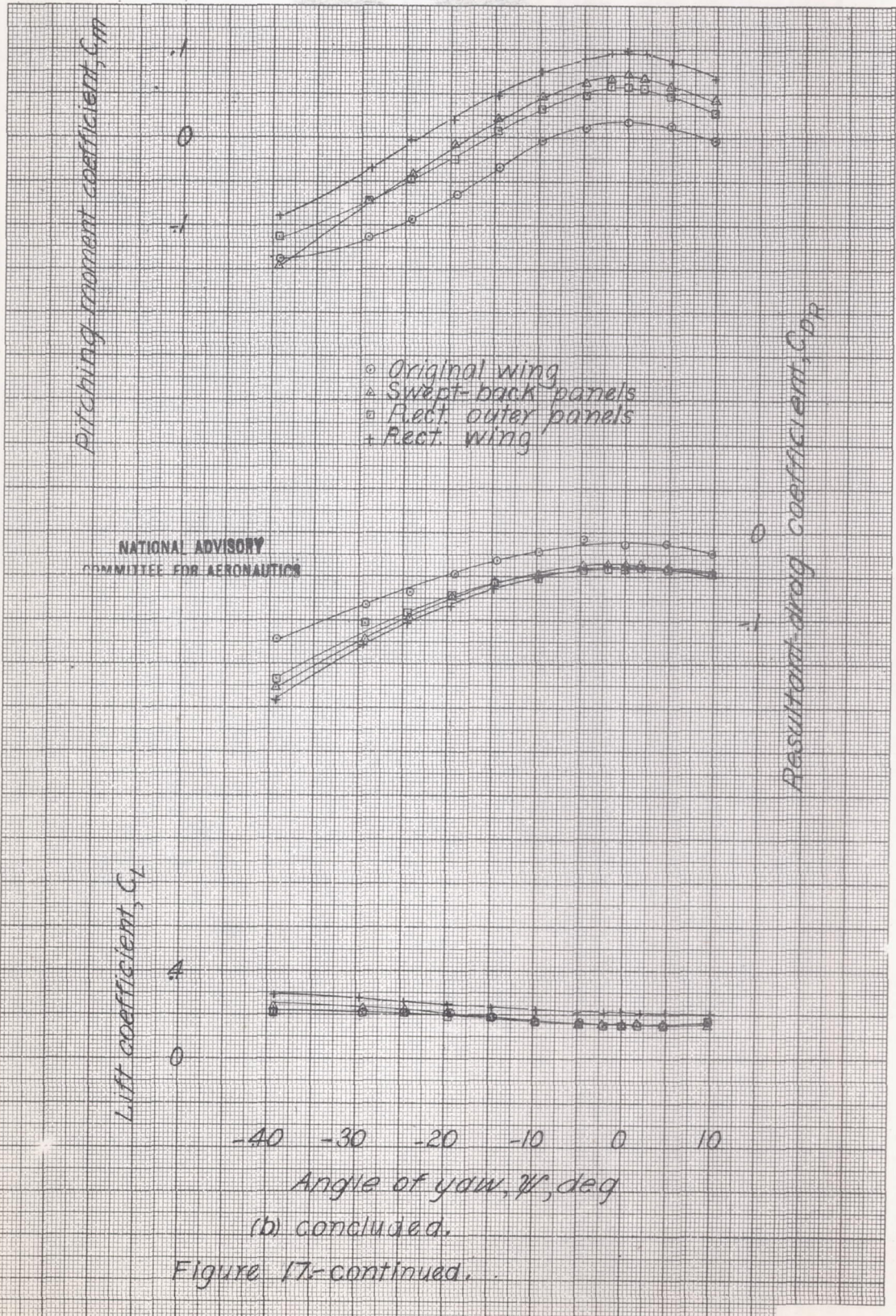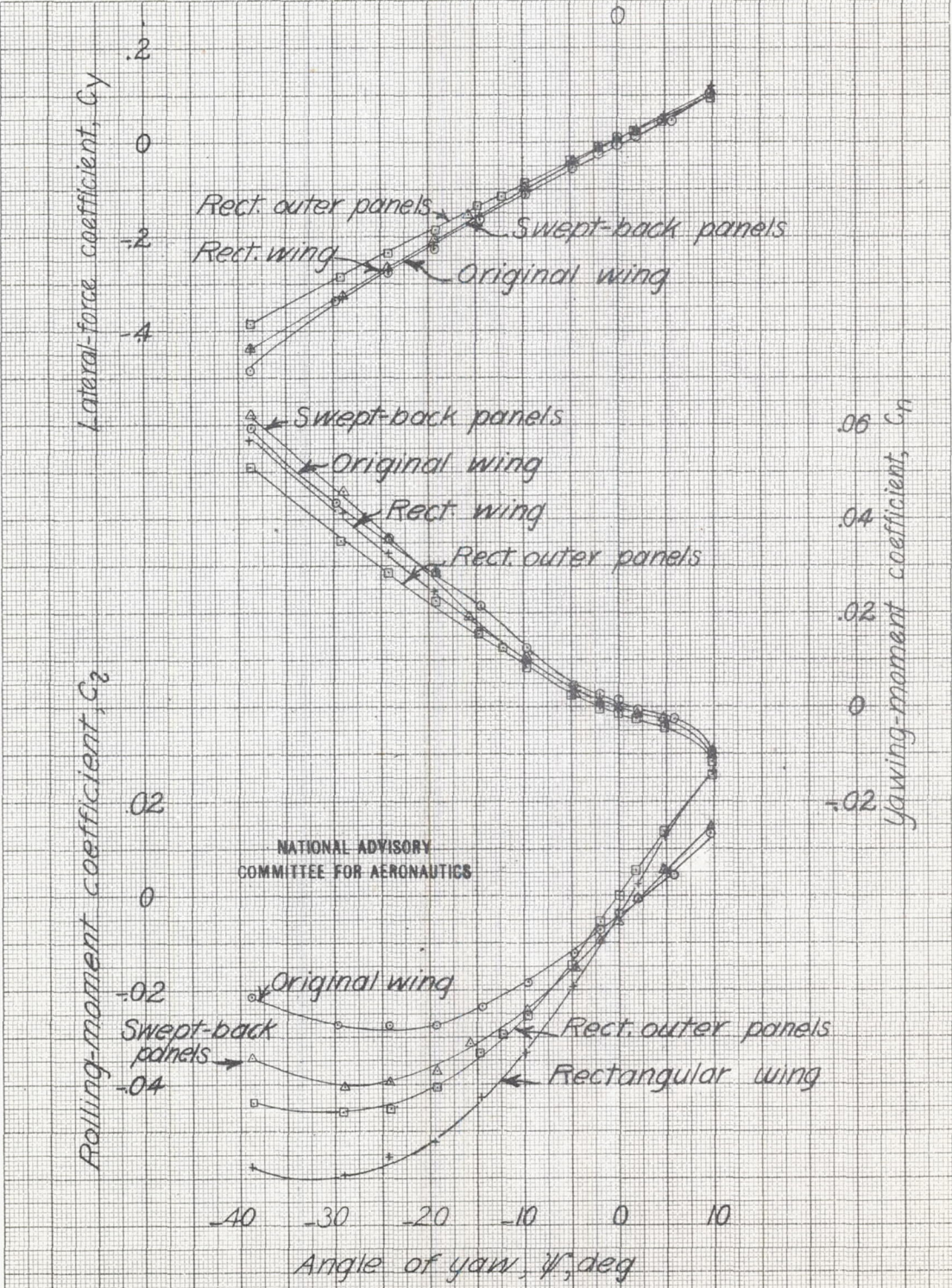
(c) Propeller windmilling, $\alpha \approx 10.7°$

Figure 17 .-Continued.

Pitching-moment coefficient, C_m

0

-.1

-.2

Resultant-drag coefficient, C_{DR}

1

0

○ Original wing
△ Swept-back panels
□ Rect. outer panels
+ Rectangular wing

Lift coefficient, C_L

1.2

.8

.4

NATIONAL ADVISORY
COMMITTEE FOR AERONAUTICS

-40   -30   -20   -10   0   10

Angle of yaw, ψ, deg

(c) Concluded.
Figure 17.- Continued.

Lateral-force coefficient, C_Y

.2

0

-.2

Rect. panels "A"   Swept-back panels
        "B"

-.4   Original wing

-.6   Rect. wing

Swept-back panels, $\beta = 23°$

Original wing, $\beta = 30°$ .04

Rect. wing, $\beta = 23°$

.02

Rect. panels "A"
$\beta = 23°$ "B"

0

-.02

Yawing-moment coefficient, C_n

Rolling-moment coefficient, C_ℓ

.02

0

-.02   Original wing   Rect. panels "A"
                                    "B"
Swept-back panels   Rect. wing

-.04

-40   -30   -20   -10   0   10

Angle of yaw, ψ, deg

(d) Take-off power, $\alpha \approx 9°$.

Figure 17.- continued.

L-787
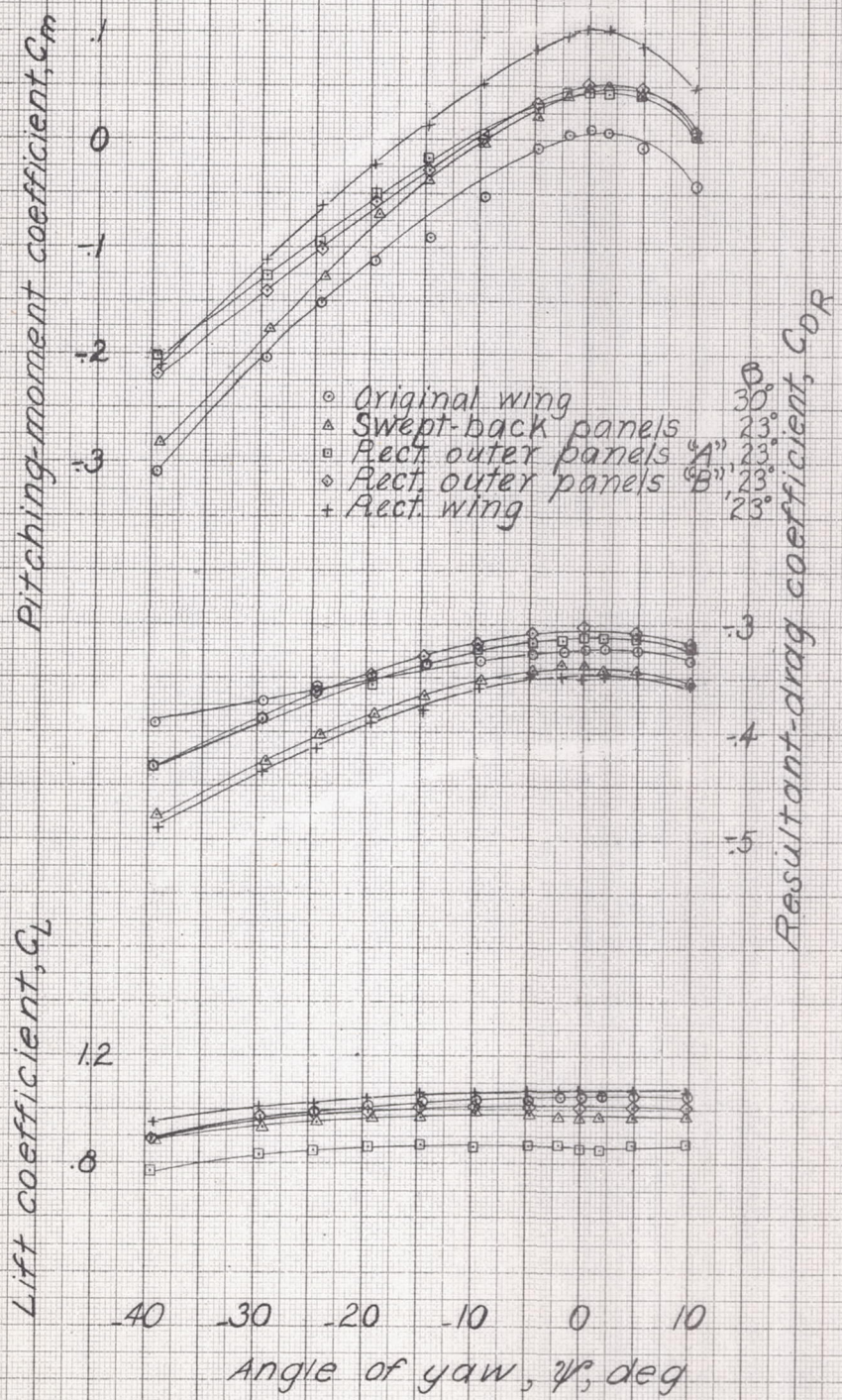
(d) Concluded.

Figure 17.-Concluded.

NATIONAL ADVISORY
COMMITTEE FOR AERONAUTICS

Lateral force coefficient, C_Y

Rolling-moment coefficient, C_l

Yawing-moment coefficient, C_n

0

.2

Rect. outer panels

Original wing — Swept-back panels

.4

Rect. wing

Swept-back panels

Rect. wing

Rect. outer panels

Original wing

.06

.04

.02

0

-.02

NATIONAL ADVISORY
COMMITTEE FOR AERONAUTICS

.02

0

-.02

Original wing

-.04

Swept-back panels

.06

Rect. outer panels

(a) Propeller windmilling, $\alpha \approx 9.2°$.

Rect. wing

-40   -30   -20   -10   0   10

Angle of yaw, ψ, deg
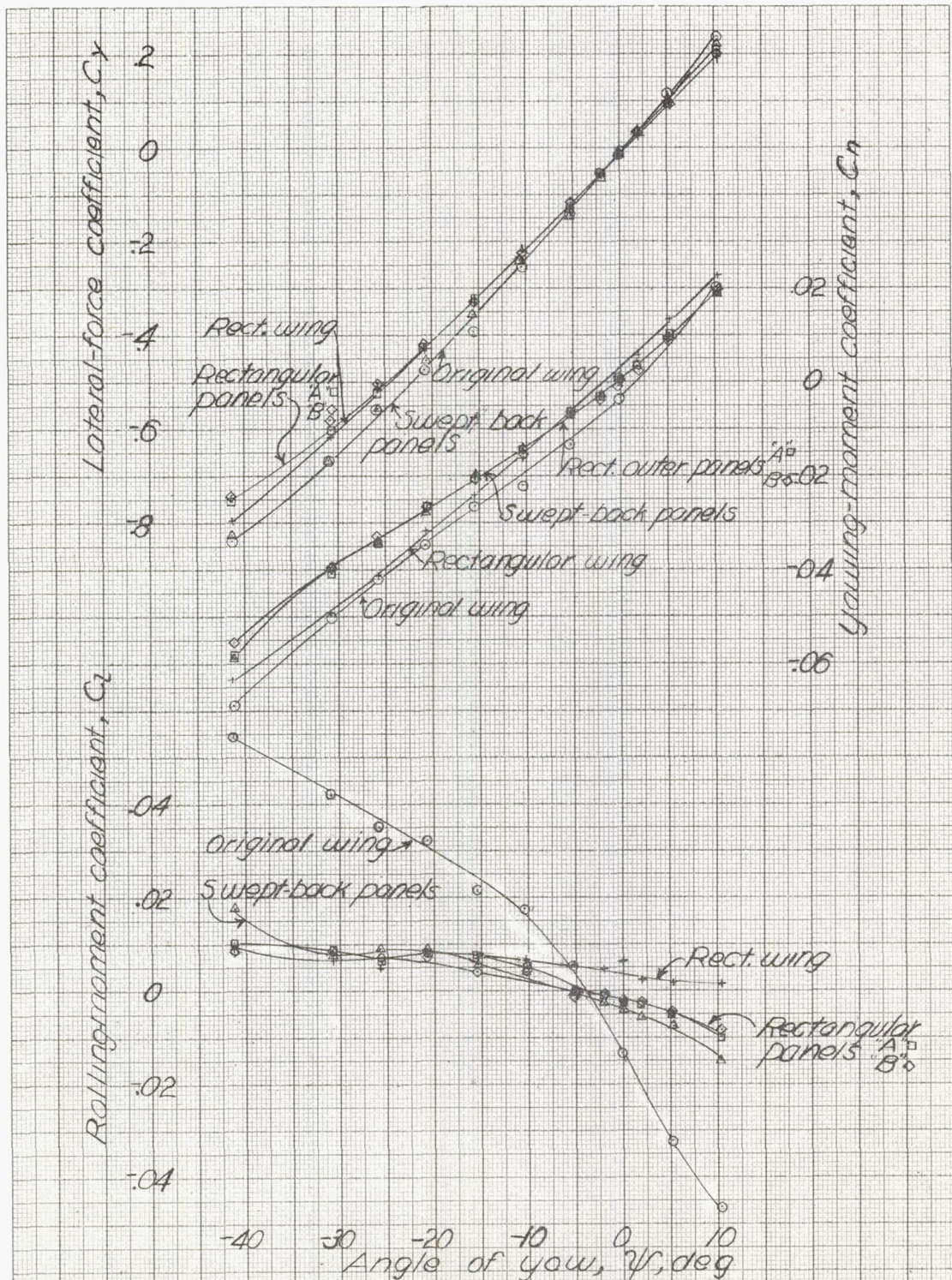
Figure 18.- Effect of wing plan form on the aerodynamic characteristics in yaw of the XBTC-2 airplane. Landing configuration.

Original wing
Swept-back panels
Rect. outer panels
Rectangular wing

NATIONAL ADVISORY
COMMITTEE FOR AERONAUTICS

Angle of yaw, ψ, deg

(a) Concluded.

Figure 18: continued.

NATIONAL ADVISORY
COMMITTEE FOR AERONAUTICS

Rectangular
Rect. outer panels "A"
Swept-back panels
Rect. outer panels "B"

Original

Angle of yaw, ψ, deg

Lateral-force coefficient, C_Y

Yawing-moment coefficient, C_n

Rolling-moment coefficient, C_l

(b) Take-off power, $\alpha \approx 11.0°$.

Figure 18: continued.

L-787

Original wing
Swept-back panels
Rect. outer panels (power A)
Rect. outer panels (power B)
Rectangular wing

Pitching-moment coefficient, C_m

Resultant-drag coefficient, C_{D_R}

Lift coefficient, C_L

Angle of yaw, ψ, deg

(b) concluded.

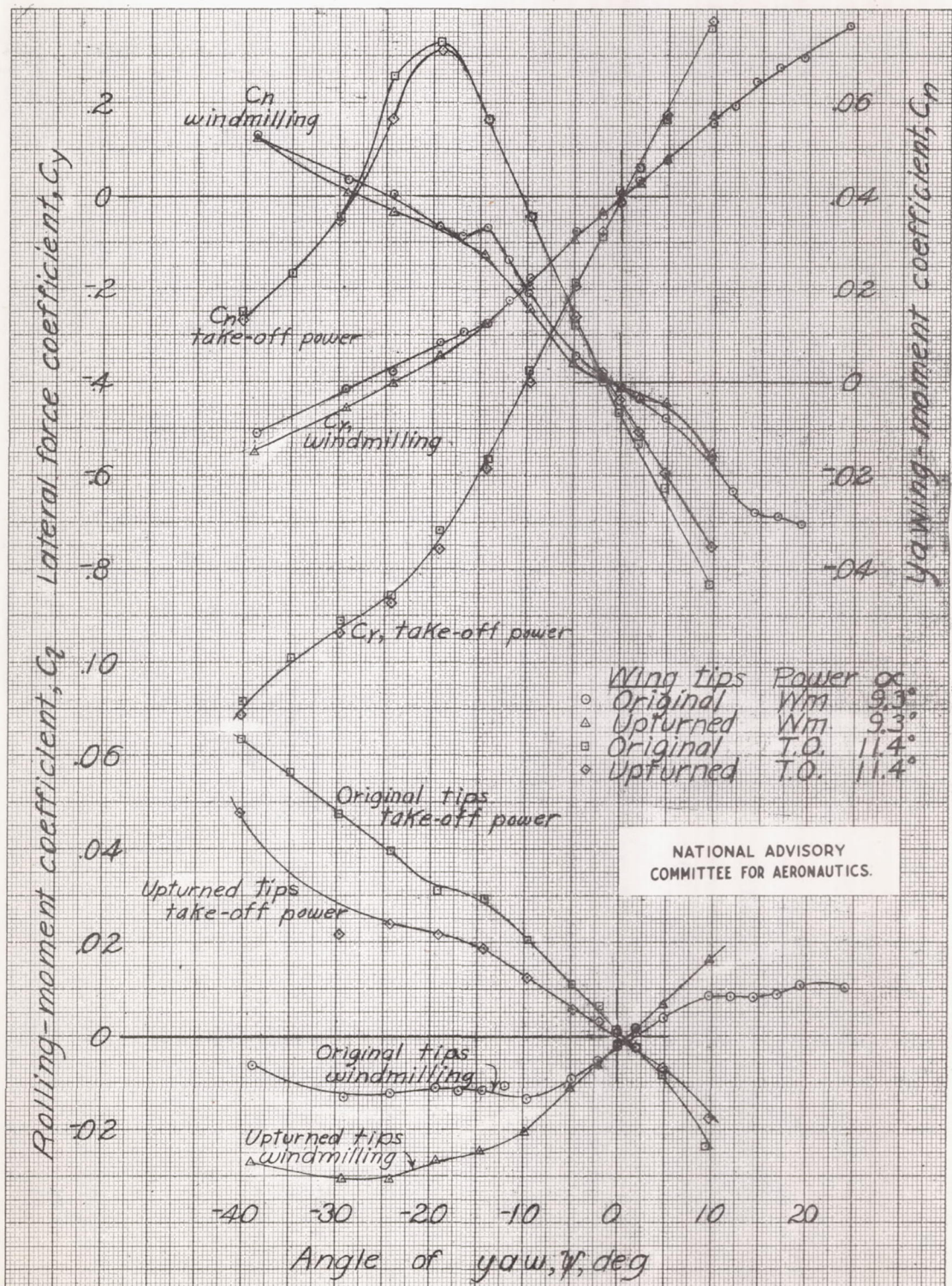Figure 18. concluded.

NATIONAL ADVISORY
COMMITTEE FOR AERONAUTICS
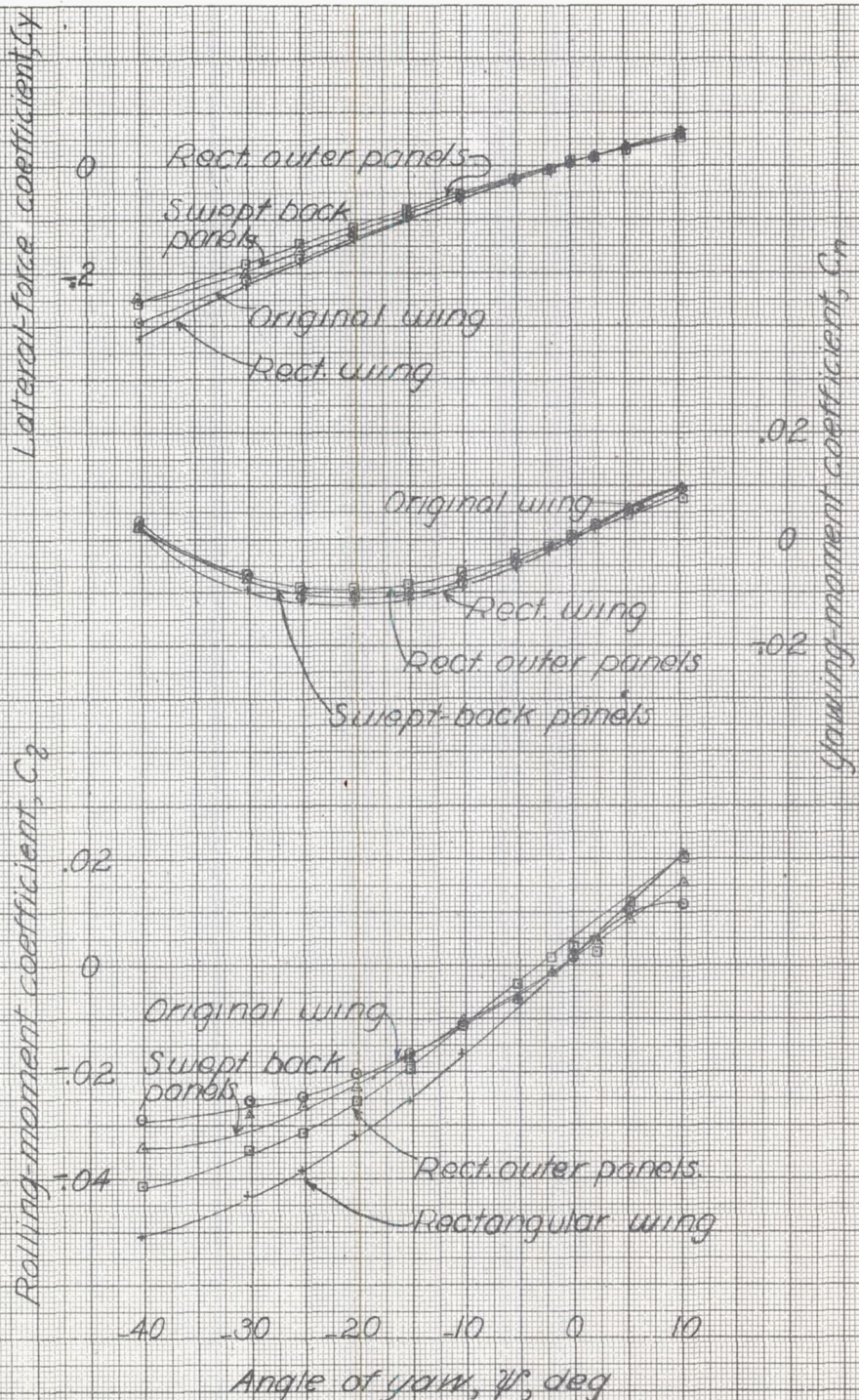
Figure 19.- Effect of wing plan form on the aerodynamic characteristics in yaw of the 1/6-scale model of the XBTC-2 airplane. Cruising configuration; Tail off.

(a) Propeller windmilling, $\alpha \approx 0.2°$.

Pitching-moment coefficient, C_m

.1

0

-.1

Resultant-drag coefficient, C_{DR}

Original wing
Swept-back panels
Rect. outer panels
Rectangular wing

.1

0

-.1

Lift coefficient, C_L

.4

0

-40   -30   -20   -10   0   10

Angle of yaw, ψ, deg

(a) Concluded.

Figure 19.- continued

Lateral-force coefficient, C_Y

Rect. outer panels

Rect. wing

Swept back panels

Original wing

Yawing-moment coefficient, C_n

.02

0

-.02

Original wing

Rect. outer panels

Rect. wing

Swept-back panels

Rolling-moment coefficient, C_l

.02

0

-.02

-.04

Swept back panels

Original wing

Rectangular wing

Rect. outer panels

-40   -30   -20   -10   0   10

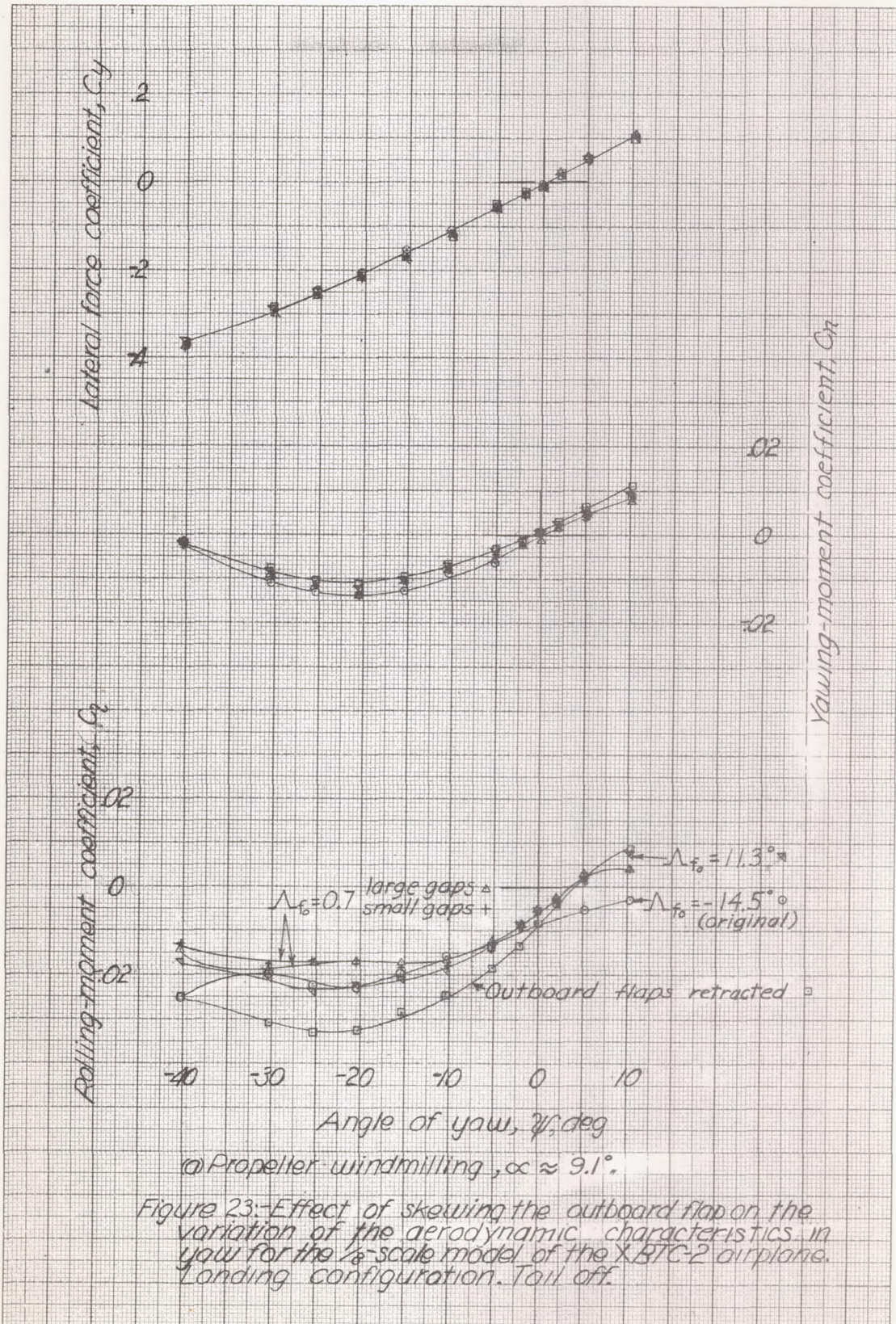Angle of yaw, ψ, deg

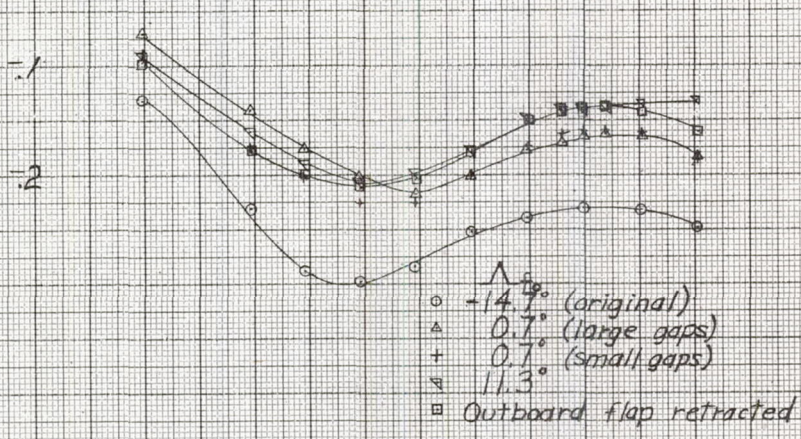(b) Take-off power, $\alpha \approx 0.2°$.

Figure 19.- continued.
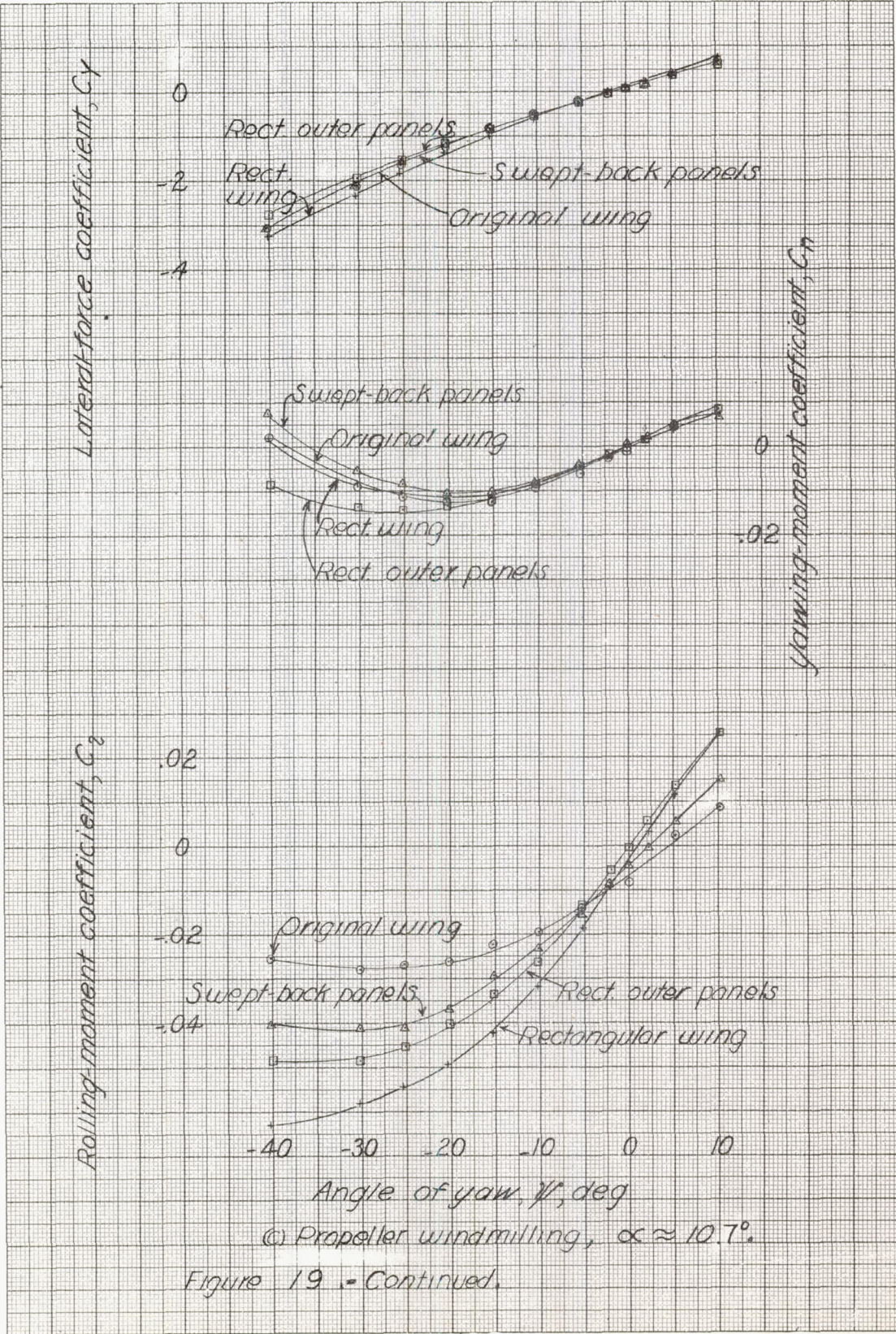
Pitching-moment coefficient, C_m

Resultant-drag coefficient, C_{DR}

Lift coefficient, C_L

.1

0

-.1

0

-.1

.4

0

Swept-back panels □
Rectangular wing +
Original wing ○
Rect. outer panels △

-40   -30   -20   -10   0   10

Angle of yaw, ψ, deg

(b) Concluded.

Figure 19.- continued.

Figure 19 .- Continued.

(c) Propeller windmilling, $\alpha \approx 10.7°$.

Original wing
Swept-back panels
Rect. outer panels
Rectangular wing

(c) Concluded.
Figure 19.- continued.

L-787
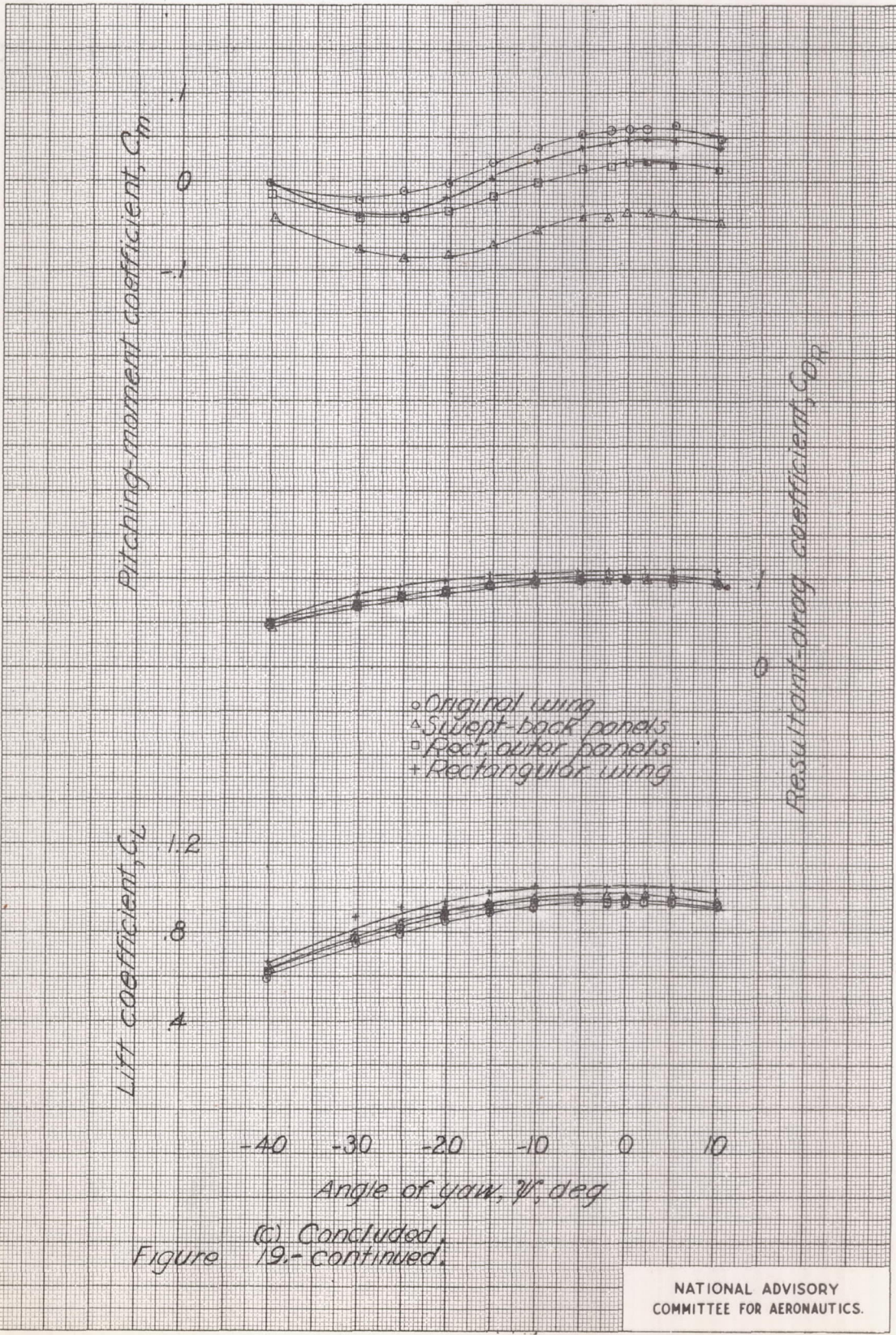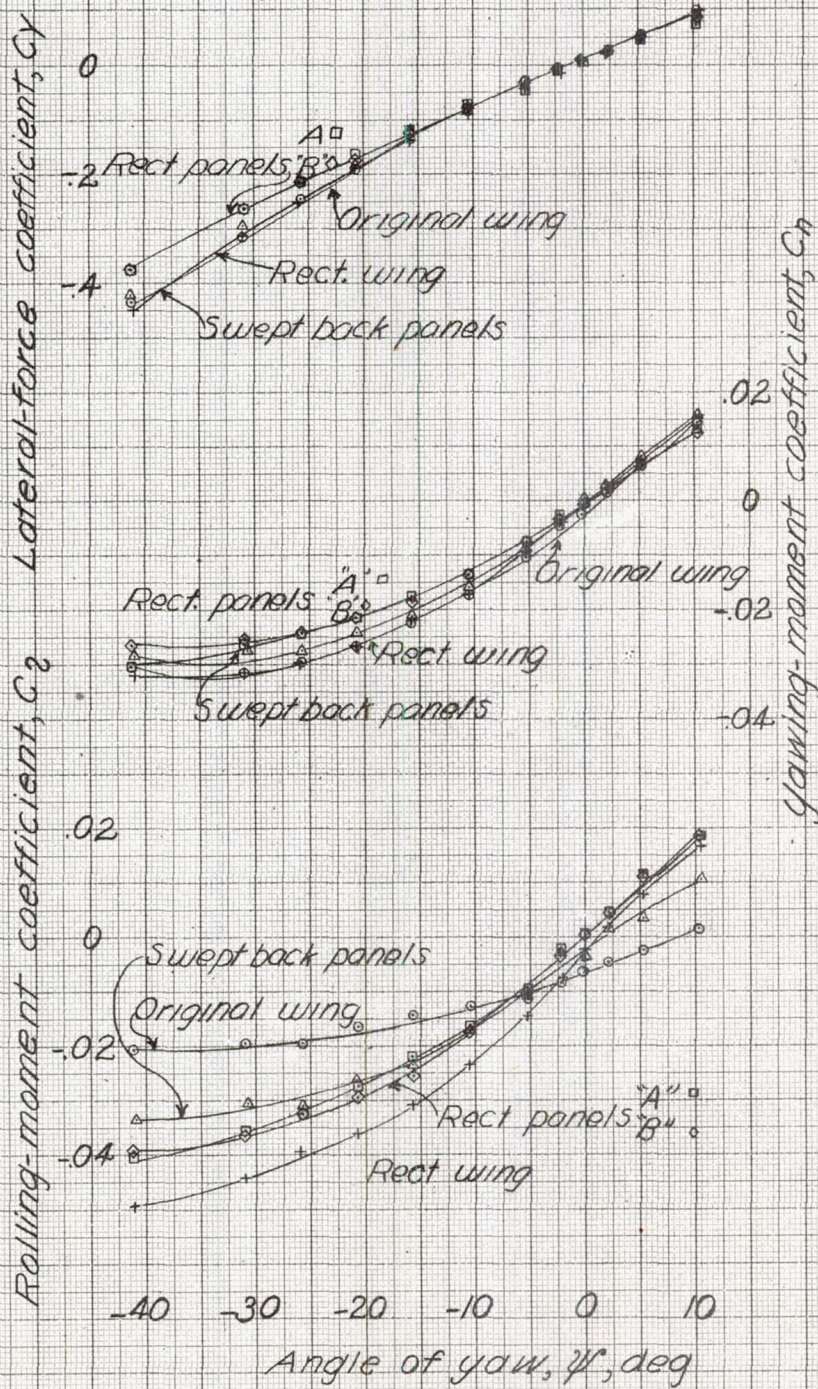
(d) Take-off power, $\alpha \approx 9.0°$.

Figure 19.—continued.

Pitching-moment coefficient, C_m

Resultant-drag coefficient, C_{DR}

Lift coefficient, C_L

○ Original wing
△ Swept-back panels
□ Rect. outer panels "A"
◇ Rect. outer panels "B"
+ Rect. wing

.1
0
-.1

-.2
-.3
-.4
-.5

1.2
.8
.4

-40   -30   -20   -10   0   10

Angle of yaw, ψ, deg
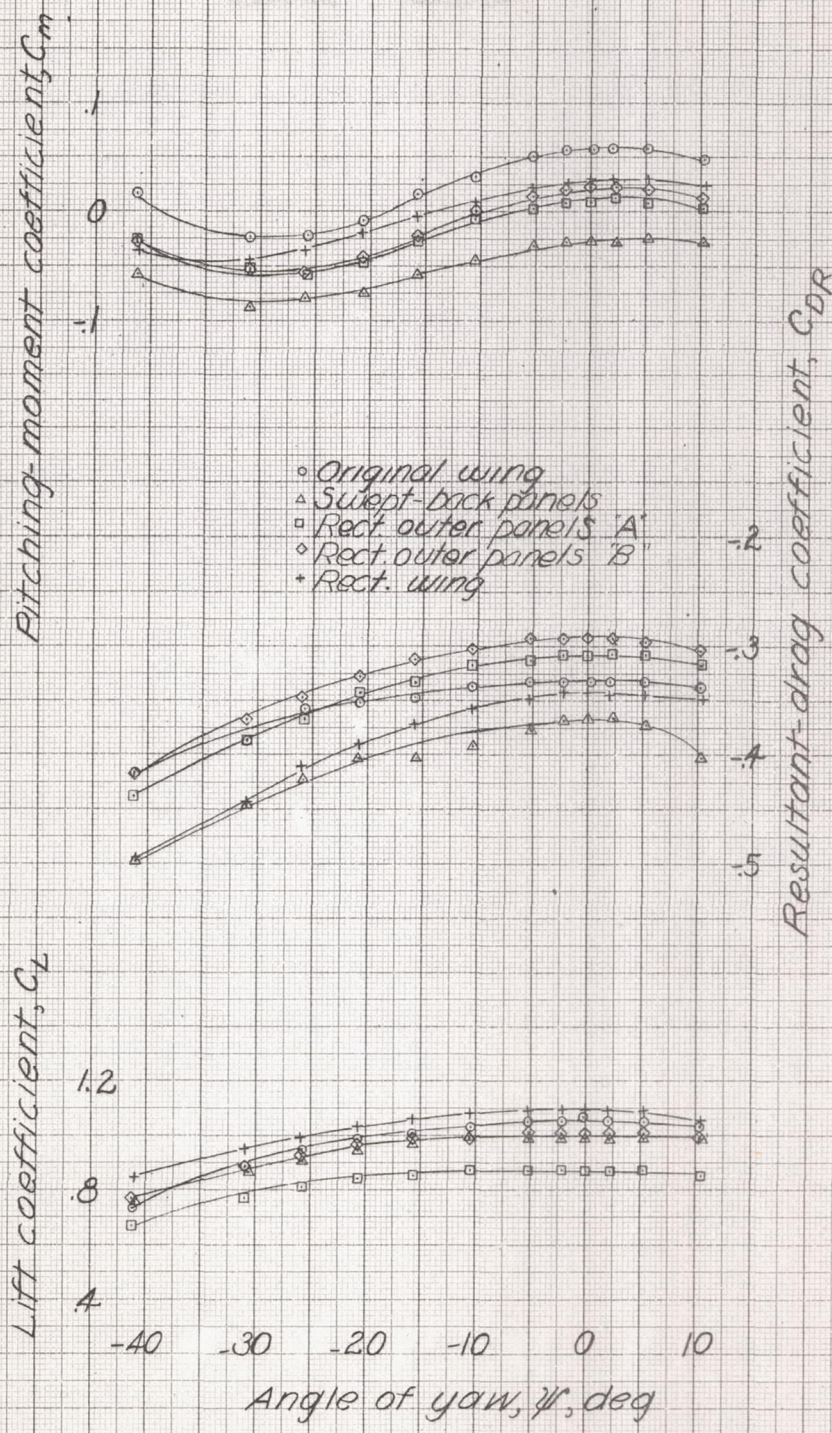
(d) Concluded.

Figure 19.- concluded.
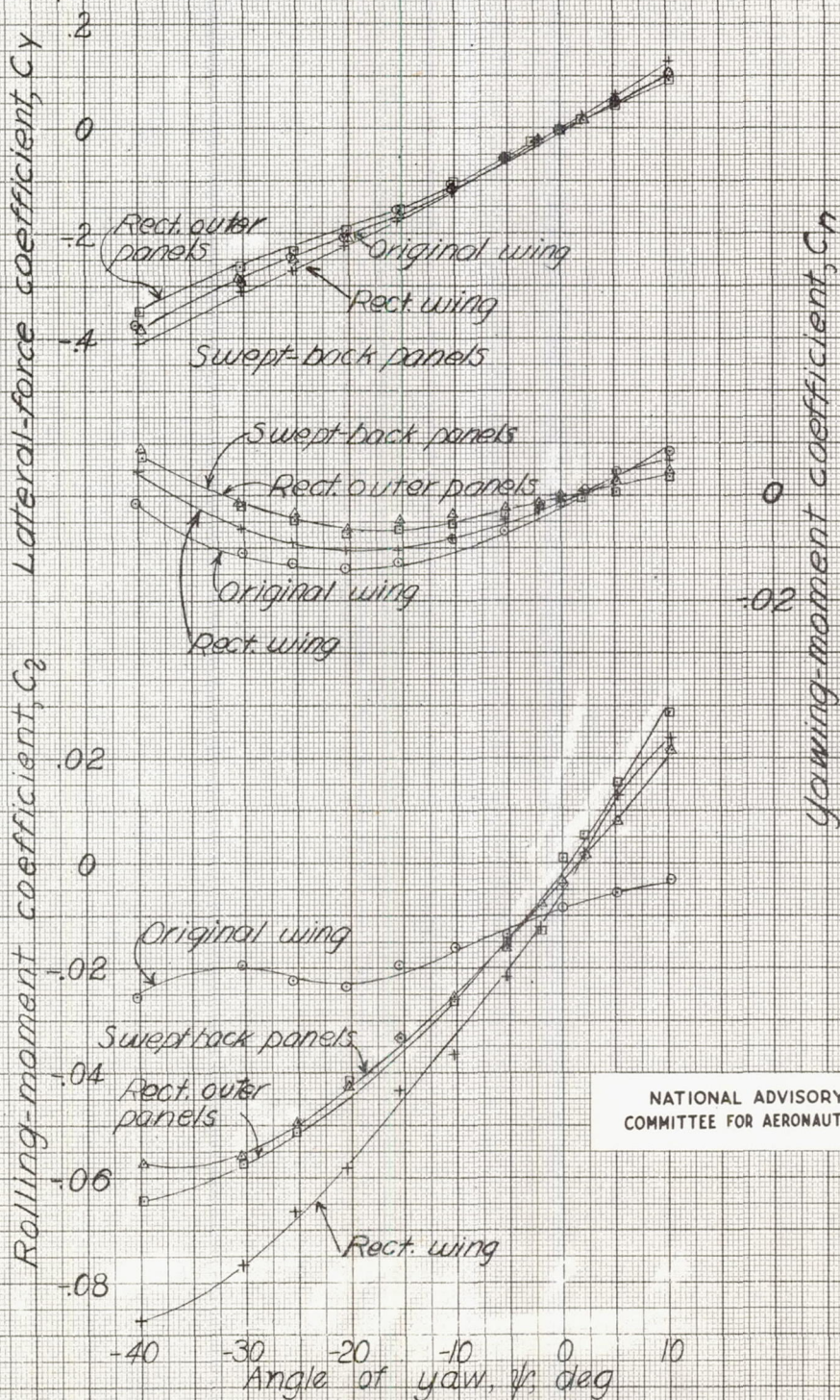
(a) Propeller windmilling, $\alpha \approx 9.2°$.

Figure 20.- Effect of wing plan form on the aero-dynamic characteristics in yaw of the XBTC-2 airplane. Landing configuration; Tail off.

Pitching-moment coefficient, C_m

Resultant-drag coefficient, C_{DR}

Lift coefficient, C_L

o Original wing
◇ Swept-back panels
□ Rect. outer panels
+ Rectangular wing

-40   -30   -20   -10   0   10

Angle of yaw, ψ, deg

(a) Concluded.

Figure 20.- continued.

(b) Take-off power, $\alpha \approx 10.6$.

Figure 20.— continued.
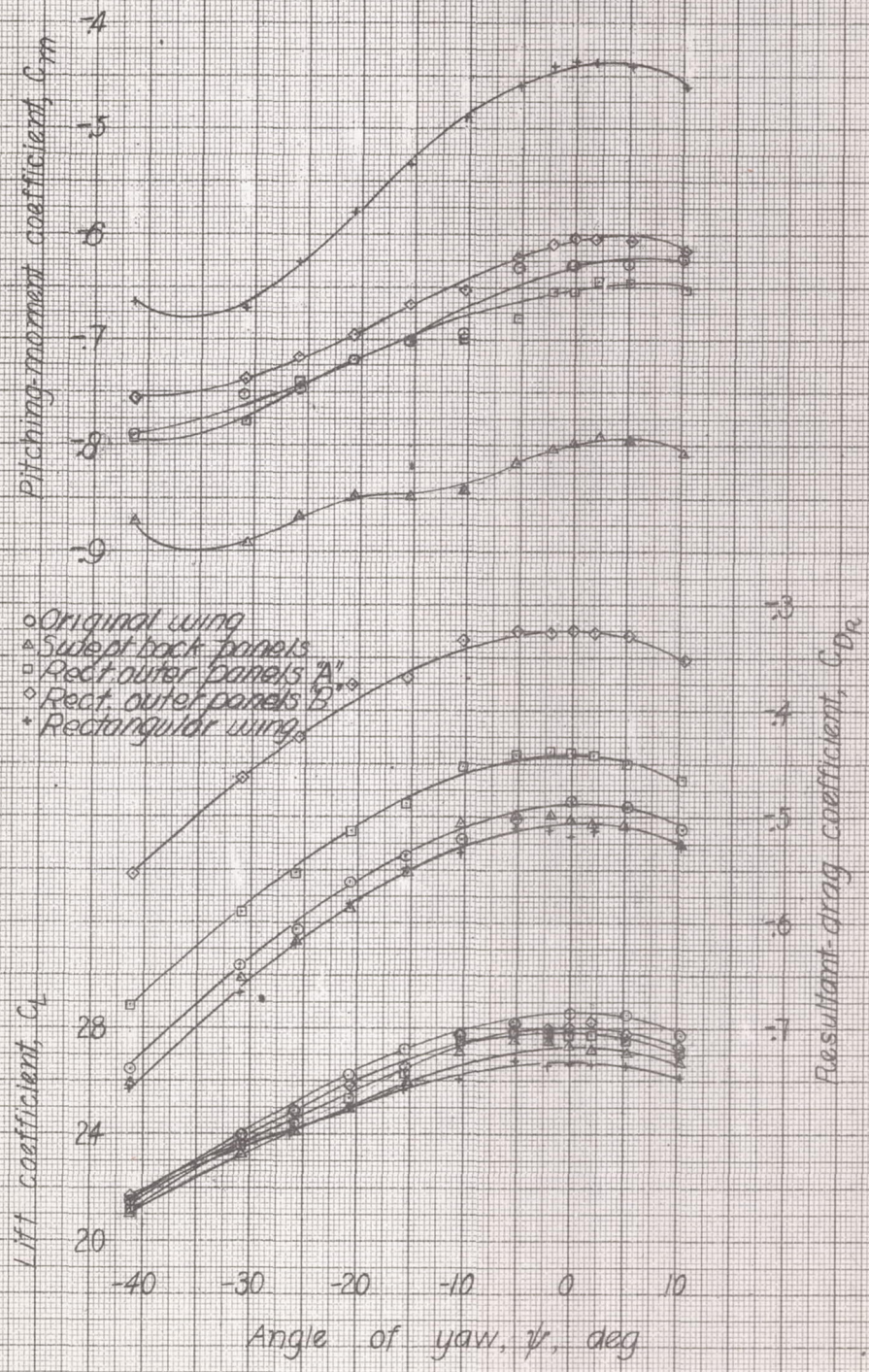
(b) Concluded.

Figure 20.- concluded.
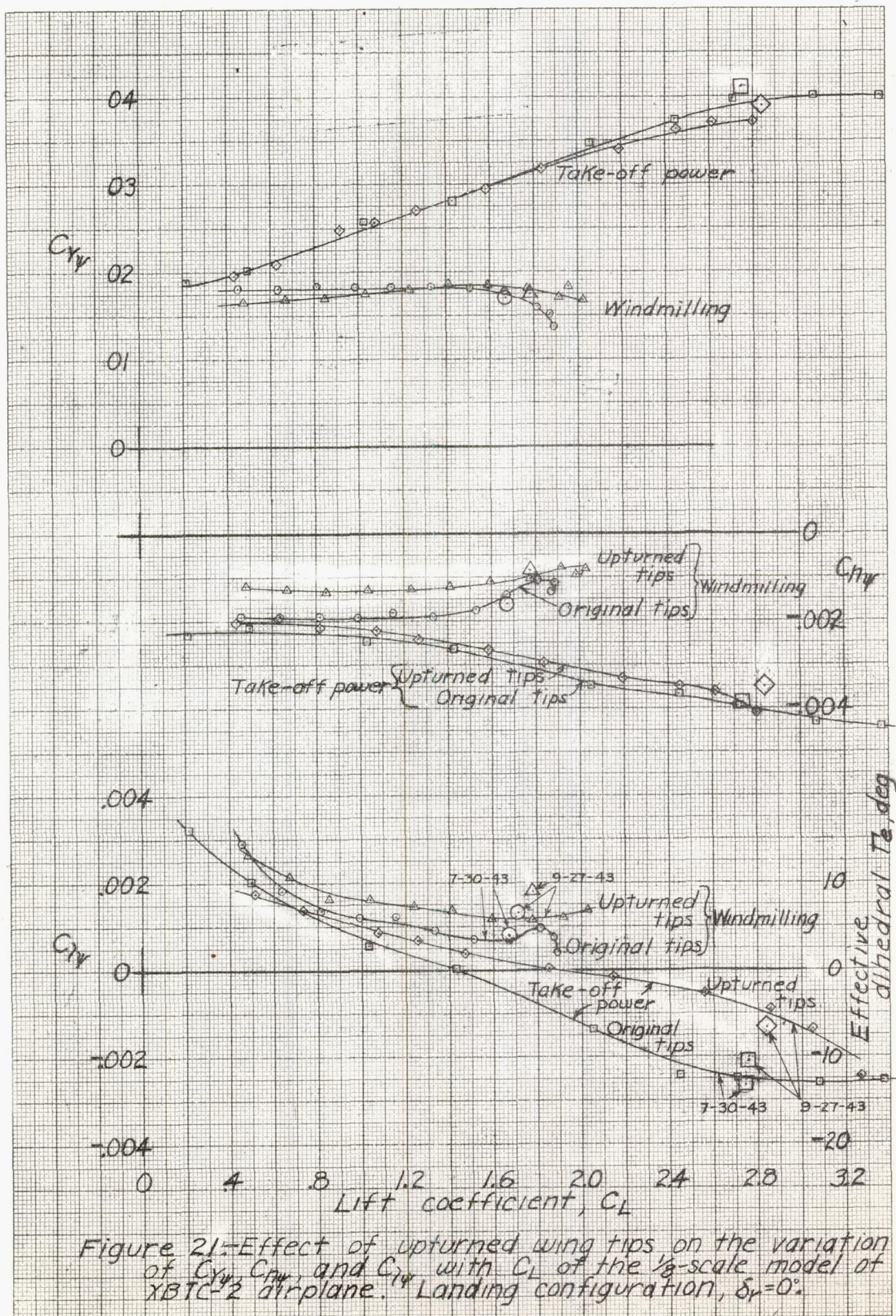
Figure 21.- Effect of upturned wing tips on the variation of C_{Y_ψ}, C_{n_ψ}, and C_{l_ψ} with C_L of the ⅓-scale model of XBTC-2 airplane. Landing configuration, $\delta_f = 0°$.

Figure 22. Effect of upturned wing tips on the aero-dynamic characteristics in yaw of the 1/8-scale model of the XBTC-2 airplane. Landing configuration, $\delta_r = 0°$ Dorsal D_1.
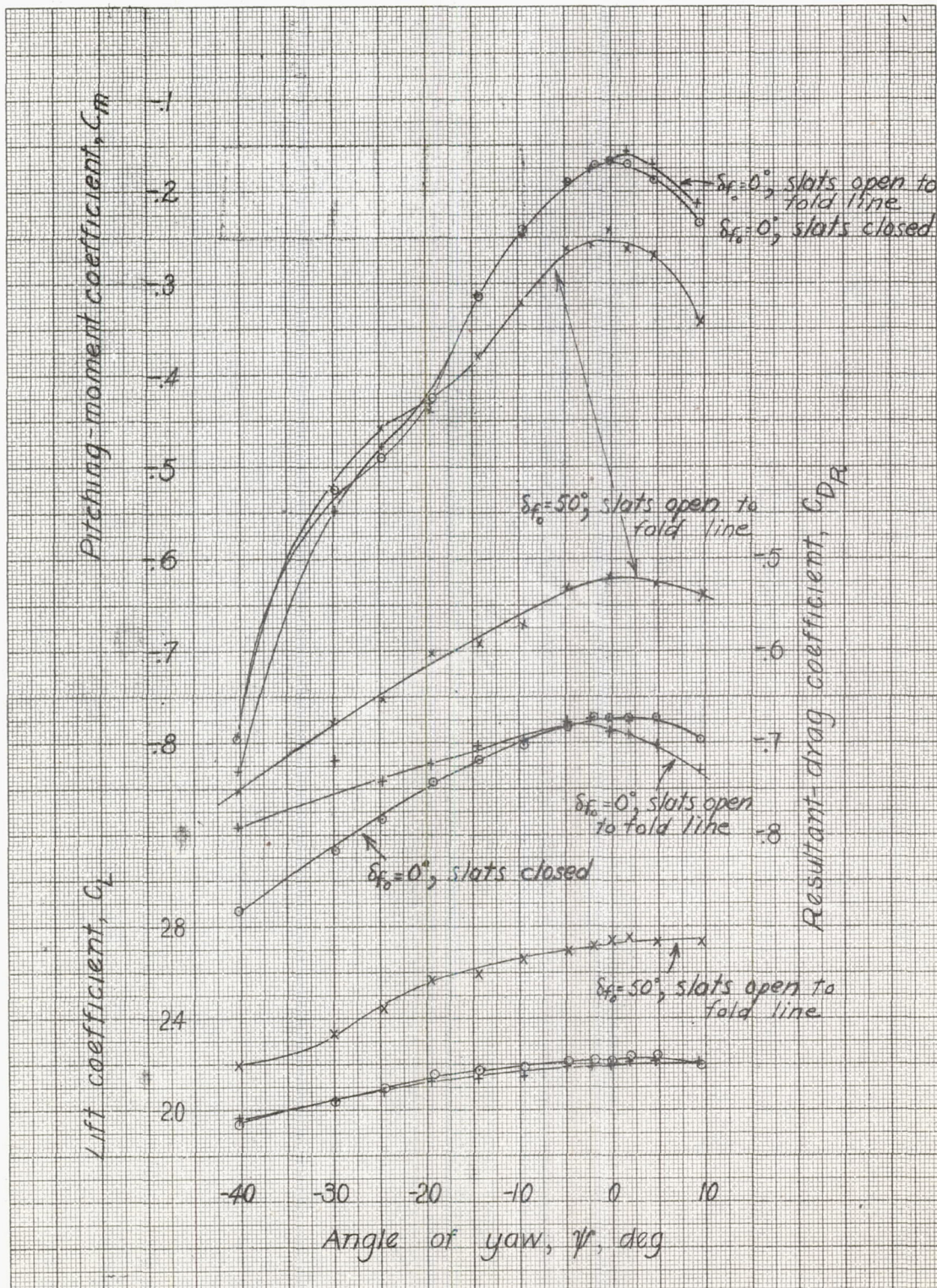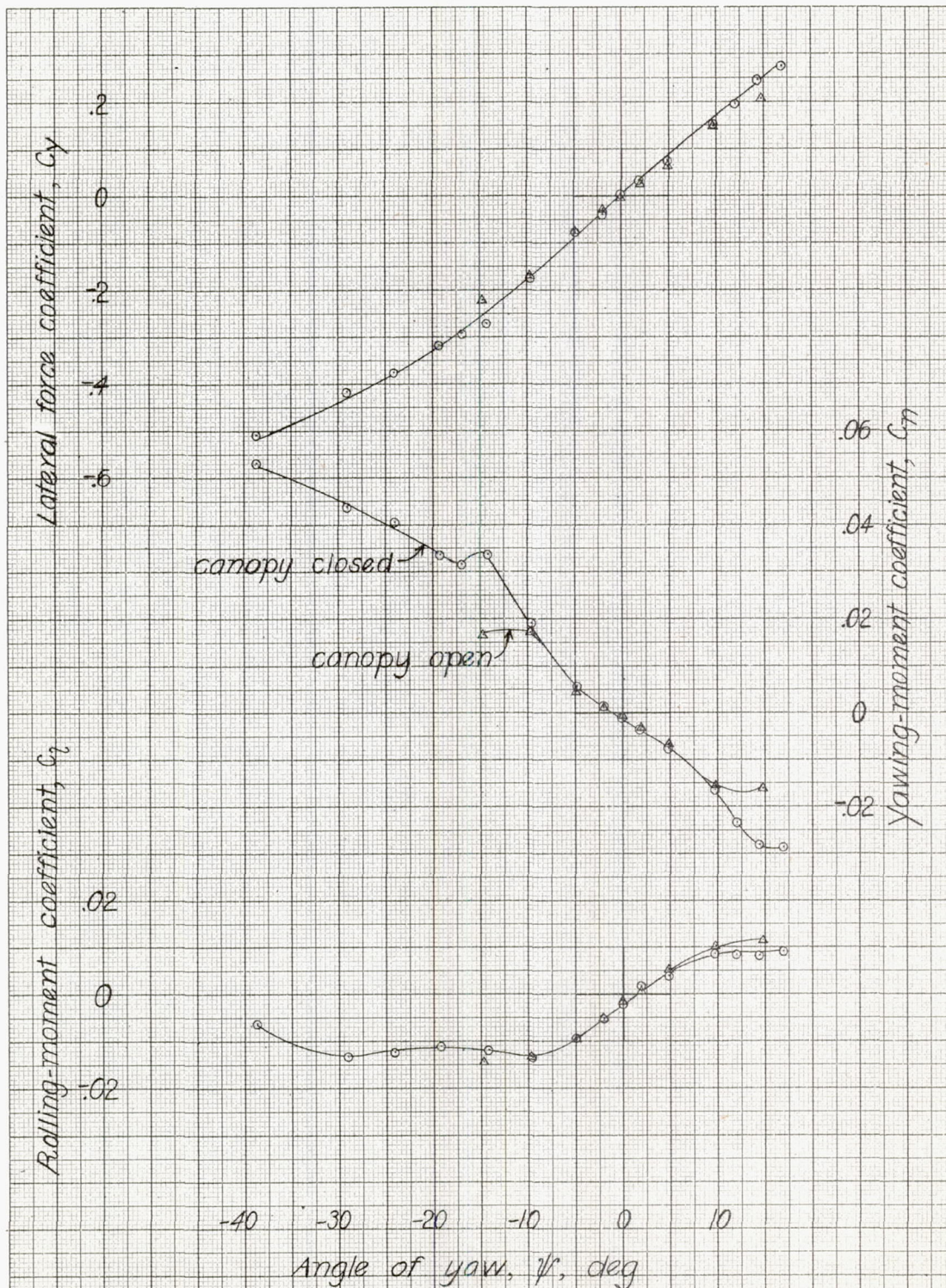
Figure 22.—Concluded.

Figure 23.- Effect of skewing the outboard flap on the variation of the aerodynamic characteristics in yaw for the ⅛-scale model of the XB7C-2 airplane. Landing configuration. Tail off.

(a) Propeller windmilling, $\alpha \approx 9.1°$.

Angle of yaw, ψ, deg

Rolling-moment coefficient, C_l

Lateral force coefficient, C_Y

Yawing-moment coefficient, C_n

$\Lambda_{f_o} = 0.7$ large gaps
small gaps

$\Lambda_{f_o} = 11.3°$

$\Lambda_{f_o} = -14.5°$ (original)

Outboard flaps retracted

Pitching-moment coefficient, C_m

$-.1$

$-.2$

Resultant drag coefficient, C_{DR}

.3

.2

.1

$\wedge_{f_o}$
○ $-14.7°$ (original)
△ $0.7°$ (large gaps)
$+$ $0.7°$ (small gaps)
▽ $11.3°$
☐ Outboard flap retracted

Lift coefficient, C_L

16

12

8

○ $\wedge_{f_o} = -14.5°$ (original)
△ $\wedge_{f_o} = 0.7°$
▽ $\wedge_{f_o} = 11.3°$
☐ Outboard flaps retracted

-40 -30 -20 -10 0 10

Angle of yaw, ψ, deg

(a) Concluded.

Figure 23-Continued.

(b) Take-off power, $\alpha \approx 10.5°$.

Figure 23.-continued.

Pitching moment coefficient, C_m

.5

-.6

-.7

-.8

Resultant drag coefficient, C_{D_R}

-.5

-.6

-.7

$\Lambda_{f_0} = -14.5°$ (original)

$\Lambda_{f_0} = 0.7°$ (small gaps)

Lift coefficient, C_L

.28

.24

.20

-40   -30   -20   -10   0   10

Angle of yaw ψ, deg

(b) Concluded.

Figure 23.- Concluded.

NATIONAL ADVISORY
COMMITTEE FOR AERONAUTICS.
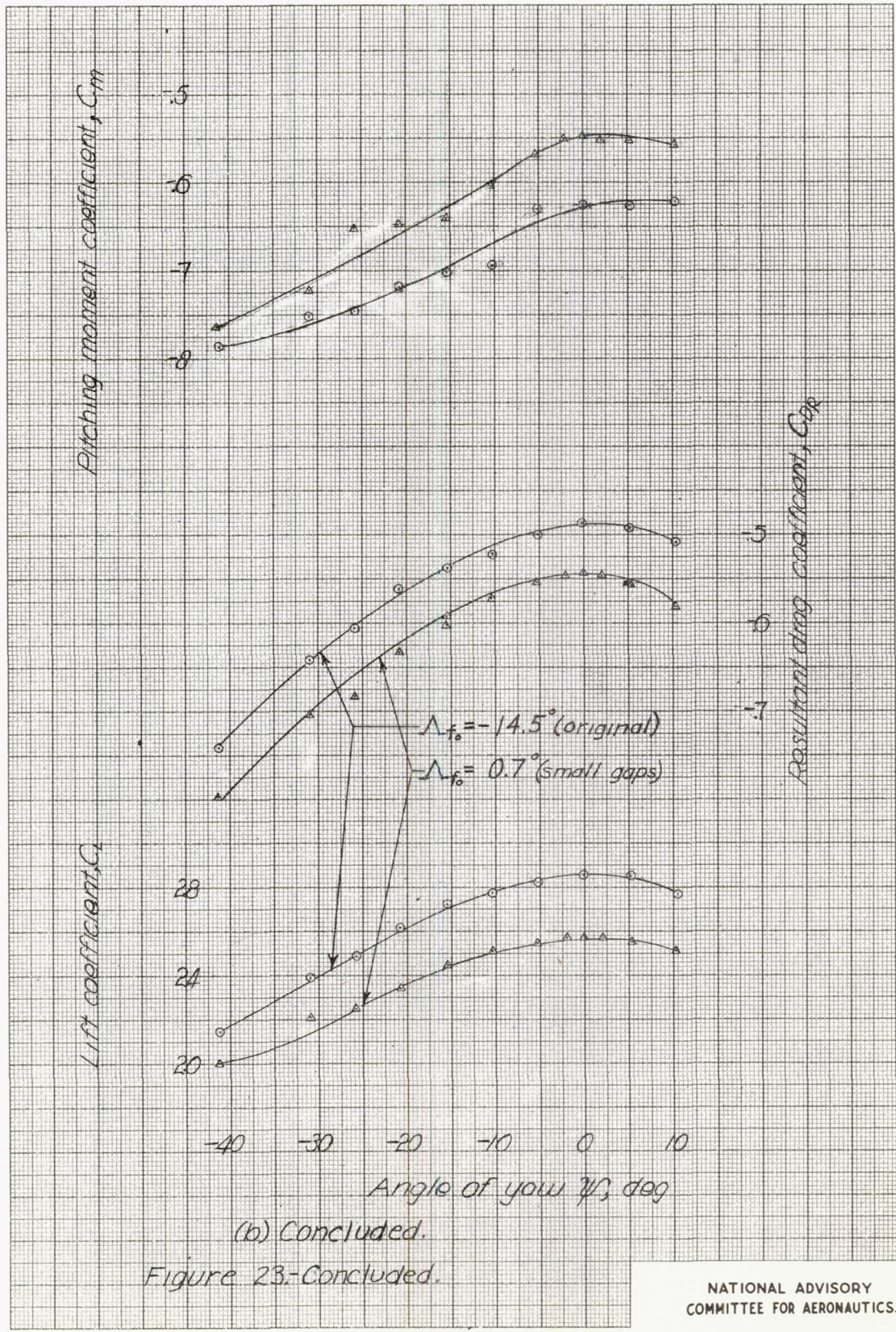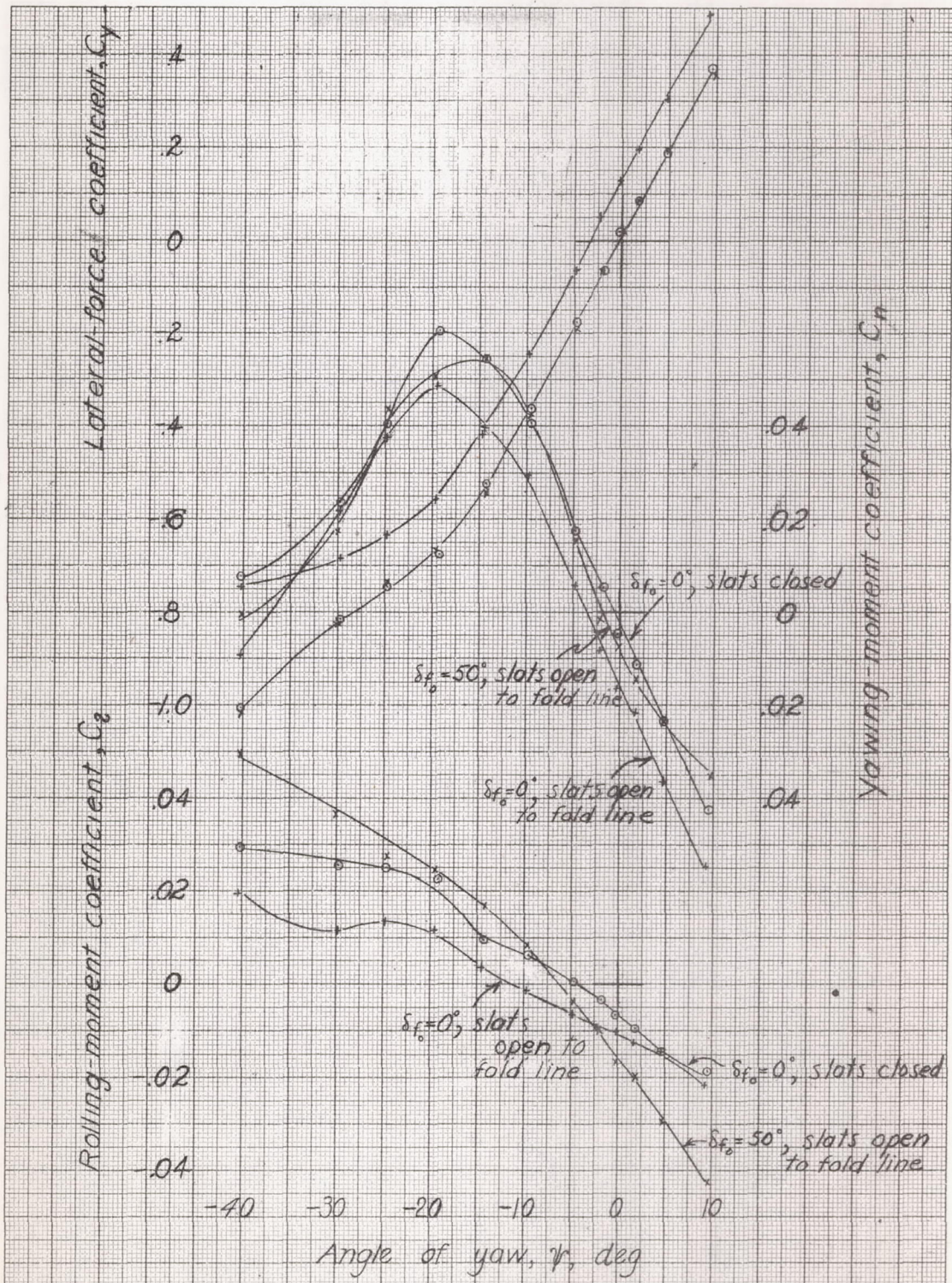
Figure 24.-Effect of outboard flap and slats on the aerodynamic characteristics in yaw of the 1/8-scale model of the XBTC-2 airplane. Landing configuration. Take-off power. $\alpha = 10.3°$.

Figure 24.- concluded.
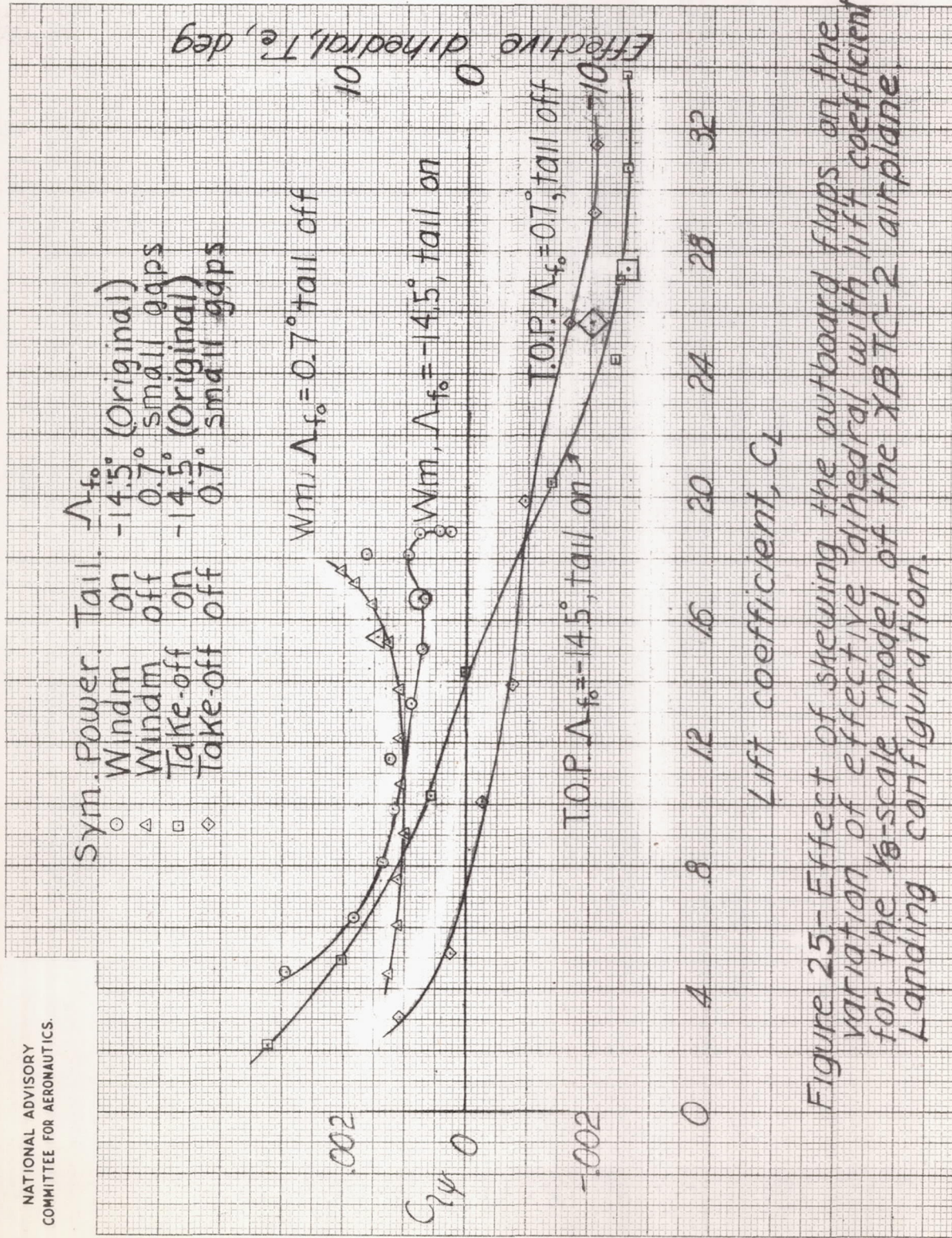
Figure 25- Effect of skewing the outboard flaps on the
variation of effective dihedral with lift coefficient
for the 1/8-scale model of the XBTC-2 airplane.
Landing configuration.

Figure 26.- Effect of canopy opening on the aerodynamic characteristics in yaw of the 1/8- scale model of the XBTC-2 airplane. Landing configuration. Propeller windmilling. $\delta_f = 0$. $\alpha \approx 9.3°$ $C_L \approx 1.7$ at $\psi = 0°$.
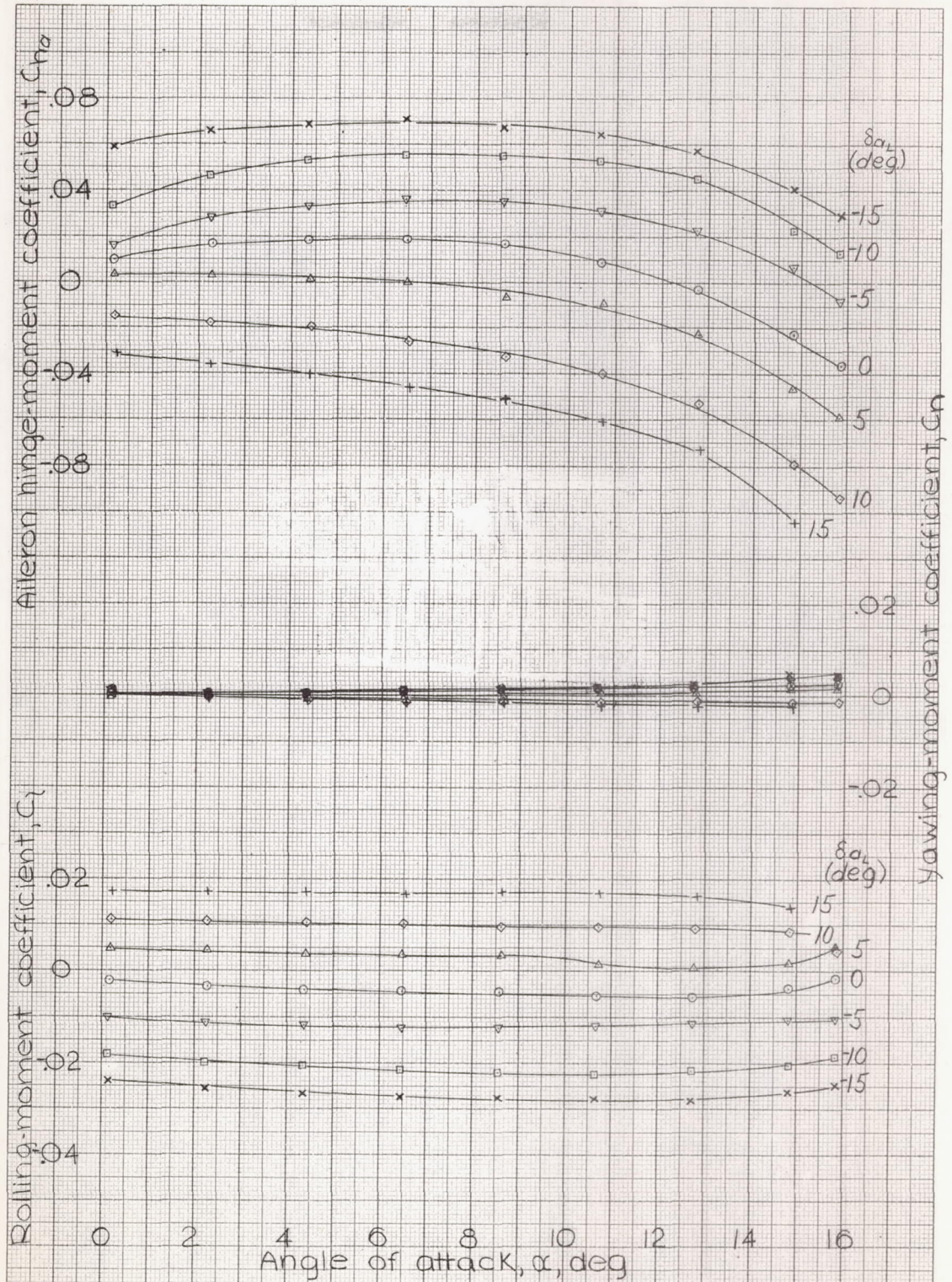
(a) Cruising configuration.

Figure 27.- Aileron characteristics of the 1/8-scale model of the XBTC-2 airplane. Transition fixed at .10 c_w Original wing.

(b) Landing configuration. (L.E. slot open to fold line.)

Figure 27.- Concluded.
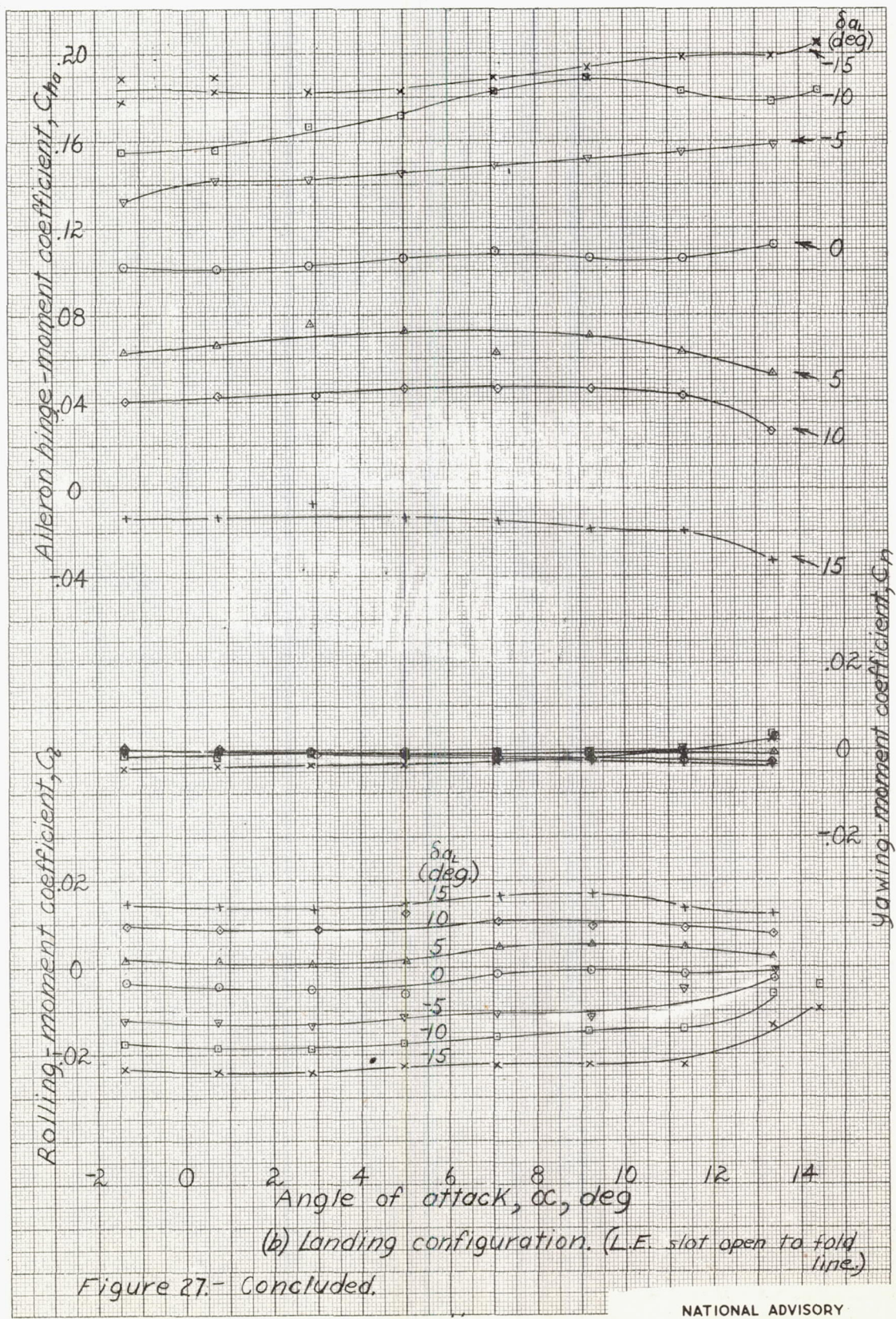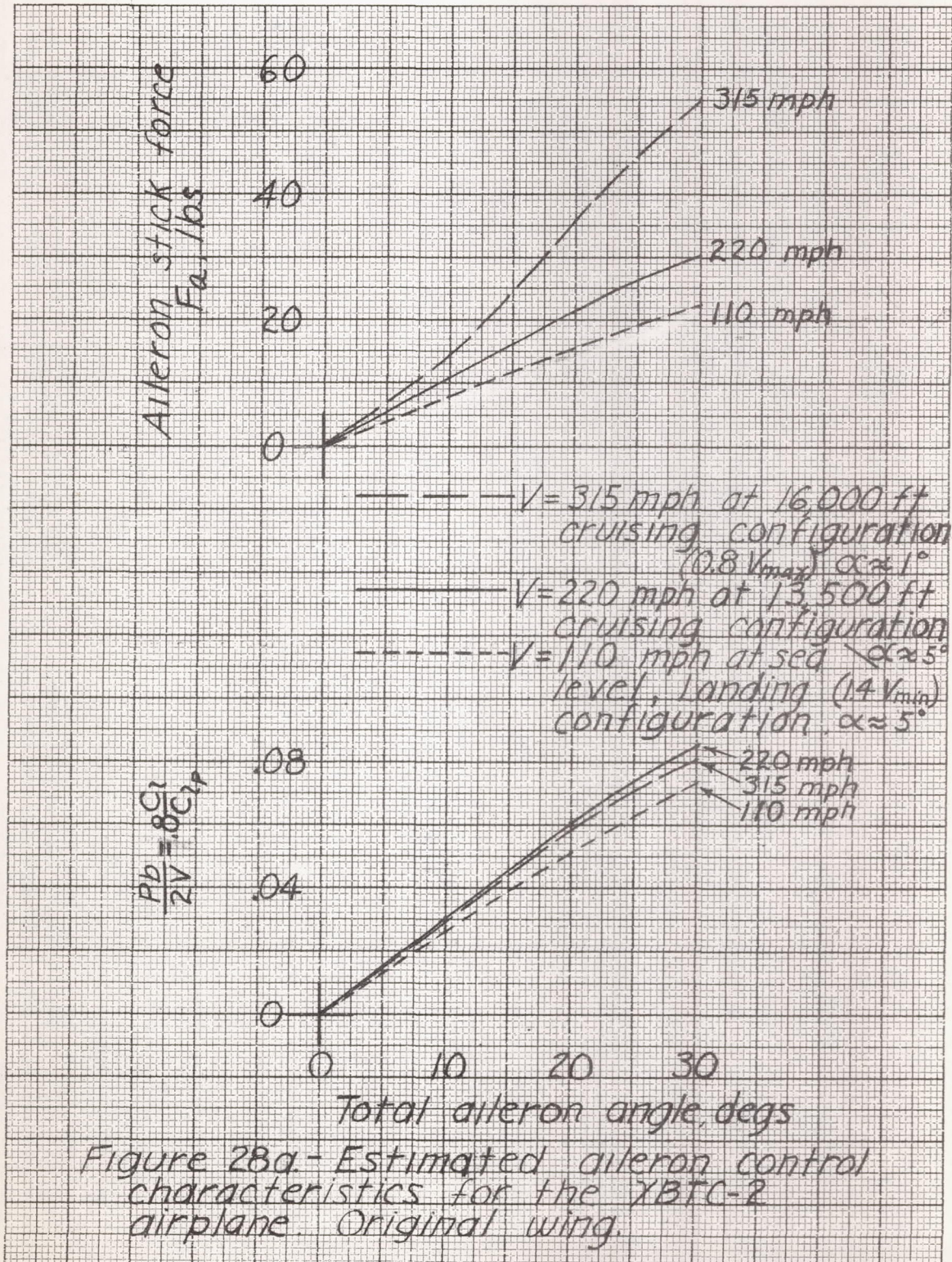
Figure 28a. - Estimated aileron control characteristics for the XBTC-2 airplane. Original wing.

Aileron stick force F_a, lbs

60

40

20

0

315 mph

220 mph

110 mph

— — — $V = 315$ mph at 16,000 ft
cruising configuration
(0.8 V_{max}) $\alpha \approx 1°$
———— $V = 220$ mph at 13,500 ft
cruising configuration
——— $V = 110$ mph at sea $\alpha \approx 5°$
level, landing (1.4 V_{min})
configuration $\alpha \approx 5°$

$\frac{Pb}{2V} = .8 \frac{C_l}{C_{l_p}}$

.08

.04

0

220 mph
315 mph
110 mph

0   10   20   30

Total aileron angle, degs
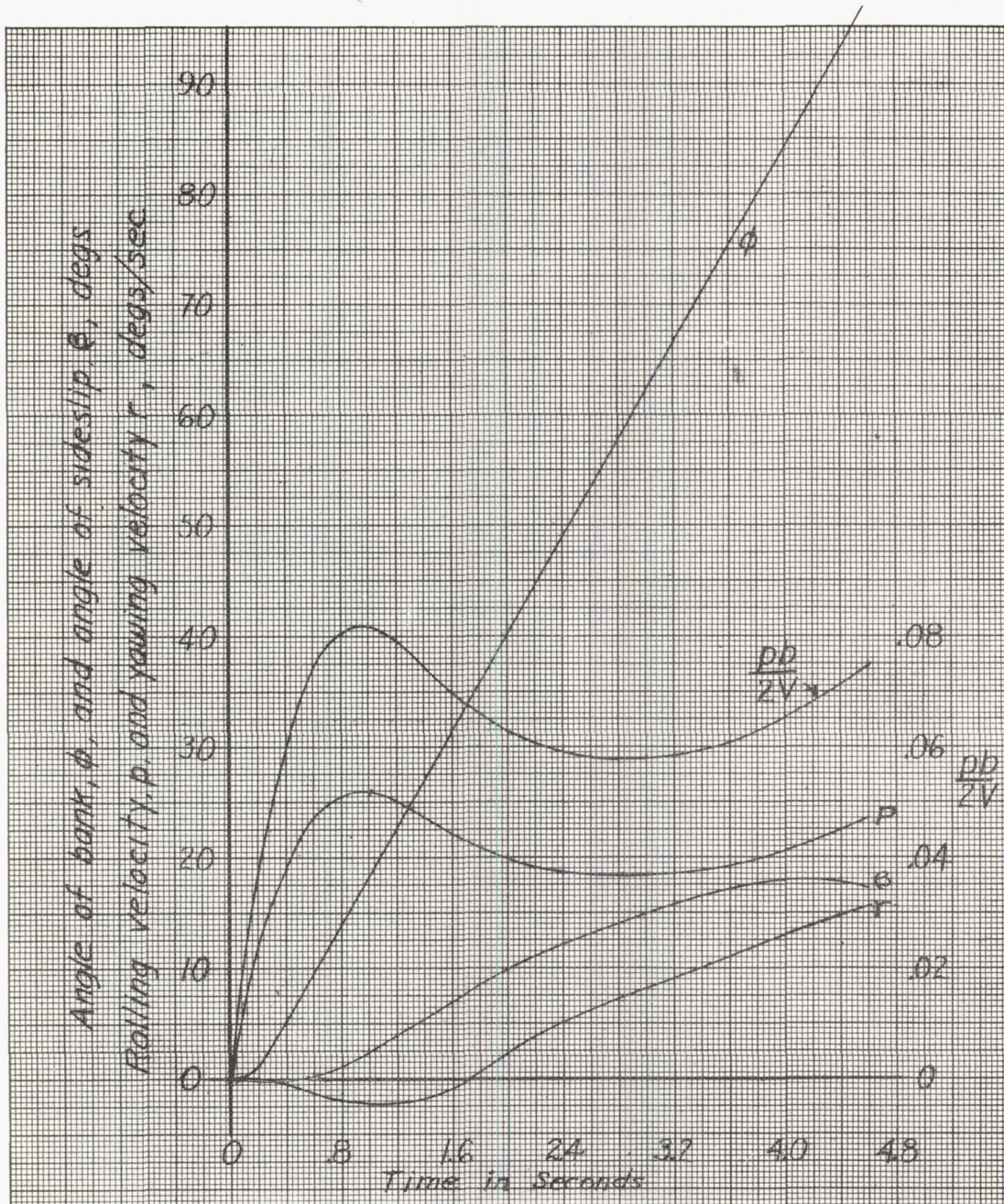
Figure 28b.-Theoretical time history of the rolling sideslipping and yawing motions of the XBTC-2 airplane as a consequence of an abrupt full-right aileron deflection. V=144 mph at sea level. Landing configuration. Swept-back outer panels. Propeller windmilling. $\delta_r = 0°$.
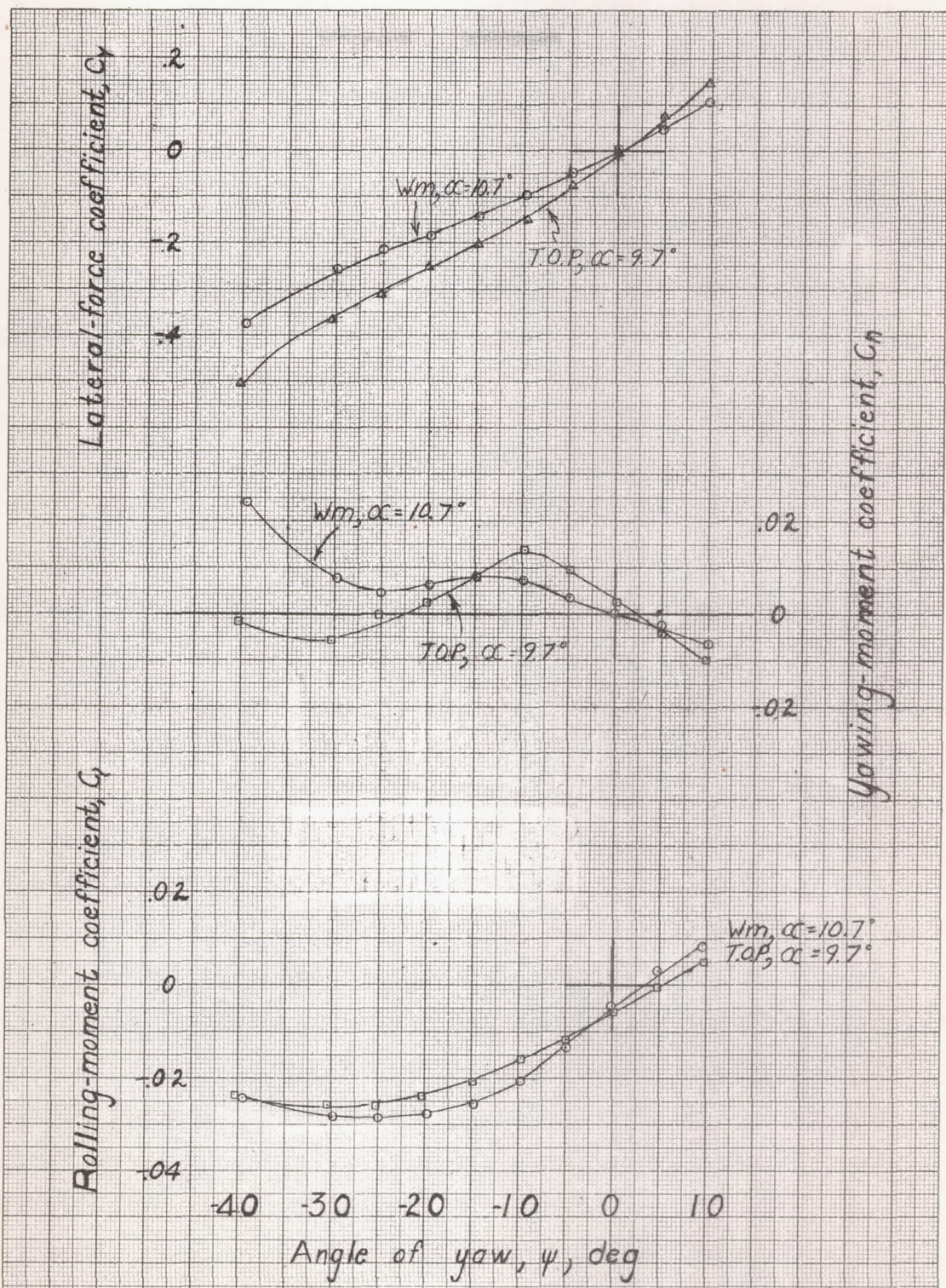
(a) Cruising configuration, Original tail and dorsal.

Figure 29.- Effect of free rudder on the aerodynamic characteristics in yaw of the 1/8-scale model of the XBTC-2 airplane. Rudder stops ±30°.

Lateral forces coefficient, C_Y

Revised tail
dorsal D_1

Revised tail
no dorsal

Original tail
original dorsal

Yawing-moment coefficient, C_n

Rolling-moment coefficient, C_l

Angle of yaw, ψ, deg

(b) Landing configuration, Windmilling
$\alpha \approx 9.3°$, $C_L \approx 1.7$ at $\psi = 0°$
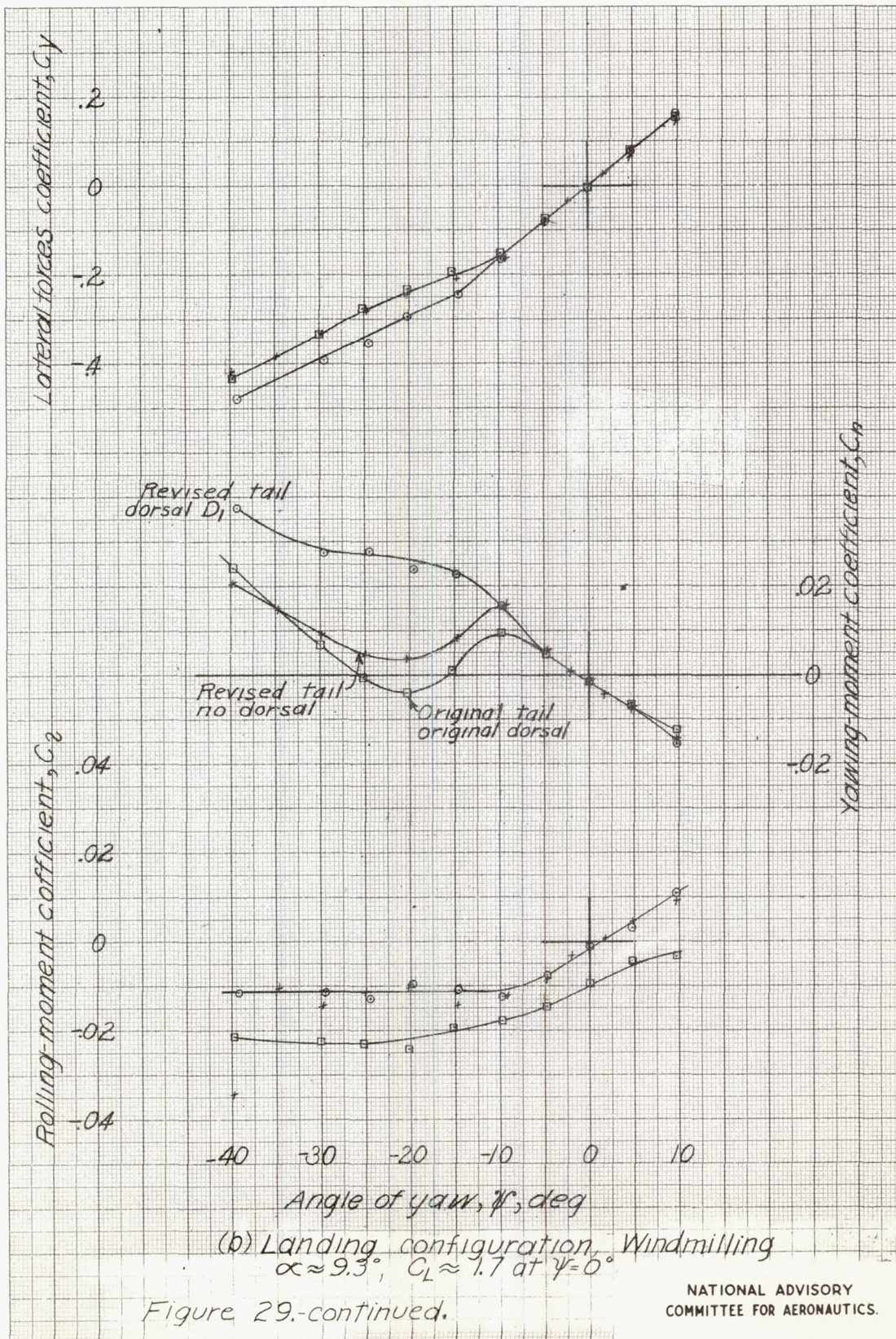
Figure 29.-continued.

NATIONAL ADVISORY
COMMITTEE FOR AERONAUTICS.
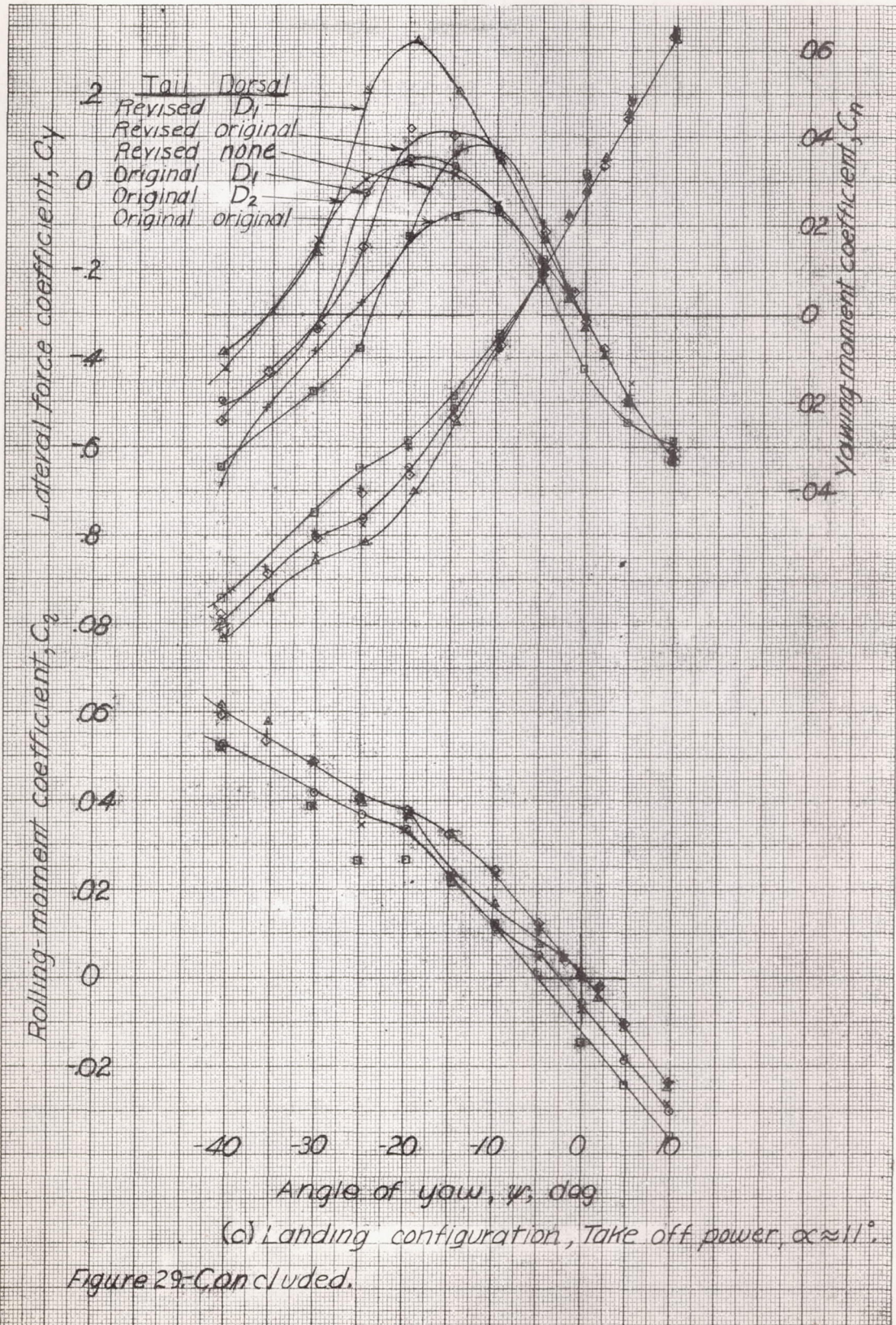
(c) Landing configuration, Take off power, $\alpha \approx 11°$.

Figure 29.- Concluded.
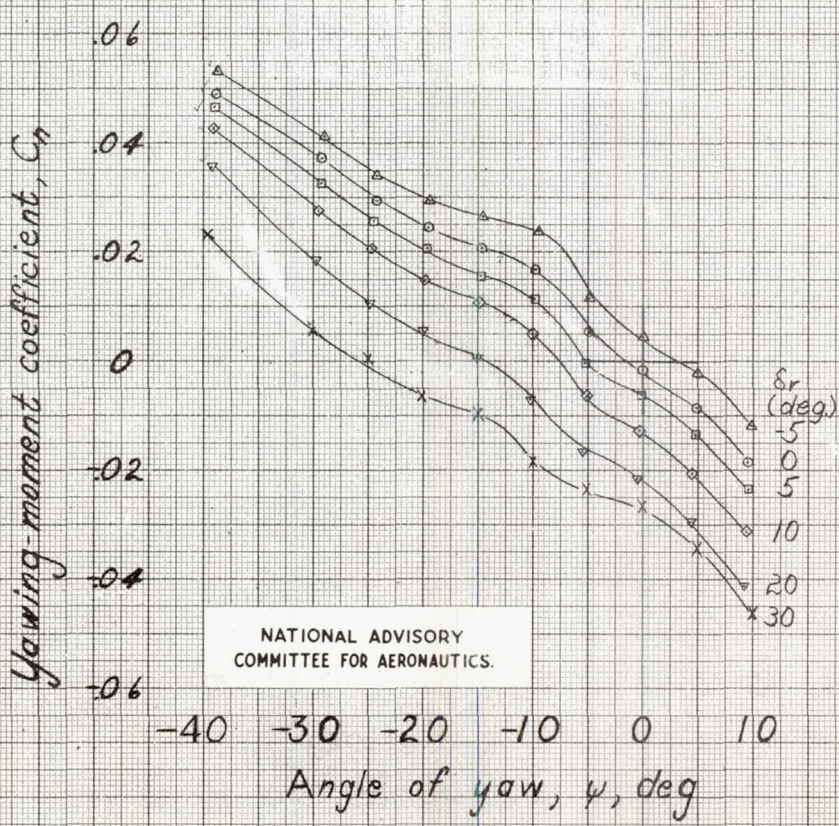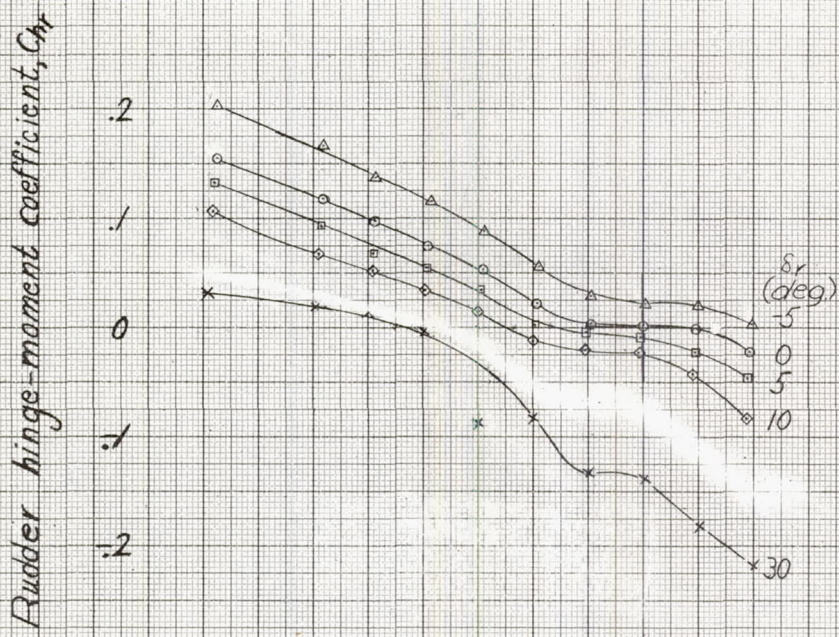
Figure 30- Effect of rudder deflection on the aerodynamic characteristics in yaw of the 1/8-scale model of the XBTC-2 airplane. Windmilling, landing configuration. Original vertical tail. $\alpha \approx 9.2$. Original dorsal.

$C_L \approx 1.66$ at $\gamma = 0°$

NATIONAL ADVISORY
COMMITTEE FOR AERONAUTICS.
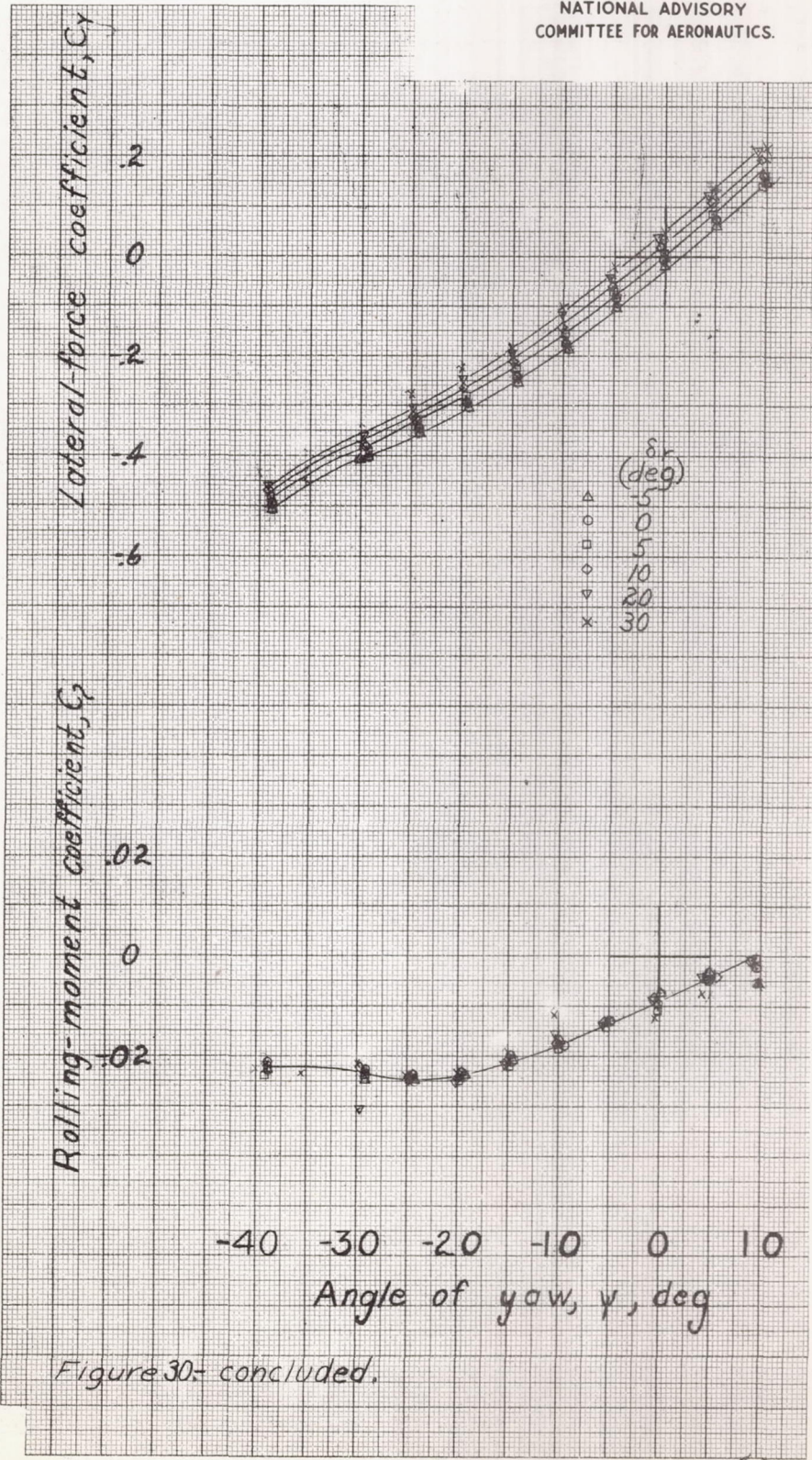
Figure 30.- concluded.
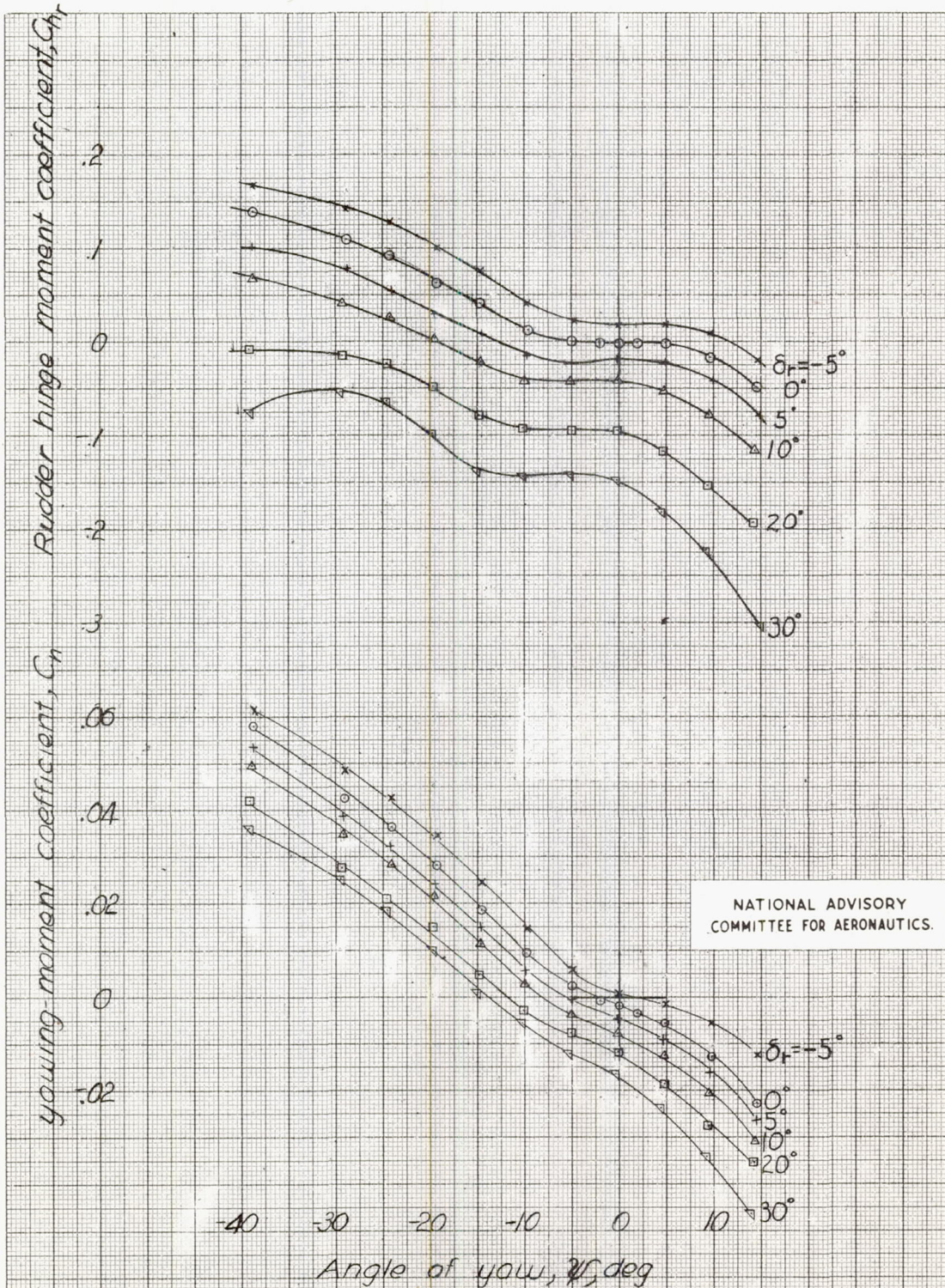
Figure 31.- Effect of rudder deflection on the aerodynamic characteristics in yaw of the $\frac{1}{5}$-scale model of the XBTC-2 airplane with the revised vertical tail $\alpha \approx 6.5$. Cruising configuration. Propeller windmilling Dorsal D_1.

Figure 3i.- Concluded.

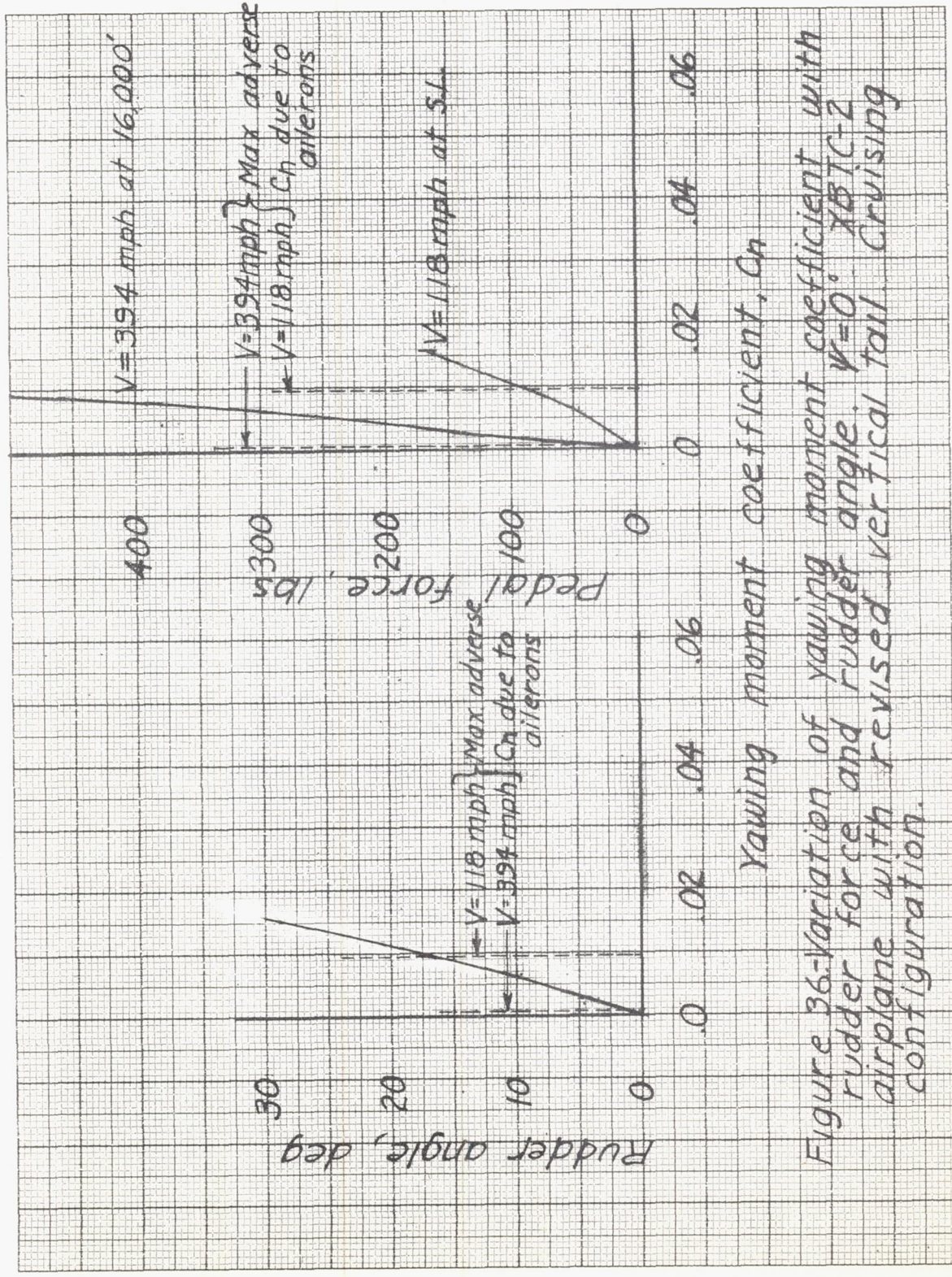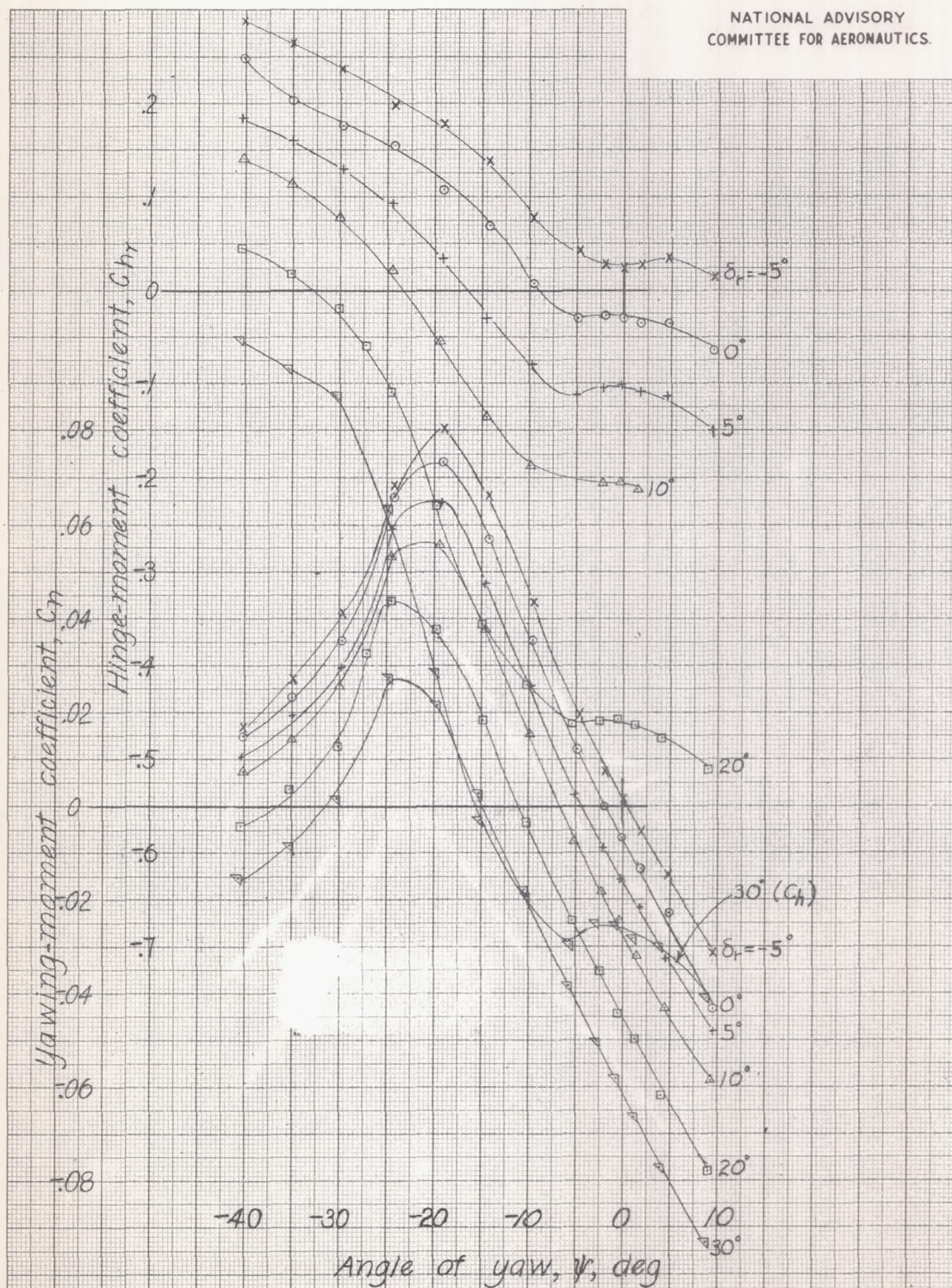Figure 32.- Effect of rudder deflection on the aerodynamic characteristics in yaw of the $\frac{1}{8}$-scale model of the XBTC-2 airplane with the revised vertical tail. $\alpha \approx 9.3°$ Landing configuration. Propeller windmilling. Dorsal D_1.
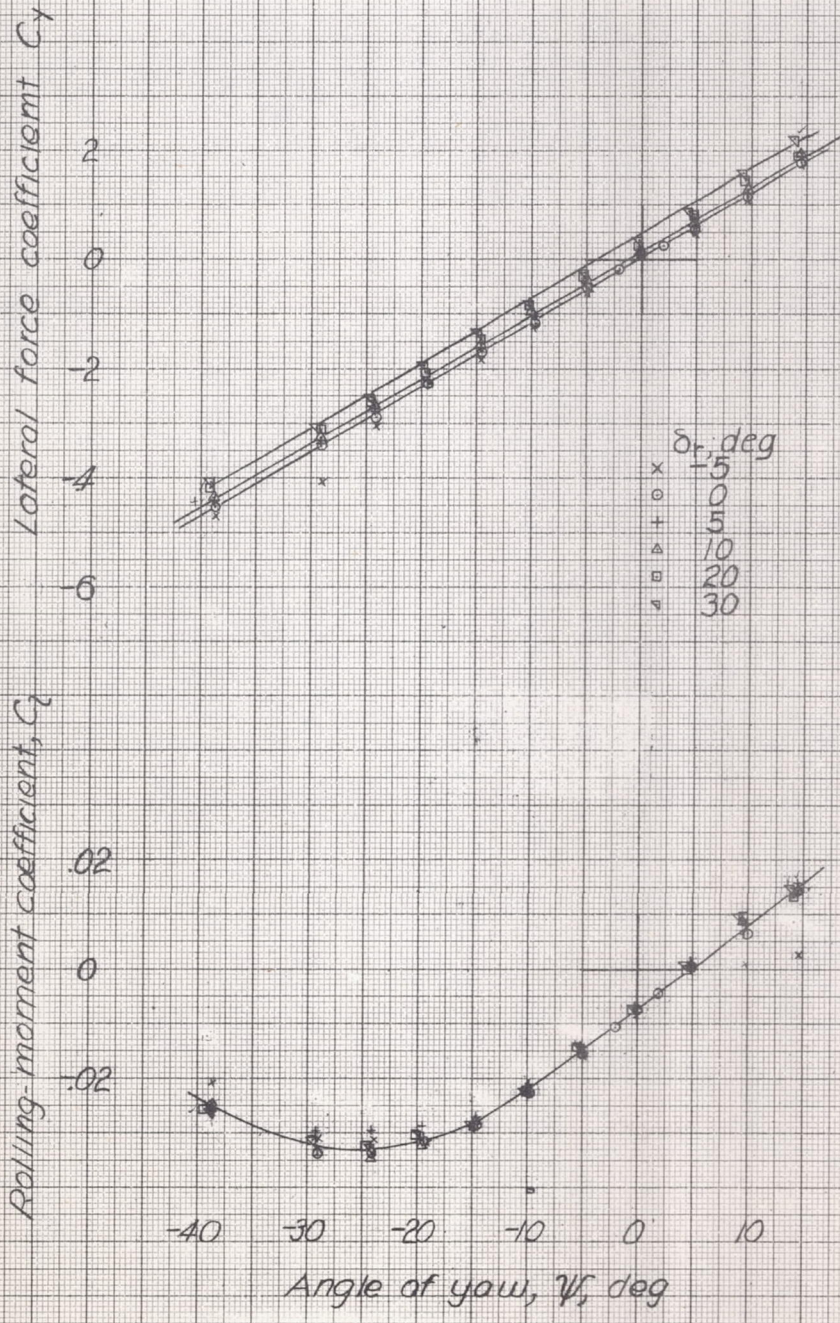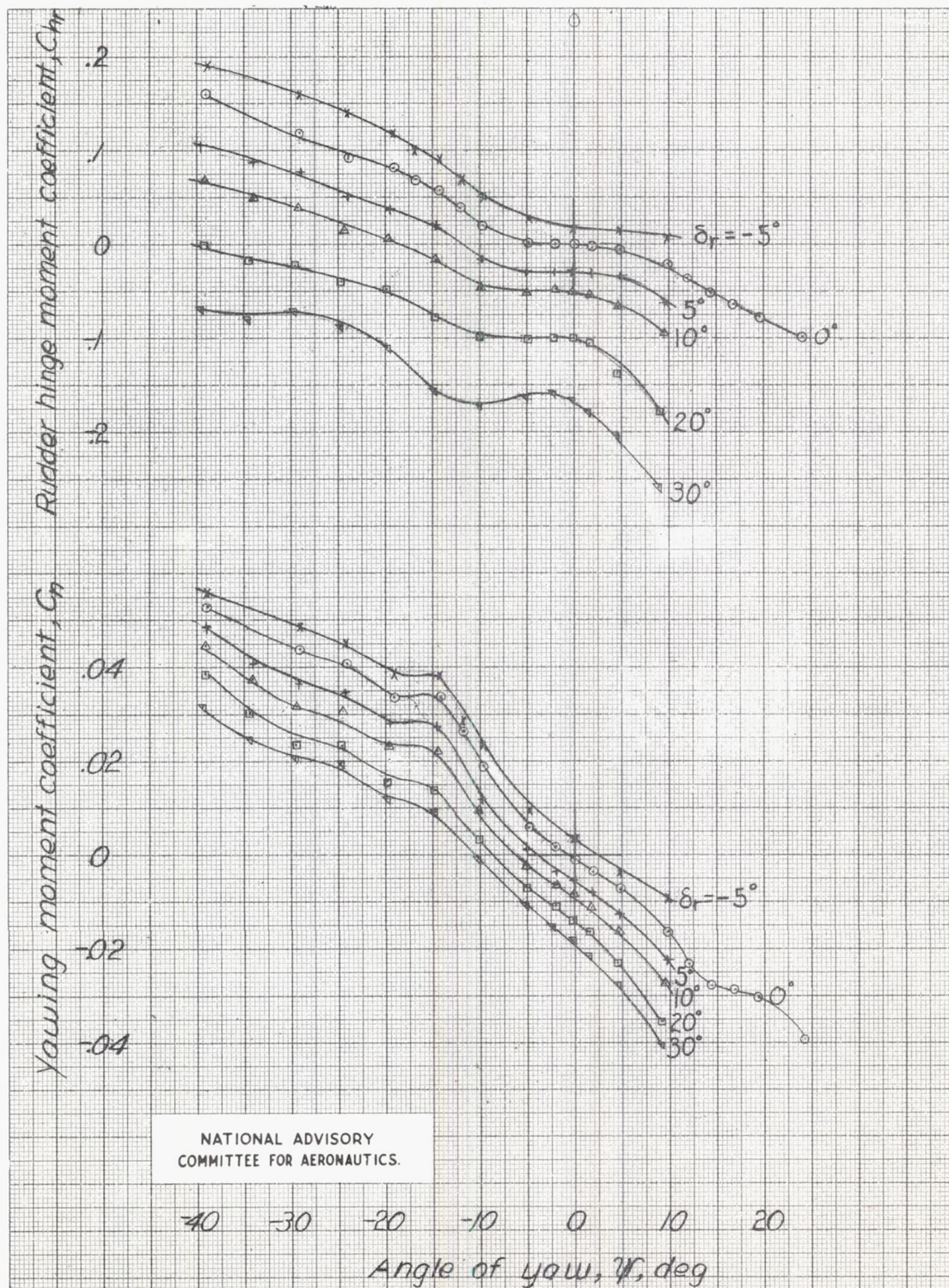
$C_L \approx 1.71$ at $\Psi = 0°$
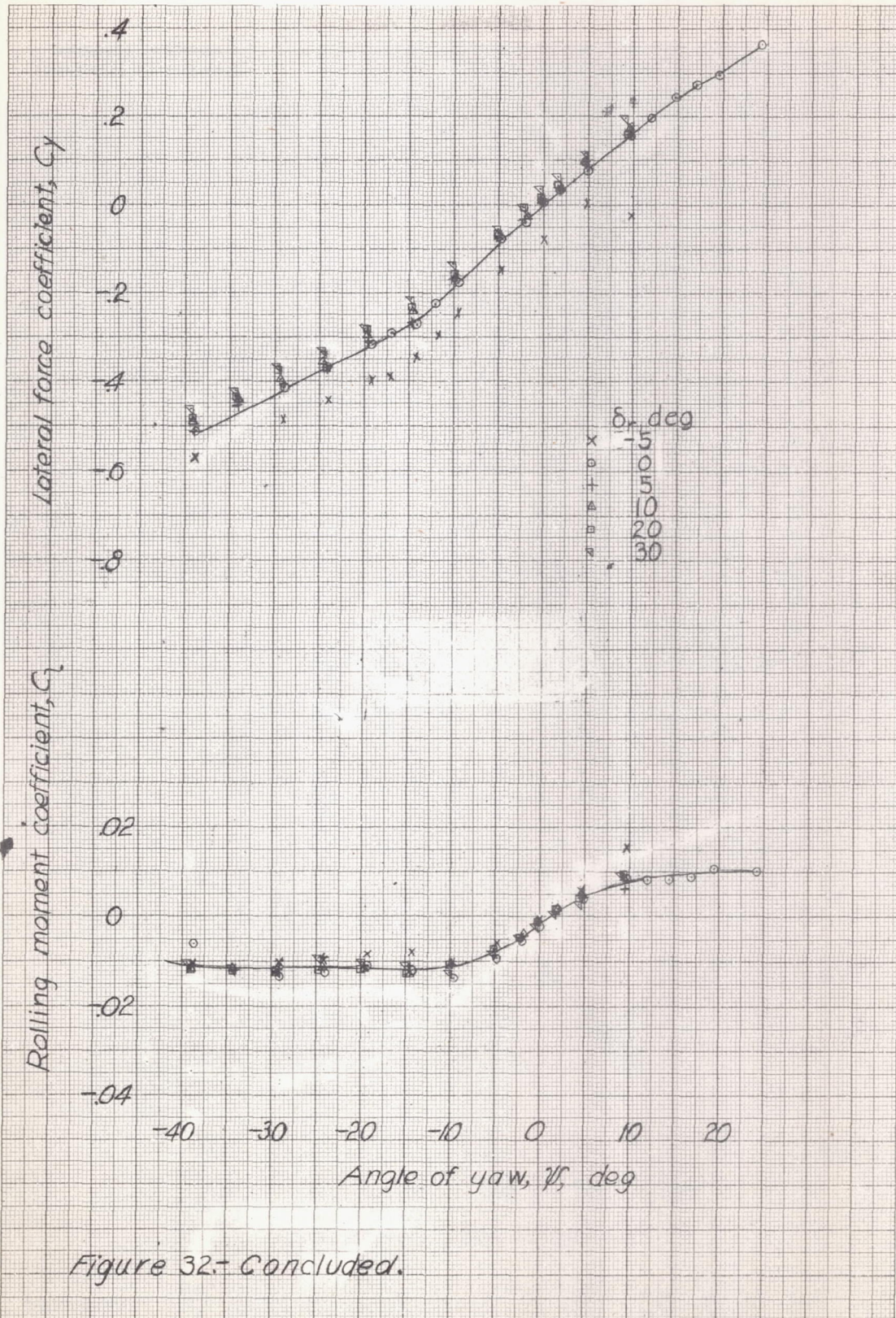
Figure 32.- Concluded.

Figure 36.- Variation of yawing moment coefficient with rudder force and rudder angle. $\psi=0°$. XBTC-2 airplane with revised vertical tail. Cruising configuration.

Yawing moment coefficient, C_n

Pedal force, lbs

Rudder angle, deg

V=394 mph at 16,000'

V=394 mph
V=118 mph } Max adverse C_n due to ailerons

V=118 mph at S.L.

V=118 mph
V=394 mph } Max adverse C_n due to ailerons

Figure 33.- Effect of rudder deflection on the aerodynamic characteristics in yaw of the ⅓-scale model of the XBTC-2 airplane with the revised vertical tail. α≈11.4° Landing configuration. Take-off power. Dorsal D_1.
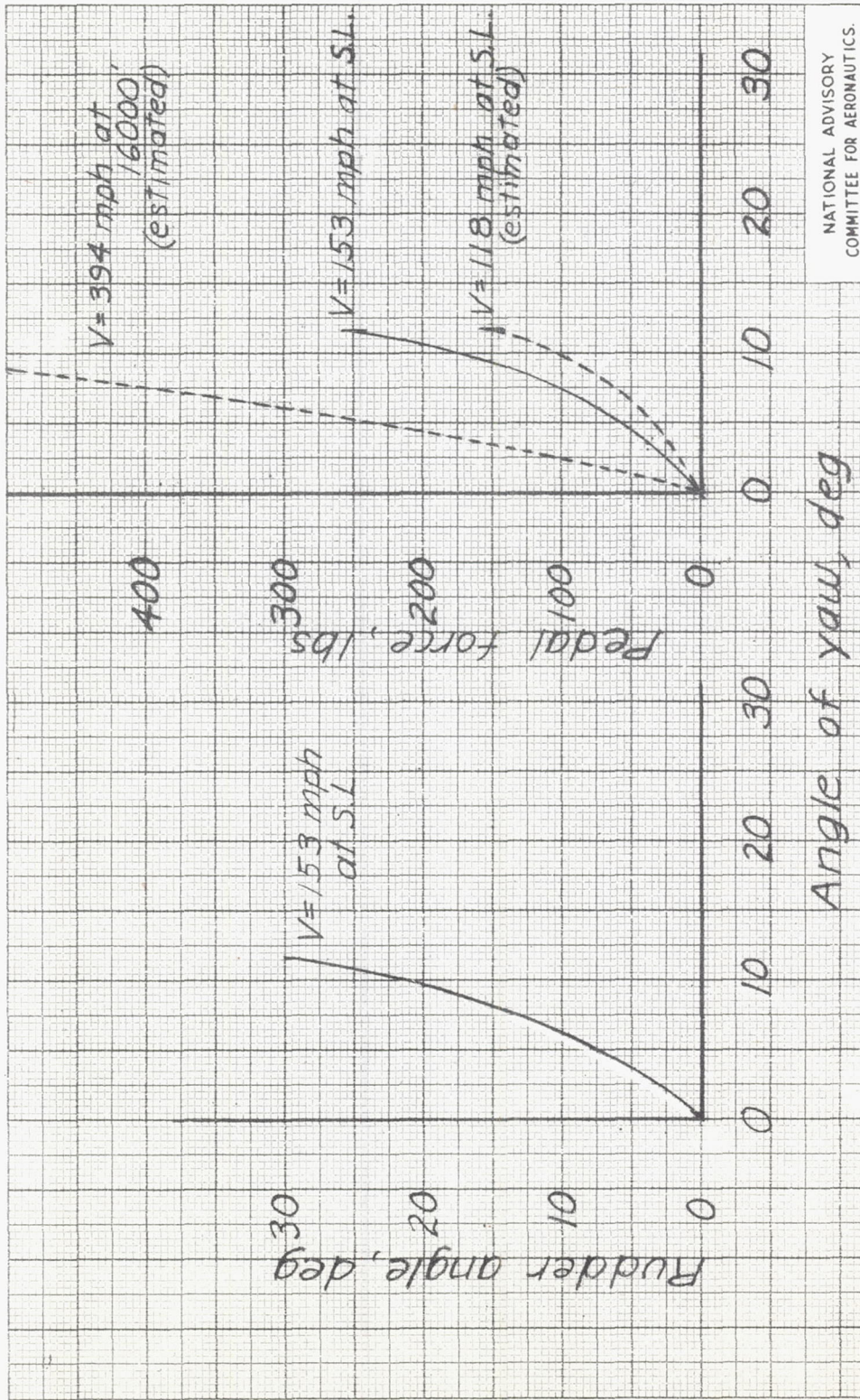
$C_L \approx 2.77$ at $\psi = 0°$

Figure 33.- Concluded.

L-787
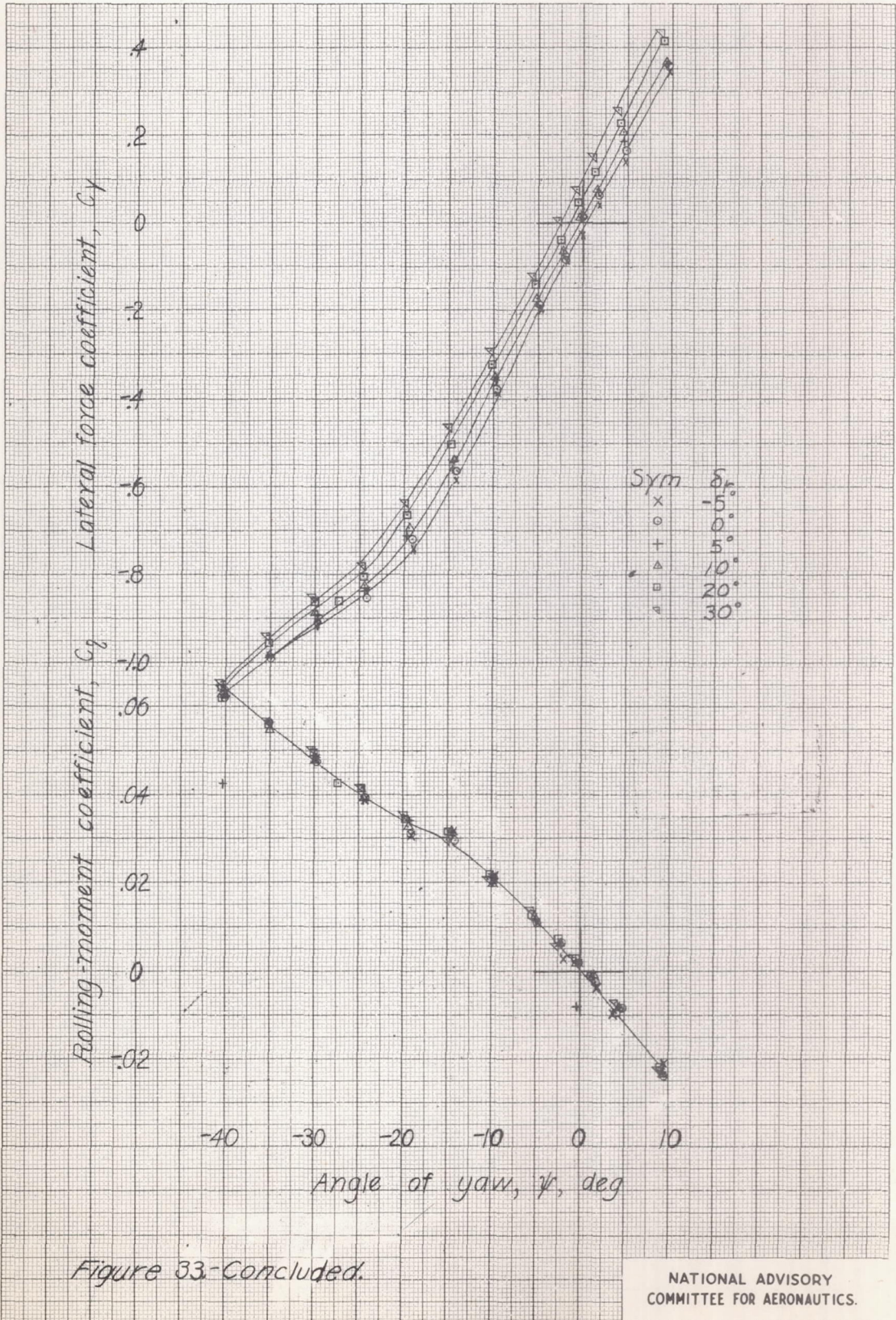
Figure 34.- Variation of rudder force and rudder deflection for trim with angle of yaw. XBTC-2 airplane with revised vertical tail. Cruising configuration. Dorsal D. Windmilling.
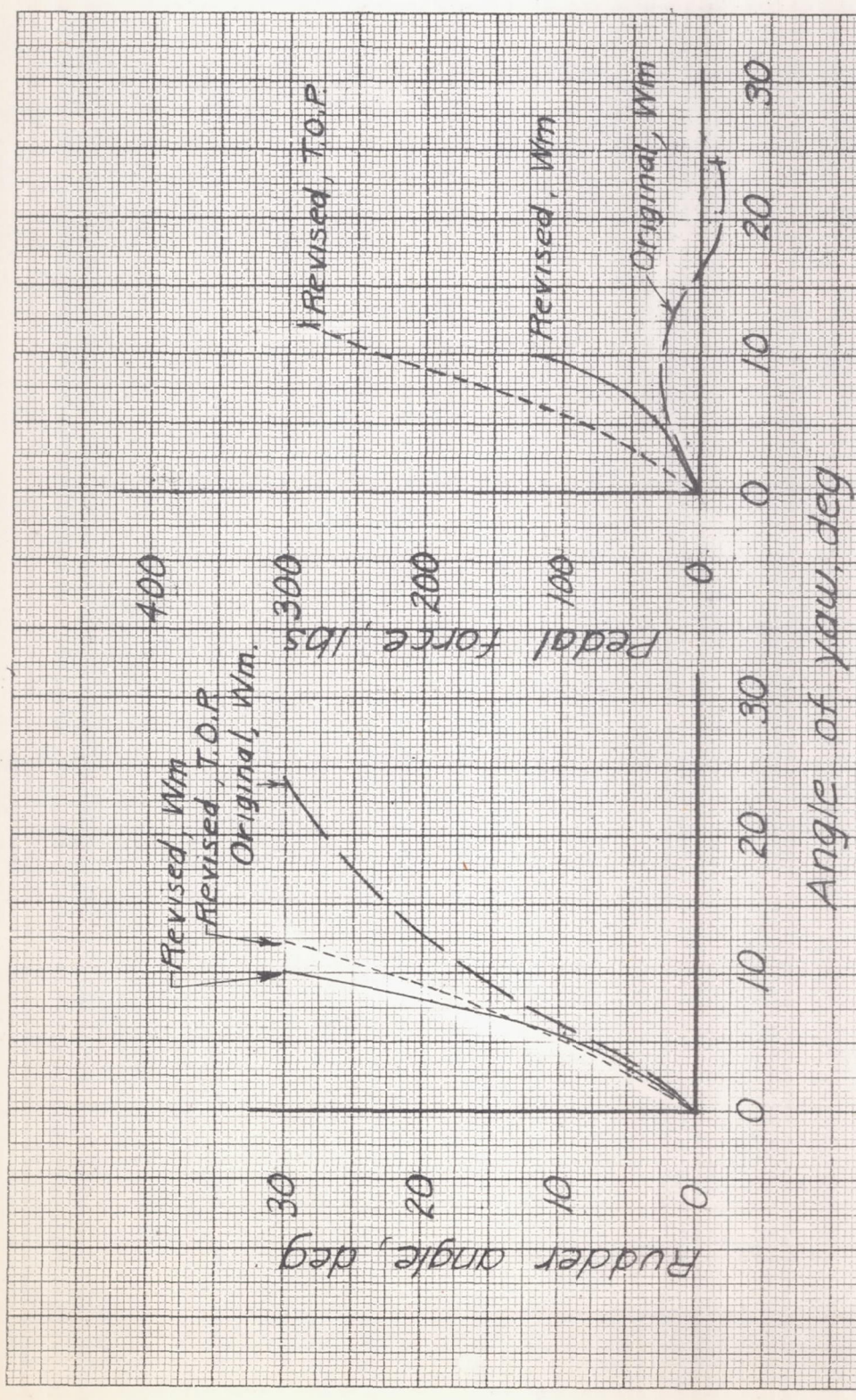
Figure 35.- Variation of rudder force and rudder deflection for trim with angle of yaw. XBTC-2 airplane with original and revised vertical tails. Landing configuration. $C_L = 1.74$. $V = 91.4$ mph. Original dorsal with original tail, dorsal D_1 with revised tail.
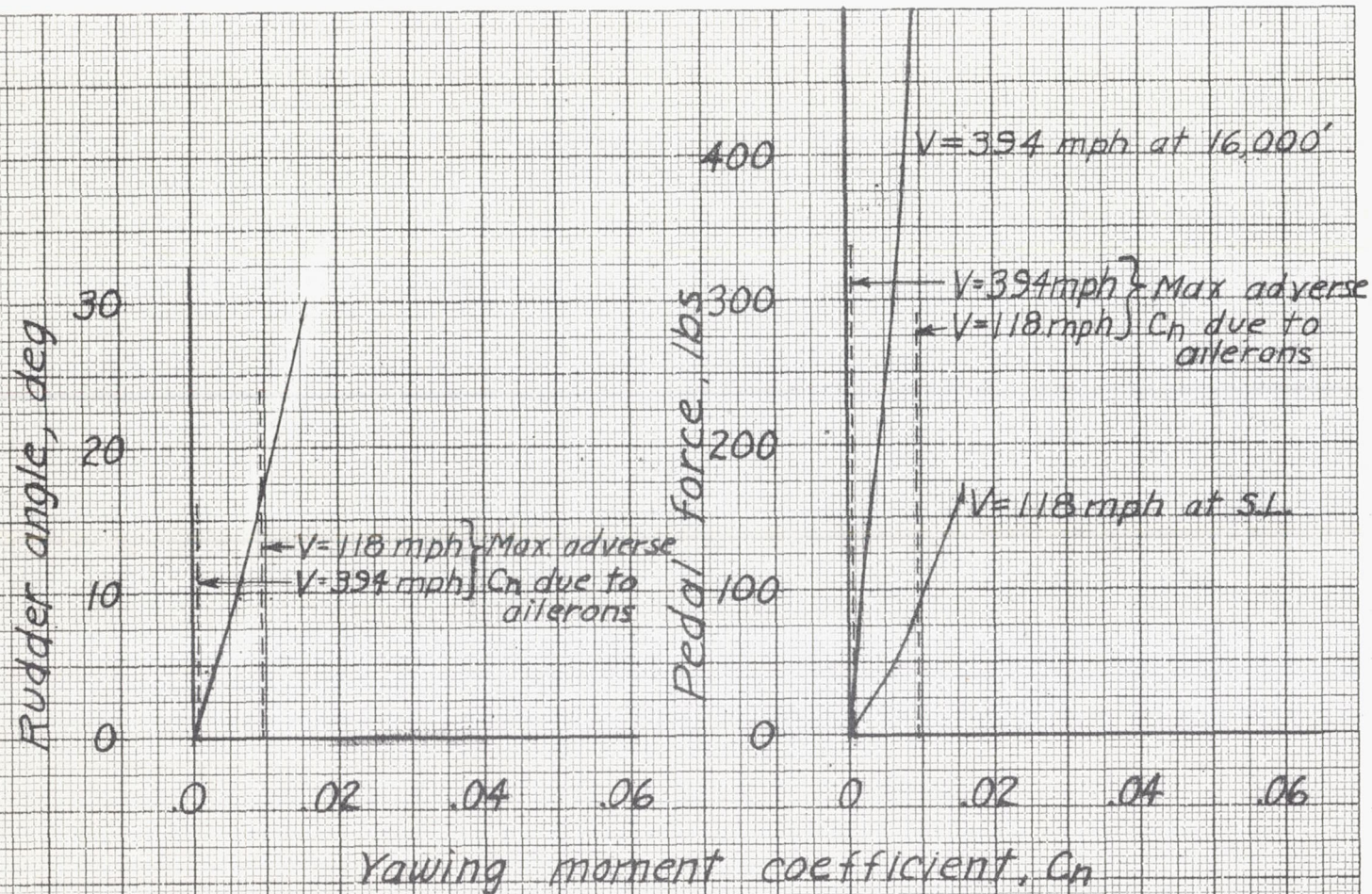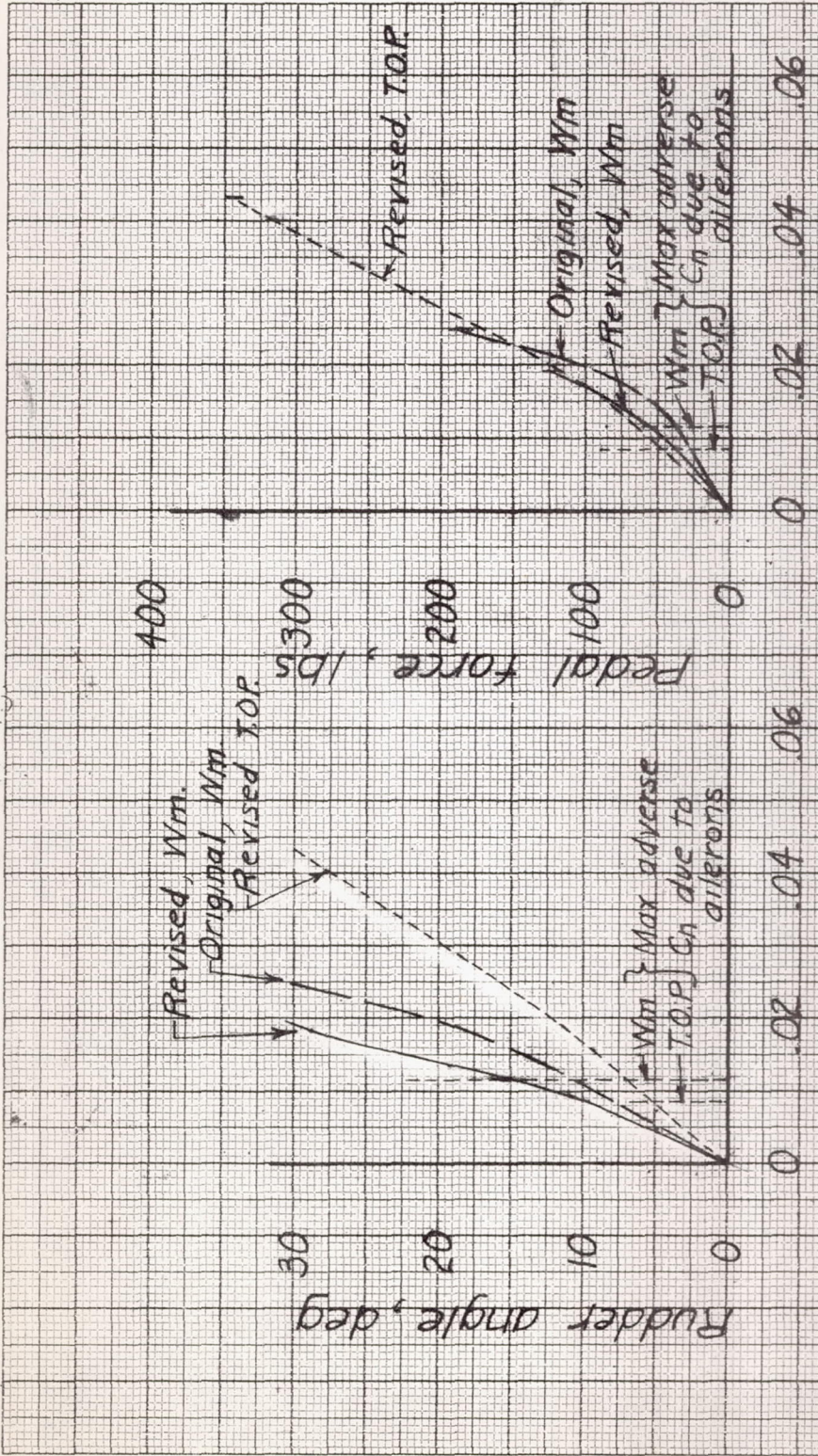
Figure 36.- Variation of yawing moment coefficient with rudder force and rudder angle. $V=0°$. XBTC-2 airplane with revised vertical tail. Cruising configuration.

L-787

Figure 31.-Variation of yawing-moment coefficient with
rudder force and rudder angle. ψ=0°. XBTC-2
airplane with original and revised vertical tails.
Landing configuration. C_L=1.74, V=94.4 mph.